Heat and mass transfer processes in absorption systems.

Sabir, Hisham

HEAT AND MASS TRANSFER PROCESSES IN ABSORPTION SYSTEMS

by

HISHAM SABIR

A thesis submitted for the degree of
Doctor of Philosophy
in the Faculty of Engineering of the
University of London

Department of Mechanical Engineering
King's College London
1993

Acknowledgements

I would like to express my deep sense of gratitude to my supervisor Dr. G. A. Vinnicombe for his much appreciated contributions to this study and his valuable guidance throughout.

I also wish to thank the Saudi Ministry of Higher Education and the Arab–British Chamber Charitable Foundation for their generous financial support.

My thanks are also due to Mr. C. Edwards and Mr. M. Harrington for their valued assistance and patience.

Abstract :

This thesis presents a theoretical and experimental study of the absorption refrigeration system and includes a literature survey which reviews previous relevant work.

The study includes a computer simulation of a complete absorption refrigeration system with non–volatile absorbent. The programme calculates the system's operation conditions for given outside and design conditions. The components' behaviour is described in terms of heat transfer and mass transfer effectivenesses. The simulation enabled the study of the effects of the system's conditions on its performance and for this results are presented and discussed.

The experimental work was undertaken to validate the simulation programme. It involved the building and testing of a complete $LiBr/H_2O$ refrigeration system. The results of the experimental studies compared reasonably well with the model. The discrepancies were explained largely in terms of heat losses from the system to the ambient which were not included in the model.

The work also includes a more detailed study of the performance of the system's absorber and develops a simplified method of predicting this performance. The method is suitable for use on personal computers because of its limited need for computing speed and memory and is therefore an alternative to the finite difference method which requires more extensive computing facilities. However, this simplified method does need the prior knowledge of the heat and mass transfer coefficients. A simply implemented correction factor was found to be

necessary to ensure good agreement between the method and the published data.

Two special factors relating to the behaviour of absorbers have also been investigated analytically, i.e., the effects of waves and entrained non–condensable gases. The enhancement of the heat and mass transfer due to the actions of waves in the falling film type absorbers is analytically investigated by solving the combined energy and diffusion equations using an Alternating Direction Implicit (ADI) finite difference method. The results for flows with low Reynold's Number are presented and discussed. The detrimental effects of the presence of non–condensable gases on performance is presented using data for an air–LiBr/H_2O combination and it is shown that the reduction in heat and mass transfer as a result of the non–condensable gas can be offset by introducing turbulence into the vapour/gas mixture in the absorber.

To summarise; the novelty and uniqueness of the work presented here include: a) the use of the absorber's heat effectiveness to obtain the overall solution of the absorption system, b) the simplified method to estimate the absorber's performance, c) the use of a velocity profile that denies mixing in the problem of combined heat and mass transfer in liquid wavy films and the subsequent proof that the improvement in heat and mass transfer rates are due to the vertical component of velocity that exists only in the wavy flow, and d) the method of estimating the effect of the presence of air on the absorption process.

Table of Contents :

List of Figures :

List of Tables :

1–Introduction :

1.1–General :

In today's practice, refrigeration can be performed by one of several methods. These methods are :

(1) Vapour compression
(2) Vapour absorption
(3) Air expansion
(4) Vapour jet
(5) Thermoelectric

The vapour compression system is, by far, the most widely used in refrigeration and air conditioning applications. Next to it is the vapour absorption system which is commonly used where a cheap, or free, source of low temperature heat is available. Air expansion, vapour jet, and thermoelectric systems are used in small and specific areas.

1.2–Vapour Absorption Systems :

This work will be dedicated to the performance of the vapour absorption system and its main component; the absorber.

Vapour absorption refrigeration cycles were first invented in the early 19^{th} century. They formed the early developments of refrigeration systems. However, when the vapour compression systems later dominated the field with their better performance and their relatively small number of components, absorption systems were eclipsed for many years. Recently however, they have received renewed interest as the cost of electricity escalated and the issue of environment became more and more important.

The main components of the vapour absorption system, with non–volatile absorbent, are the boiler, condenser, evaporator, absorber, heat–exchanger, and the solution pump. The boiler, absorber, heat–exchanger, and the solution pump perform the combined effect of the compressor in the vapour compression system. They deliver the refrigerant, at high pressure, to the condenser and remove it, at low pressure, from the evaporator. There are two cycles in the absorption system. The refrigerant cycle in the condenser and evaporator which is the same as that of the compression system, and the absorbent cycle in the boiler, absorber and heat–exchanger.

The working fluid in absorption systems is a pair of absorbent/refrigerant liquids (solid absorbents are also used). There are two main absorbent/refrigerant pairs in absorption systems. The $LiBr/H_2O$ and the H_2O/NH_3. The $LiBr/H_2O$ pair is used where moderate cooling temperatures are required because water, the refrigerant, can not be cooled below zero degree Celsius. The H_2O/NH_3 pair is used to achieve lower temperatures. However, since the water, the absorbent in this case, is volatile a rectifier is needed to ensure high purity of the ammonia vapour. Another difference between the two absorption systems is that the $LiBr/H_2O$ system operates at sub–atmospheric pressures because of the low vapour pressure of water. This makes the system operate under the risk of inward air leakage which, as will be seen from this study, can seriously affect its performance, and will also be impossible to eradicate without interruptions to the system's operation. The H_2O/NH_3 system, on the other hand, works at high pressures due to the high vapour pressure of the ammonia. This eases the problem of leakage (which will be outward

leakage in this case) because the working fluids can be replenished without interrupting the operation of the whole system.

1.3–Comparison between Absorption and Compression Systems :

Heat, the input energy to absorption systems, is considered a low grade form of energy and is readily available as waste in large power plants and factories. It is also available from alternative energy sources e.g solar, biomass, geothermal, etc. It is, therefore, either free or much cheaper than the mechanical work needed to drive the compressor of the vapour compression system. However, heat has less thermodynamical availability than work which means that the heat ratio (Hr) of the absorption system, defined as the ratio of the evaporator's power to the input heat, is less than the coefficient of performance (COP) of the compression system, defined as the ratio of the evaporator's power to the compressor's work. However, Hr is not directly comparable to the COP because of the difference between heat and mechanical work. To be able to compare the two quantities, one must consider the heat that was originally supplied to the heat engine which produced the work and calculate an equivalent heat ratio for the vapour compression system. Even then, the heat ratio calculated for the compression system will still be higher than that of the absorption system. This is due to the irreversibilities of the absorption system which is higher than the irreversibilities of the combined heat engine/vapour compression system. One source of irreversibility is the inability of the absorption system to utilize the high temperature heat which is used by the heat engine. Another source of irreversibility in the absorption system is the departure from equilibrium in the vapour absorption and generation processes. Of course, there is a small mechanical work input to the absorption system in the form of the power of the solution pump.

However, this is much smaller than the work needed to drive the compressor of the compression system since the liquid has a smaller volume than an equivalent mass of vapour. In the Platen–Munters aqua–ammonia absorption system the solution pump is eliminated by using hydrogen gas to equalize the pressure throughout the system. In addition to saving the power of the pump this system has the benefit of having no moving parts. However, it will be clear in the course of this study that the performance of the system is seriously affected by using the hydrogen gas.

It is concluded that when a cheap, or free, source of low temperature heat is available, absorption systems become economically attractive. Their ability to utilize the heat from the alternative sources of energy directly makes them an attractive option from the environmental point of view.

1.4–Absorbers :

It will be clear during the course of this study that the absorber is the most important component of the absorption system. Therefore, great attention must be paid to its performance.

Absorbers are the devices where the liquid absorbent absorbs the vapour refrigerant to remove it from the evaporator and allow it to be reproduced in the boiler thus maintaining a continuous flow throughout the system. The absorption process is complicated in that the change of phase takes place at a varying temperature. This is due to the heat of absorption which can be positive (exothermic process) or negative (endothermic process). The temperature of the absorbent will rise or fall depending on the type of process, however, in both the $LiBr/H_2O$ system and the H_2O/NH_3 system absorption is an exothermic process

and the temperature will increase if the absorber is not cooled to keep the process continuous.

There are different types of absorbers used in todays refrigeration practice to meet the requirement. In particular there are the bubble column absorber, the foam absorber, and the film absorber. The bubble column absorber consists of two concentric vertical tubes. The inner tube is occupied by the solution through which the vapour ascends in a rising column of bubbles, while the cooling medium flows in the outer tube. In the foam absorber the solution is sprayed by a nozzle or stirred to improve the mass transfer while the cooling takes place in a separate heat exchanger. In film absorbers the solution flows in a thin film down a horizontal bundle of tubes, a wetted packed column, or a plate, while the coolant flows on the other side of absorber plate (or inside the absorber tubes).

Film absorbers are very popular because of their high performance. They achieve high effectiveness due to the thinness of the absorbent's flow which maximizes the ratio of the surface area to mass flow rate and minimizes the penetration length. This results in a high mass transfer rate from the vapour refrigerant to the liquid absorbent and a high heat transfer rate from the absorbent to the coolant.

1.5–Outline of Present Work :

As it was mentioned earlier this work will be concerned with the study of the absorption system and its absorber. In this context, a computer model simulating the overall performance of the absorption system was developed and the results from which were compared to the results obtained from the experimental work carried out to validate the model. To study the absorber, a simplified method of predicting its

performance was developed and the effect of two factors, i.e., absorbent's waves and the loss of vacuum, on this performance was analyzed.

2–Literature Survey :

The body of literature relevant to the areas investigated in this dissertation vary in size between the particular areas. Some areas are extensively investigated while some are less well researched. For convenience, this review is divided into sections corresponding to the subject division adopted in this work.

2.1–Simulation of the Overall Performance of Absorption Systems :

The revived interest in absorption systems in the past two decades has generated a growing need for reliable and effective system simulation to investigate new concepts for advanced cycles and working fluids. Not surprisingly, most of the work in this area is relatively recent.

Vliet et al [1] devised a computer model for a LiBr/H_2O absorption system with specific design features for the components. The governing equations were obtained from mass, species, and energy balances, as well as fluid flow, heat transfer, and mass transfer correlations for each of the components. The heat transfer in the absorber was modelled by a fixed heat transfer coefficient. Their results were presented in terms of the effect of the generator temperature on the system's COP. No experimental validation was reported.

Takeshita et al [2] developed a computer model for a residential gas fired absorption heat pump based on R22–DEGDME pair. Their model accounted for the pressure loss around the cycle. This was necessary because the heat of vaporization of the R22 is relatively small, therefore its mass flow rate has to be large resulting in a large pressure drop. Thus, it could not be ignored in this particular case whereas in other

cases the pressure drop is ignored. The model, however, did not account for the heat losses. The model was validated by experimental work and good agreement was reported.

Grossman and Perez–Blanco [3] reported the development of a simple code to aid the conceptual design of an absorption heat pump for waste heat utilization using $LiBr/H_2O$ and $LiCl/H_2O$ pairs. Later Grossman and Michelson [4] created a flexible, modular computer programme to simulate the absorption systems. The programme has the capability of modelling various systems employing different working fluids. Each component of the system is simulated in a different subroutine containing the equations that describe the physical processes that take place in this component. The user has to supply information on (a) the physical system i.e., the number of stages, the nature of the system (whether a chiller, heat pump, heat transformer, etc), the way the flow is arranged, specify the working fluids and (b) the initial guess values of the solution and the allowed tolerance of convergence. The programme then calls up the relevant component subroutines which in turn invoke the relevant data base that contain the properties of the specified fluid. A solver then solved the set of the nonlinear equations starting from the initial seed values and iterating until the preset tolerance criteria is satisfied. A distinctive feature of the programme is that it imposes temperature constraints on the solution to ensure that heat is transferred in the right direction. If the direction is wrong then the current intermediate solution values are changed to comply with the restraint. This feature is required because the nature of the governing equations, most of them being nonlinear, can lead to many solutions and only one of which is the actual physical solution for the design point chosen. They carried out experimental work on a $LiBr/H_2O$ heat pump

to validate the analytical results and when comparing the results found that the computer generated COP of the system was 16% higher than its experimental value at high temperatures and between 7% and 12% higher at lower temperatures. They attributed the discrepancy to heat losses from the system to the ambient which the programme did not account for. Later, Grossman and Gommed [5] introduced an improved version of the same programme with considerably extended user–oriented simulation capability and applicability. The programme results were reported to have very good agreement with the experimental results of a $LiBr/H_2O$ heat transformer. They also reported successful results in simulating various other cycles and working fluids. However, they noted that some problems were encountered in fluids with volatile absorbents such as H_2O/NH_3 due to their complex behaviour at large concentrations of the absorbent in the vapour phase. Gommed and Grossman [6] employed the same code to investigate the performance of various systems using the $LiBr/H_2O$ fluid pair. They generated complete performance maps under varying operating conditions for systems in single stage and several double stage configurations.

Iedema [7] developed a computer simulation for a $LiBr/ZnBr/CH_3OH$ heat pump based on a heat and mass transport model that utilizes empirical relations as derived from experimental results which eliminates the need for the use of components effectivenesses. No experimental validation has been reported in his case.

Alvares and Trepp [8] introduced a computer model of an existing solar driven aqua–ammonia refrigeration system. They adopted an "approach to equilibrium factor" for the generator and absorber which is a measure of deviation from equilibrium concentration in those devices. The same principle is used later in this work under the name

of "mass effectiveness". Another feature of their simulation is the allowance of heat losses from the generator.

Butz and Stephan [9] developed a computer simulation of a commercially available heat pump. They simulated each component by partial differential equations resulting from the unsteady heat and mass balance. The equations are reduced to a set of ordinary differential equations by discretization with respect to space. They are then, along with their accompanying algebraic equations, solved using an available solver package. Their analytical results had good agreement with the actual performance of the heat pump.

It can be seen that there is a fair amount of computer simulations of absorption systems. Some of it, however, were created for existing systems using the conditions of these systems to calculate the heat and mass transfer rates. This means that these models can not be used for other systems without altering the code. Other simulations relied on the user input of the conditions to facilitate the calculations. This complicates the use of the model and the process of converging to the solution. To circumvent these difficiencies, a computer simulation of an absorption system where the performance of the components is characterized by "heat and mass effectivenesses" will be presented in this study. The use of effectivenesses allows the components to be treated as "black boxes" and eliminates the need to specify heat and mass transfer coefficients and areas. It is believed that the code, which will simulate the basic LiBr/H_2O system, will not need solution constraints of the type used in [4] which were necessitated by the fact that the code [4] was designed for a wide range of applications using the same initial solution guess.

Where Γ is the mass flow rate per unit width (kg/m s), and μ is the dynamic viscosity (kg/m s)

2.2–Heat and Mass Transfer in Falling Film Absorbers :

The absorber is the most complex of the components in an absorption system and, fortunately, has been subjected to extensive specialised study.

Absorbers, where the absorbent is freely falling in a thin film over wetted packed columns, over a bundle of horizontal tubes, or over cooled plates are widely used in absorption systems. They achieve high effectiveness by virtue of the thinness of the absorbent's flow [10] which maximizes the ratio of the surface area to mass flow rate and minimizes the penetration length, hence aids the process of both heat transfer to the coolant and mass transfer of the vapour refrigerant.

2.2.1–Film Hydrodynamics :

The nature of the film flow, whether laminar or turbulent, smooth or wavy, and hence the amount of heat and mass transfer, will depend on the Reynold's Number.

Aragaki et al [11] who experimentally studied falling films of water over smooth vertical tubes concluded that the flow is laminar up to Reynold's Number ($Re = \Gamma/\mu$) = 170 and turbulent at $Re > 900$ with a transitional region between. ✳

Benjamin [12], who observed the wave formation in laminar flows reported that film flows with $Re < 5$ appears to have smooth surfaces.

Rotem and Neilson [13] concluded after surveying a significant amount of available information that there are three distinct regimes of film flow depending on Reynold's Number :

Laminar flow without rippling of the free surface at $Re < 7$

Laminar flow with rippling (wavy) at $7 < Re < 250$
Turbulent flow at $Re > 250$

Hounkanlin and Dumargue [14], who conducted experimental work with falling films of soda solution observed that the flow is :
smooth laminar or wavy at $18 < Re < 200$,
transitional between laminar and turbulent at $200 < Re < 1000$, and
turbulent at $Re > 1000$

Now, the values of Re for the applications of absorption refrigeration is unlikely to exceed 300 [15] and is therefore likely to lie in the laminar wavy range. Therefore it is this region which will be concentrated upon in the rest of this study.

A good body of literature is available on the nature of waves in film flow regimes. Tailby and Portalski [16] and Stainthorp and Allen [17] concluded after studying the wave motion photographically that the wave characteristics depend on the flow rate, the physical properties of the liquid, and its distance from the leading edge. Salazar and Marshall [18] concluded after detailed optical studies using laser technique that waves are primarily of two dimensional nature up to Re = 375. Brauner and Maron [19] recorded the variation of film thickness and the mass transfer rate in an inclined plate. They observed that : (a) there is an inception line at which high frequency, shallow ripples start to develop, (b) that as they travel downstream they overlap each other thus generating larger lumps of liquid with lower frequencies, higher amplitudes, and greater velocities, and (c) that further down stream these waves eventually become steady–periodic roll waves which have a pronounced influence on the mass transfer. They also noted that the wave characteristics will depend on the film Re, the plate inclination,

and the distance from the inception line. The same authors later [20] developed a physical model for hydrodynamic mechanisms of gravity rolling waves in thin liquid film based on periodic distortion of the hydrodynamic boundary layer in the wave front and the following recovery in the wave trail. They described the roll waves as being highly disturbed lumps of liquid travelling along a thin substrate at a speed several times greater than the mean film velocity. Their model, which agreed well with experimental results for flows with Re < 1000 and over a wide range of inclinations, predicted that the fraction of liquid travelling in the substrate does not exceed 20% of the total amount of liquid at low rates and approaches 3—4% at Re > 2000.

2.2.2–Heat and Mass Transfer :

In many cases the absorption process is exothermic where heat, known as the heat of absorption, is released. This is certainly the case in the absorption fluid pairs that are most commonly used in refrigeration i.e., $LiBr/H_2O$ and H_2O/NH_3. However, since the concentration seeks equilibrium at its temperature and vapour pressure, the rise in temperature associated with this released heat will reduce the concentration variation i.e., impairs further absorption. Consequently cooling is essential if high concentration variation is to be achieved.

Several workers have addressed the problem of vapour absorption by thin liquid films and the associated heat and mass transfer processes. Javdani [21] solved the diffusion equation for a wavy falling film analytically by assuming the concentration to consist of two parts, a mean part and a fluctuating part which he approximated by a simple periodic function. His approach showed good qualitative agreement with experimental data.

Grigoreva and Nakoriakov [22] presented an exact solution to the simultaneous heat and mass equations by putting the temperature and concentration in the form of Fourier expansions of the dimensionless axial and vertical coordinates and using the boundary conditions to obtain the constants of the expansions.

Beschkov and Boyadjiev [23] employed a finite difference method to solve the equation of vapour diffusion into a thin liquid film flowing in a laminar wavy manner. They used the velocity profile and wave characteristics computed by Penev et al [24] and obtained data on mass transfer which agreed well with their own experimental work.

Grossman and Heath [25] solved the the combined energy and diffusion equations for a turbulent film using a "method of lines". According to this method the non–dimensional film domain is divided into thin strips by lines parallel to the longitudinal axis whereby the derivatives with respect to the other axis (vertical) can be expressed in finite difference form; thus reducing the equation into a set of ordinary differential equations in the longitudinal variable alone which they solved by an available ODE integrator using the relevant boundary conditions.

Ibrahim [26] solved the diffusion and the energy equations of a smooth laminar flow simultaneously using a hybrid method consisting of an analytical solution at the entry region and a numerical solution thereafter thus obtaining accurate results at reduced mesh size. He reported good agreement with the published data.

Urakawa et al [27] also solved the combined heat and mass equations. They devised two separate approaches; one implementing the finite difference method, and the other using algebraic temperature and

✳ In this study a method of estimating the performance of the absorber was presented. The method, which is suitable for use on PCs due to its simplicity and its limited need of memory, calculates the temperature and concentration of the absorber and its overall effectiveness from given heat and mass transfer coefficients which can be obtained from relevant experimental or analytical data. From the computed temperature and concentration profiles the method can then calculate the heat and mass effectivenesses of the absorber which are used by the overall computer model, of chapter 3, to simulate the performance of the absorber. The method was compared to the hybrid method of Ibrahim [26] and was corrected to give good agreement between the two methods. The method is simpler than the finite difference method approach even when this approach is reduced to solving the approximated equations for a single space variable by using the "method of lines" as was introduced in [25]. It is also much simpler than the exact solution presented in [22] which was obtained using a set of restrictive conditions. The method, by using predetermined heat and mass transfer coefficients, goes one step further than the simplified method introduced by Perez–Blanco [28] who applied energy and mass balances to the absorber and used values for the mass transfer coefficient calculated by Ruchenstein and Berbente [29] but simplified the heat transfer problem by assuming pure conduction across the absorbent film. The second method of Urakawa et al [27] in which they approximated the concentration and temperature profiles by non–linear algebraic equations is simple enough but appears to be less accurate as they reported some differences between this approach and their own finite difference solution in the temperature field at the entry region.

concentration profiles across the film thickness. They compared the results of both methods and found that the temperature differed slightly at the entry region but became equal rapidly as the flow length increased, while the concentration values agreed well.

Perez–Blanco [28] obtained heat and mass transfer rates for a falling film absorber analytically by applying heat and mass balance over an absorber element and using the mass transfer coefficient from Ruchenstein and Berbente [29] and assuming pure heat conduction across the film thickness. The results agreed to within 10% with his own experimental work.

Cosenza and Vliet [30] experimentally studied the absorption of water vapour into a thin film of $LiBr/H_2O$ solution flowing over horizontal tubes. They correlated the heat transfer characterized by the film Nusselt Number to the film Reynold's Number for tube diameter of 19 mm as : $Nu_{film} = 0.3\ (Re_{film})^{.46}$.

Zheng and Worek [31] used fibre–optic holographic method to measure the heat and mass transfer rates during the humidification of air by a film of $LiCl/H_2O$ solution. They obtained data that compared to other experimental results to within 5% error. More work on this area is reviewed below where it is more relevant.

2.2.3–Effect of Waves :

Many investigators noticed the significant improvement to heat and mass transfer due to the presence of waves.

Budov et al [32] reported, based on experimental observations, that the oscillatory motion resulting from wavy flow causes an intensification of the heat transfer.

Oliver and Atherinos [33] experimentally studied the absorption of carbon dioxide into a thin film of aqueous sodium bicarbonate solution. They reported that the mass transfer was enhanced by up to 250% by the waves.

Pokusaev et al [34] observed the desorption of carbon dioxide from a water film and reported that the intensification of mass transfer due to waves reached 5.4 times that of smooth flow.

Ruckenstein and Berbente [35] concluded after surveying the works of several investigators that the enhancement of mass transfer in wavy films is up to 150% over that of smooth films and the heat transfer increases by 20—30%. Later [29] they obtained a velocity profile based on the solution of the equation of motion in the form of Fourier series and they showed that the wave motion may amplify the local mass transfer rate by a factor of two. They qualitatively explained the unequal enhancement of the heat and mass transfer by the fact that thermal diffusivity in liquids is large as compared to the coefficient of molecular diffusion; it is therefore possible that the apparent diffusivity, due to the wave motion, be negligible against thermal diffusivity, but of the same order with, or even larger than, the coefficient of molecular diffusion. This explanation is sufficient in the case of heat and mass transfer across the film interface where both processes are exposed to the same wave intensity. However, in the absorbers of refrigeration systems where the mass transfer occurs at the interface and the heat is transferred across the solid wall, the discrepancy is further explained by the fact that the effect of waves is larger at the interface than at the solid wall. This view is supported by Brauner and Maron [19] who experimentally studied the mass transfer from a solid wall into a falling liquid film. They concluded that in the case of large rolling waves

increasing the flow rate, though increases their intensity, produces little effect on the mass transfer because increasing the waviness at high liquid flow rates does not necessarily enlarge its effect deep in the liquid film close to the solid boundary. They also noted that small waves have little or no effect on the mass transfer for the same reason. They further speculated that waves will have more effect in case of vapour absorption at the free surface. The same conclusion was reported by Beschkov et al [36] when they experimentally investigated the dissolution of gypsum in a vertical water film. They also made similar speculations about vapour absorption at the interface.

Beschkov and Boyadjiev [23] who solved the diffusion equation of vapour in wavy laminar flows numerically, reported that their model predicted an improvement of 100% in mass transfer across the free surface of the film. This agreed, to a satisfactory degree, with their own experiment of carbon dioxide desorption from a wavy water column.

One of the explanations given for the observed enhancement in heat and mass transfer in wavy flows is that it is due to the increase of interfacial area. However, Brauer, as quoted in [23], showed that the interfacial area increase due to the ripples is less than 10%. Portalsky and Clegg [37] have shown that at any Reynold's Number the regular (roll) waves contributed more to the area increase than the small ripples and the random motion. They obtained an imperically corrected formula for the percentage area increase after extensive experimentation with different liquids. Their formula reads :

$$\Delta A\% = 374\left(\frac{\nu^2 \, Re}{\lambda^{4/3} \, g}\right)^{2/3}$$

where, ν, λ, and g are the liquid's kinematic viscosity, the wave length, and the gravitational constant respectively. Accordingly, the interfacial area increase for water at Re = 100 is less than 0.2%. Therefore, to attribute the amplification of the heat and mass transfer rate solely to the interfacial area increase is, obviously, not satisfactory.

At present the literature suggests that the improvement is primarily due, at lower Reynold's Number, to the presence of the vertical component of the velocity and the convection heat and mass transfer associated with it, and as the Reynold's Number increases and the wave characteristics develop, circulation currents and eddies start to evolve and further enhance the heat and mass transfer.

Ibrahim [26] suggested that for flows with Re < 100 a model with regular wave characteristics and no mixing should be applied to estimate the improvement in heat and mass transfer.

Penev et al [24] solved the complete Navier–Stokes equation for a falling liquid film assuming the waves to be regular and two dimensional i.e., the thickness of the film does not vary with its width. They found that under such conditions the liquid elements travel along unclosed trajectories and there can be no surface renewal, and the improvement is primarily due to the vertical component of the film velocity. However, they noted that the assumption of uniform wave celerity (velocity) may not exist in real film systems and recommended that more detailed description of wavy film flow should be based on taking into account a discrete spectrum of celerities, under which description, they noted, it is possible to account for the formation of circulation currents of liquid elements in the film.

Howard and Lightfoot [38], having developed a method of predicting rates of gas absorption into laminar rippling films, suggested that depending on the wave amplitude and its celerity there is a region around the wave peak where a reverse flow (with respect to coordinates moving at the wave velocity) is possible i.e., circulation of the liquid elements. Brauner and Maron [19] who recorded time traces of simultaneous local film thickness and mass transfer rate in a falling liquid film found them to have the same periodicity with the mass transfer rate having a small phase lag behind the film thickness. They interpreted the sudden relaxation of the wall shear stress just before the wave front and its subsequent steep rise as being the result of the picking up and mixing of the thin substrate into the following wave front. According to the above observations, and as mentioned earlier, they later [20] devised a theoretical model for the hydrodynamic mechanisms associated with rolling waves based on a periodical distortion of the hydrodynamic boundary layer in the wave front followed by a recovery in the wave trail. Maron and Brauner [39] offered a piecewise approach whereby the wave is viewed in terms of composite zones for each a characteristic mechanism is suggested. According to them and depending on the wave characteristics, there exists a region engulfing the wave peak where the local interfacial velocity exceeds that of the wave. As a consequence eddies take place and become responsible for the amplification of the local mass transfer.

It must be noted, following the above review, that the improvement of mass transfer due to the action of waves reported by Pokusaev et al [34] at more than five folds is an overestimation since most investigators estimate the range of improvement between 100% and 200%.

* , i.e., because of the enhanced heat and mass transfer due to the mixing of the liquid and the agitation of the vapour by the liquid waves

Following the literature review and the fact that improvement in heat and mass transfer were recorded for wavy flows over a wide range of Reynold's Number, it can be concluded that for flows with low amplitudes and wave velocities the heat and mass transfer are improved by means of convection associated with the perpendicular (to the direction of the flow) component of the velocity, and as the amplitude and celerity increase, circulation and mixing take place and contribute to improving the transfer rates.

The broad picture which has emerged from this review on wave effects is that while the enhancement of heat and mass transfer due the mixing effect of the waves is obvious, the enhancement due to the vertical velocity is less clear and is not substantiated enough from the literature. It was, therefore, considered necessary to clarify this point. Thus, the findings of Penev et al [24] will be applied to find the heat and mass transfer in a low Re wavy flow in order to validate their hypothesis.

It is also felt that the current methods of absorber analysis are very complicated and there is therefore a need for a much simpler model for design work. To fill this gap, such a method will be developed in this work. This simplified method should have good agreement with the existing, more complicated, methods.

2.2.4–Effect of Non–Condensable Gases :

The presence of a non–condensable gas in a condensing vapour is known to create diffusion resistance which must be taken into account as well as the resistance of the liquid [40].

The little work done in this area is primarily concerned with the effect of non–condensable gases on the condensation of vapours into liquid films, and perhaps the first effort to quantify the effect of the presence of such gases on the performance of falling film absorbers came in 1980 when Burdukov et al [41], conducting an experimental study on the absorption of water vapour by thin films of aqueous Lithium Bromide, observed the effect of the presence of air on the mass transfer of vapour into the liquid film. They concluded that an air content of 0.5% in the vapour reduced the mass transfer coefficient almost in half.

Lee and Rose [42] carried out experimental work to study the effect of non–condensable gases on condensation of vapours into liquid films flowing along a horizontal tube. They used combinations of steam and R113 as vapours with air and hydrogen as gases. They concluded that the presence of gases greatly impairs the heat and mass transfer of the vapour. They also noted that vapour velocities, even at small values, helped eliminate the building up of the gas at the interface hence improved the transfer rates.

Kotake [43] analyzed the effect of small amounts of non–condensable gases on the film condensation of vapours from a vapour/gas mixture. He concluded that the effect of gas is to reduce the condensation rate.

Galamba et al [44] investigated, analytically and experimentally, the melting of solid wall due to the condensation of a vapour on it. They used naphthalene and Wood's metal respectively for the solid wall material and steam with air content as the vapour/gas mixture. Their analytical model predicted heat transfer rates within a range of -7% to +18% of their experimental data. However, the experimental data

showed that the effect of the air on the heat transfer rates was much greater in the case of Wood's metal than in the case of naphthalene. They explained this from the fact that Wood's metal has a small thermal resistance and so the added resistance in the vapour/gas mixture due the presence of air presents a larger percentage, while the naphthalene has large thermal resistance and the extra resistance introduced by the air does not produce the same effect.

Bologa et al [45] performed experimental work to test the effect of an induced electrical field on the heat transfer in a vapour condensation into a liquid film in the presence of a non–condensable gas. They used combinations of R113 and hexane for vapours with air, carbon dioxide, and helium as non–condensable gases at volumetric concentration range of 0%—47%. They concluded that the deciding factor in the determination of heat transfer intensity is the ratio of the molecular mass of the gas to that of the vapour, the higher this ratio is, the greater the effect on the heat transfer.

Abdollahi [46] reported, after conducting an experimental work, a remarkable decrease in the heat transfer coefficient of a dropwise condensation of a vapour stream due to the presence of a small quantity of air.

Some experimental work on the effect of non–condensable gases on the overall performance of absorption systems has been found in the literature. Leibundgut et al [47] calculated the reduction of the overall heat ratio of NH_3/H_2O absorption heat pump with hydrogen and found that at 0.4 bar (40 kPa) of hydrogen partial pressure the reduction was more than half. It is also been reported by Young and Makiya [48] that

the heat carried by the hydrogen from the absorber to the evaporator will decrease the cooling capacity.

It is apparent from the literature that non–condesable gases will have a very significant effect on the heat and mass transfer processes in refrigeration components. However, the literature lacks good analytical studies on this effect. An effort in this area is therefore needed and will be presented in this study.

of of equations

3–Overall Solution for a LiBr/H_2O Absorption System :

3.1–Introduction :

In this chapter a computer simulation of a LiBr/H_2O water chiller is introduced. The model uses heat and mass effectivenesses to describe the performance of the various components of the system. The use of the absorber's heat effectiveness is unique to this simulation. It enables the characterization of the absorber's heat performance by a single parameter.

3.2–Basic Absorption Cycle :

Fig (3.1a) shows the basic non–volatile absorption system which is composed of five basic components: the condenser, the evaporator, the absorber, the heat–exchanger and the boiler. In addition there are two expansion valves and a solution pump. Fig (3.1b) is the absorbent's cycle on the temperature–concentration (T–C) diagram.

The refrigerant (water vapour) produced in the boiler enters the condenser at point [1], looses its latent heat to the cooling medium (usually water) and condenses. The condensate then passes through the expansion valve, mounted between points [2] and [3], to reduce its pressure to the evaporator's level. The low pressure liquid enters the evaporator at point [3] where it extracts the heat from the cooled medium and re-evaporates again. The vapour is attracted to the absorber at point [4] to be absorbed by the rich solution coming from the heat–exchanger hence forming the poor or weak solution. This process of water vapour absorption into a solution of LiBr/H_2O,

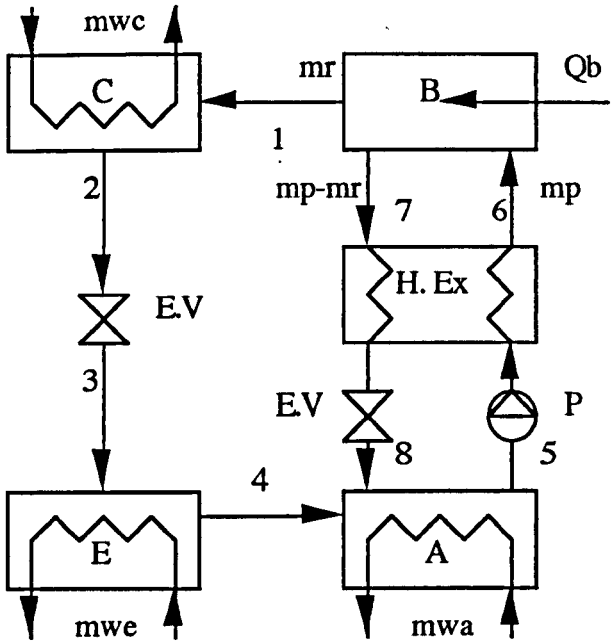

Fig (3.1a)

Schematic representation of the LiBr/H_2O system

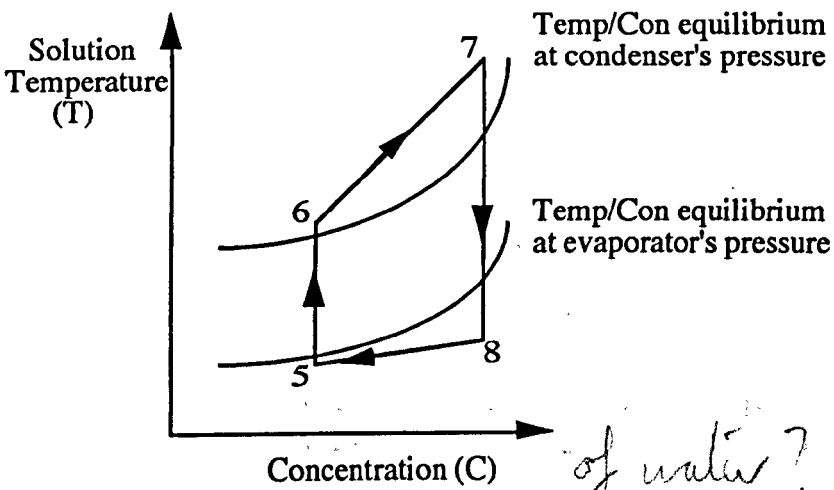

Fig (3.1b)

The absorbent cycle on the T–C diagram

represented by the process [8] to [5] on the T–C diagram of fig (3.1b), is an exothermic process during which heat is released, and for the process to continue this heat must be removed by means of a cooling medium. If the absorber is not cooled the absorbent will quickly approach equilibrium conditions at a much higher concentration than the case when cooled. This means smaller concentration variation and refrigerant mass flow rate which will result in a lower cooling capacity. This is represented on fig (3.2) where the concentration variation achieved by the adiabatic (no cooling) process is shown to be less than that achieved with cooling.

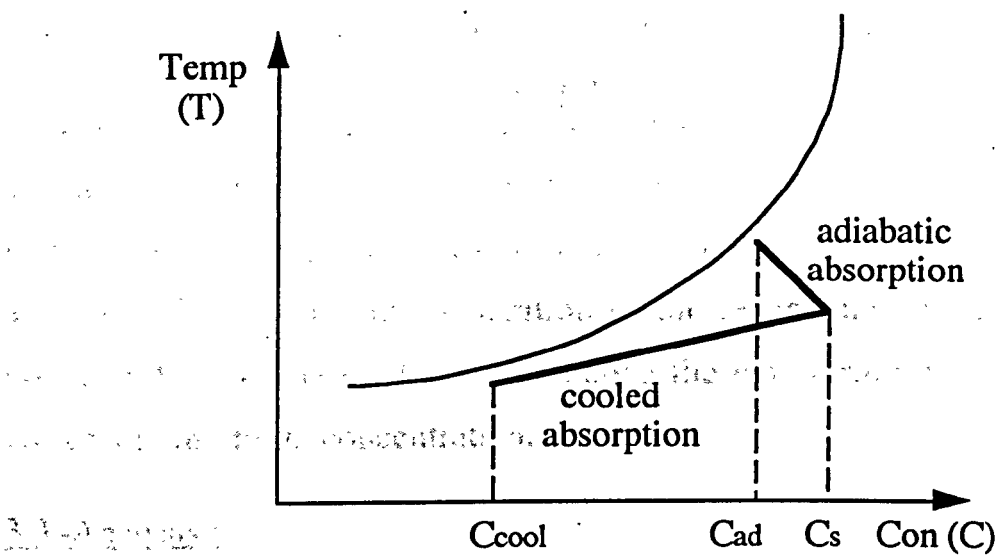

Fig (3.2)

Effect of cooling on concentration variation in the absorber

The solution, having absorbed the vapour refrigerant, is then pumped to the heat-exchanger to be preheated by the rich solution

coming from the boiler. This is represented by process [5] to [6] on the T–C diagram. It then enters the boiler where heat is added to boil off some of its water content that goes to the condenser and repeats the vapour cycle. The solution having given off water vapour becomes rich in LiBr, as represented by process [6] to [7]. It must be noted that the boiling process is less complicated than the absorption process in that the phase change and the heat addition occur at the same surface (the heating surface), whereas in the absorber the heat and mass transfer take place at two different surfaces. Returning to the cycle, the rich solution, having left the boiler, passes to the heat-exchanger, gets precooled by the weak solution and goes to the absorber through the expansion valve (process [7] to [8]) where it absorbs the water vapour coming from the evaporator and repeats the absorbent cycle.

The role of the heat–exchanger is important as it aids the absorption process in the absorber by cooling the rich solution below the equilibrium temperature corresponding to its concentration before entering the absorber. It also aids the generation of the refrigerant vapour in the boiler by heating the weak solution above the equilibrium temperature corresponding to its concentration.

3.3–Analysis :

The following analysis and the subsequent solution of the governing equations of the system enables the prediction of the system's performance given its input heat and pumping capacity, its components' effectivenesses (which include their sizes, heat transfer coefficients, and

mass transfer coefficients), and its external conditions i.e., the mass flow rates and temperatures of its cooling media.

3.3.1–Components Heat And Mass Balance :

3.3.1.1– Condenser :

A block diagram of the condenser is shown in fig (3.3) and the state points correspond to the diagram of the overall system shown in fig (3.1a).

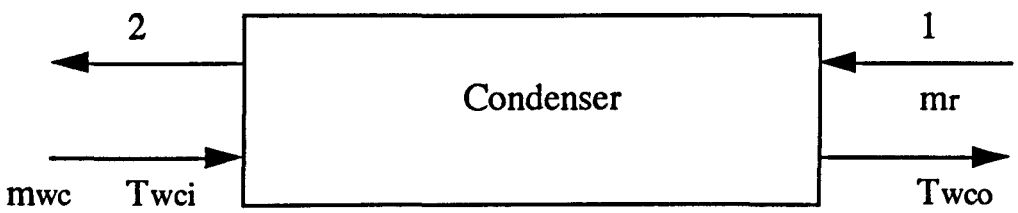

Fig (3.3)

The Condenser

The superheat, being only about 4% of the condensation heat, is neglected and the enthalpy balance on the refrigerant side gives

$$\dot{Q}_c = \dot{m}_r (h_1 - h_2) \qquad (3.1)$$

where the terms of this and all other equations are defined in the nomenclature at the end of the chapter. This is also the case in the rest of the chapters.

The enthalpy balance on the cooling water side gives

$$\dot{Q}_c = \dot{m}_{wc} C_{pw} (T_{wco} - T_{wci}) \qquad (3.2)$$

From the definition of the heat–exchanger's effectiveness [49] as seen in eqn (3.19a)

$$E_c = \frac{T_{wco} - T_{wci}}{T_c - T_{wci}}$$

So substituting in eqn (3.2) to obtain

$$\dot{Q}_c = \dot{m}_{wc} C_{pw} E_c (T_c - T_{wci}) \qquad (3.3)$$

Combining eqns (3.1) and (3.3) gives the equation that describes the condenser i.e.,

$$\dot{m}_r (h_1 - h_2) - \dot{m}_{wc} C_{pw} E_c (T_c - T_{wci}) = 0 \qquad (3.4)$$

3.3.1.2–Evaporator :

The evaporator, where the cooling duty is performed, is shown schematically in fig (3.4). The state points correspond to the diagram of fig (3.1a).

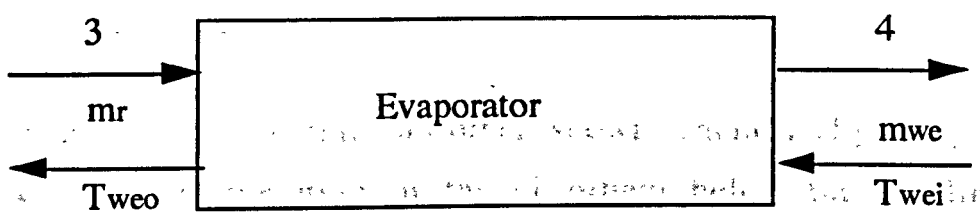

Fig (3.4)

The Evaporator

On the refrigerant side the enthalpy balance is

$$\dot{Q}_e = \dot{m}_r (h_4 - h_3) \qquad (3.5)$$

and on the heating water side

$$\dot{Q}_e = \dot{m}_{we} C_{pw} E_e (T_{wei} - T_e) \qquad (3.6)$$

where from the definition later developed in eqn (3.19b) it can be written that

$$E_e = \frac{T_{wei} - T_{weo}}{T_{wei} - T_e} \qquad (3.7)$$

For the throttling process across the expansion valve

$$h_3 = h_2 \qquad (3.8)$$

Combining eqns (3.5) and (3.6) and substituting eqn (3.8) gives the evaporator's equation

$$\dot{m}_r (h_4 - h_2) - \dot{m}_{we} C_{pw} E_e (T_{wei} - T_e) = 0 \qquad (3.9)$$

3.3.1.3–Absorber :

Heat is rejected from the absorber, shown schematically in fig (3.5), to keep the temperature of the absorbent below the equilibrium temperature corresponding to its concentration hence maintaining the absorption process.

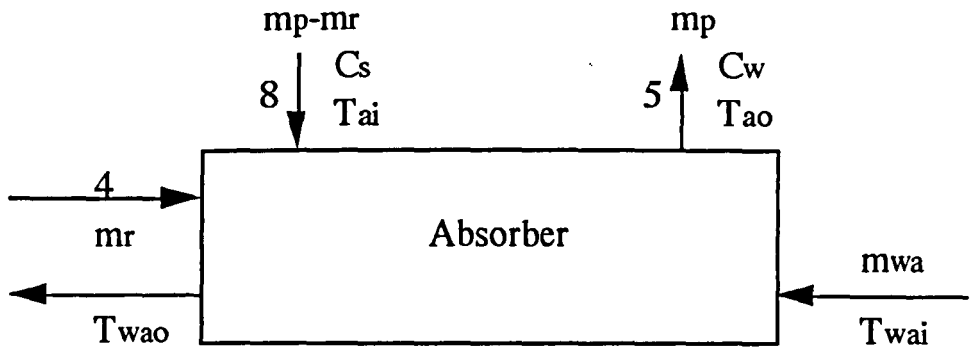

Fig (3.5)

The Absorber

Given infinite length, the absorber will yield concentration C_a which is the equilibrium concentration for the evaporator's pressure and the exit bulk temperature of the absorbent.

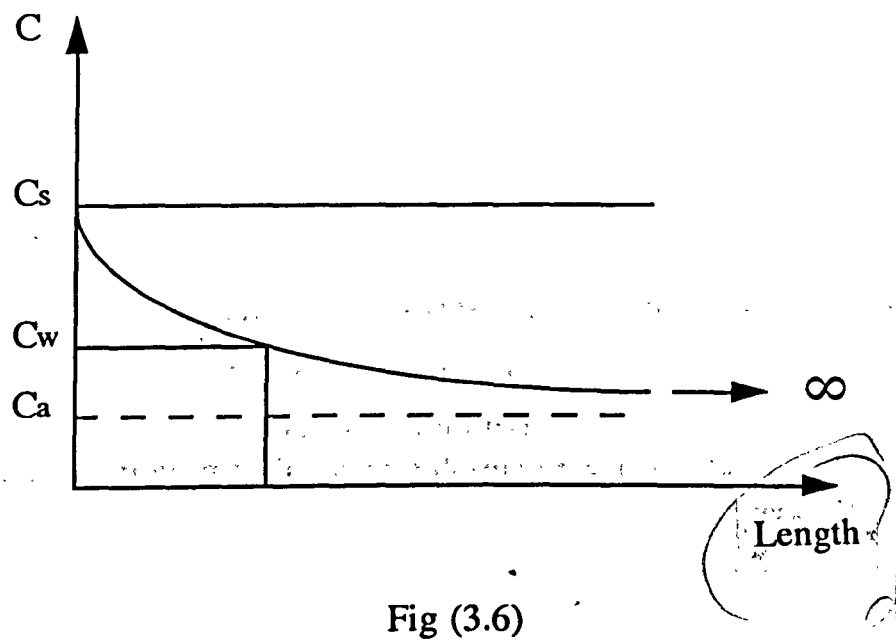

Fig (3.6)

Concentration variation with time length in the absorber

For a finite time, however, a measure of deviation from equilibrium is the "Mass Effectiveness" defined as :

$$E_{ma} = \frac{C_s - C_w}{C_s - C_a} \qquad (3.10)$$

It is noted that in chapter 4 an absorber's "Overall Effectiveness" is defined as the ratio of the actual amount of vapour absorbed to that absorbed by an ideal absorber. A method of calculating this "Overall Effectiveness", as well as the mass effectiveness (eqn (3.10)) and heat effectiveness (to be defined later) of the absorber is also presented in the same chapter and the data from it is used later in this chapter.

From eqn (3.10)

$$C_w = C_s - E_{ma} (C_s - C_a) \qquad (3.11)$$

From the conservation of mass :

$$\dot{m}_p = \dot{m}_s + \dot{m}_l$$

where $\dot{m}_p$, $\dot{m}_s$, and $\dot{m}_l$ are the mass flow rates of the weak solution, the LiBr salt, and the liquid water respectively.

The weak and strong mass ratios (concentrations) are defined respectively as :

$$C_w = \frac{\dot{m}_s}{\dot{m}_p} \qquad (3.12)$$

$$C_s = \frac{\dot{m}_s}{\dot{m}_p - \dot{m}_r} \qquad (3.13)$$

Substituting eqn (3.13) in eqn (3.12) to obtain

$$C_w = C_s \frac{\dot{m}_p - \dot{m}_r}{\dot{m}_p} \qquad (3.14)$$

Combining eqns (3.11) and (3.14) gives the mass balance of the absorber

$$C_s \dot{m}_r - \dot{m}_p E_{ma} (C_s - C_a) = 0 \qquad (3.15)$$

Now the overall heat balance for the absorber yields

$$\dot{m}_r h_4 + (\dot{m}_p - \dot{m}_r) h_{ai} - \dot{m}_p h_{ao} + \dot{m}_{wa} C_{pw} (T_{wai} - T_{wao}) = 0 \qquad (3.16)$$

At this stage, in order to proceed, it is necessary to define a heat effectiveness for the absorber similar to those applied to the condenser and evaporator.

The effectiveness of a heat–exchanger is related to the maximum possible heat transfer rate ($\dot{q}_{max}$) which could be achieved in a counterflow heat–exchanger of an infinite length. In such an exchanger the fluid with the minimum mass flow rate–specific heat product $(\dot{m}C_p)_{min}$ would experience the maximum possible temperature difference. In the case illustrated by fig (3.7), $(\dot{m}C_p)_{min} = (\dot{m}C_p)_h$ and therefore $\Delta T_h > \Delta T_c$

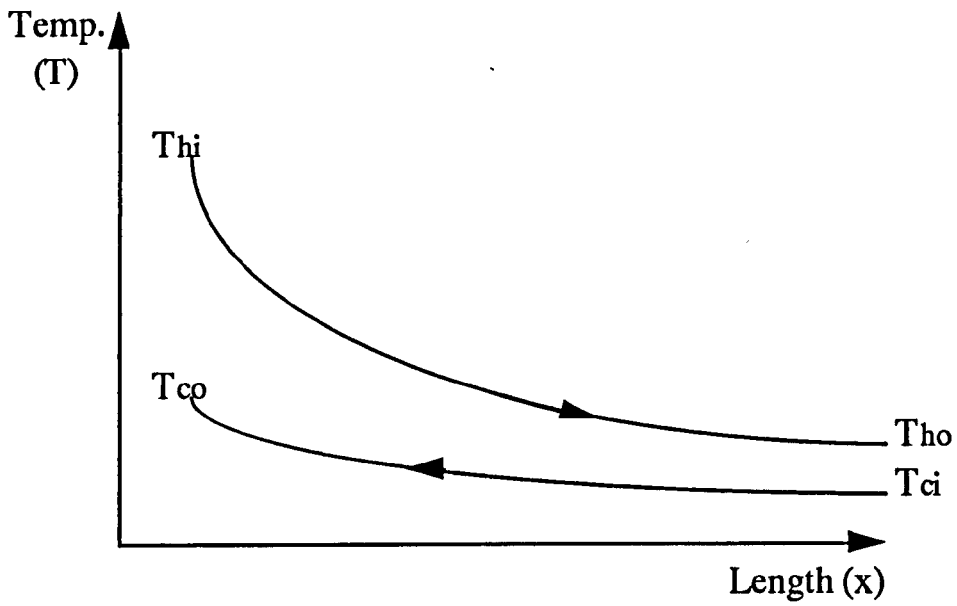

Fig (3.7)

Temperature profiles in a counter flow heat–exchanger

Consequently

$$\dot{q}_{max} = (\dot{m}C_p)_{min}\,(T_{hi} - T_{ci})$$

The heat effectiveness of the exchanger (E) is then the ratio of the actual heat transfer rate to the maximum possible rate i.e.,

$$E = \frac{(\dot{m}C_p)_h\,(T_{hi} - T_{ho})}{(\dot{m}C_p)_{min}\,(T_{hi} - T_{ci})} = \frac{(\dot{m}C_p)_c\,(T_{co} - T_{ci})}{(\dot{m}C_p)_{min}\,(T_{hi} - T_{ci})}$$

where the subscripts h and c denotes the hot and cool fluids respectively. And if $(\dot{m}C_p)_h = (\dot{m}C_p)_{min}$ as in fig (3.7) then

$$E = \frac{T_{hi} - T_{ho}}{T_{hi} - T_{ci}} \qquad (3.17a)$$

or if $(\dot{m}C_p)_c = (\dot{m}C_p)_{min}$, then

$$E = \frac{T_{co} - T_{ci}}{T_{hi} - T_{ci}} \qquad (3.17b)$$

It can be shown [49] that and expression for E in terms of the physical conditions of the heat–exchanger denoted by the number of transfer units (NTU) is :

$$E = \frac{1-\exp\{-NTU[1-((\dot{m}C_p)_{min}/(\dot{m}C_p)_{max})]\}}{1-((\dot{m}C_p)_{min}/(\dot{m}C_p)_{max})\exp\{-NTU[1-((\dot{m}C_p)_{min}/(\dot{m}C_p)_{max})]\}} \qquad (3.18a)$$

where

$$NTU = \frac{U\,A}{(\dot{m}C_p)_{min}}$$

In the case of a heat–exchanger with one fluid undergoing phase change as is the case of the condenser and evaporator, one temperature gradient is flat as shown in figs (3.8a) and (3.8b). In this case C_p of such fluid is effectively infinity and the ratio $((\dot{m}C_p)_{min}/(\dot{m}C_p)_{max})$ is equal to zero and the formula for effectiveness is then reduced to :

$$E = 1 - \exp(-NTU) \qquad (3.18b)$$

It is noted that equations (3.18a) and (3.18b) are valid only if the $\dot{m}C_p$'s are constant.

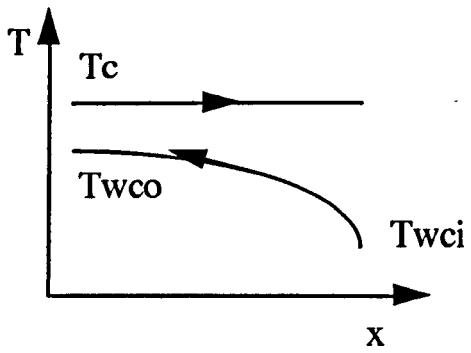

Fig (3.8a)
Temperature profiles in
the condenser

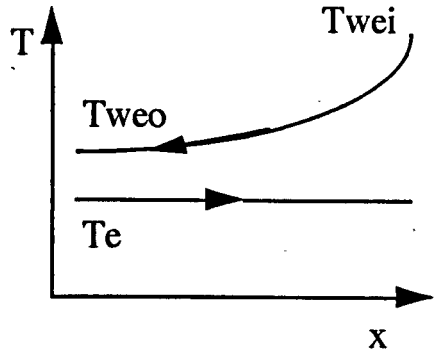

Fig (3.8b)
Temperature profiles in
the evaporator

$$\dot{q}_{max} = (\dot{m}C_p)_w (T_c - T_{wci})$$

$$E = \frac{T_{wco} - T_{wci}}{T_c - T_{wci}} \quad (3.19a)$$

$$\dot{q}_{max} = (\dot{m}C_p)_w (T_{wei} - T_e)$$

$$E = \frac{T_{wei} - T_{weo}}{T_{wei} - T_e} \quad (3.19b)$$

Now in the case of the absorber, because of the difference in nature between vapour absorption and pure condensation, the total heat transfer is a result of the combined effect of latent and sensible heat transfer. So the solution undergoes phase change and experiences temperature change at the same time. The absorber, therefore, lies between the two cases of heat–exchangers represented in figs (3.7), and (3.8a).

The heat effectiveness of the absorber is based on the coolant capacity $(\dot{m}C_p)_w$ and defined in terms of the absorbents inlet temperature and the coolant's inlet and outlet temperatures i.e.,

$$E_{ha} = \frac{T_{wao} - T_{wai}}{T_{ai} - T_{wai}} \quad (3.20)$$

✱ Note that the $\dot{m}C_p$ for the absorbent is not constant. Also note that the lines in figures (3.9a) and (3.9b) are not in reality straight lines, they are drown so for simplicity.

Unfortunately, it has not been possible to obtain an expression for E_{ha} in terms of the physical conditions as was possible in the case of heat–exchangers (eqn (3.18a)) or condensers/evaporators (eqn (3.18b)). The value of E_{ha} can only be obtained by numerical analysis. This is examined further in chapter 4.

From the definition of eqn (3.20) the heat effectiveness will have a maximum value of unity when $T_{wao}=T_{ai}$, i.e., when $\frac{(\dot{m}C_p)_{absorbent}}{(\dot{m}C_p)_{coolant}} > 1$ as shown in fig (3.9a). However, if the ratio $\frac{(\dot{m}C_p)_{absorbent}}{(\dot{m}C_p)_{coolant}}$ is less than unity the maximum heat effectiveness will be reached when $T_{wai} = T_{ao}$, and will have a value of less than unity. This case is shown in fig (3.9b) and it will be clear from the results of chapter 4 that this is the case for typical $LiBr/H_2O$ absorption systems.

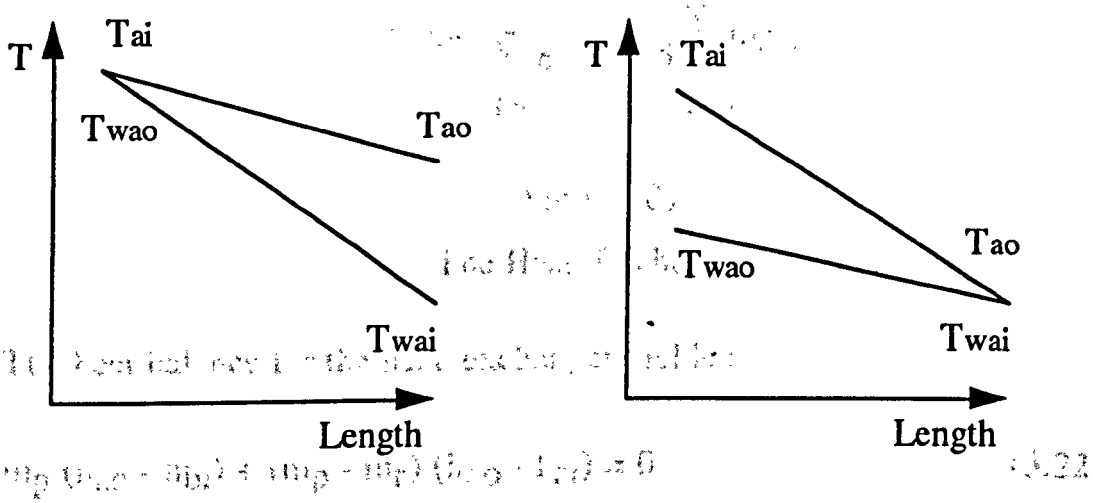

Fig (3.9a) The possible temperature profiles in the absorber $E_{max} = 1$

Fig (3.9b) $E_{max} < 1$

Returning to eqn (3.16) and introducing the heat effectiveness into it, the absorber's heat balance equation is obtained as :

$$\dot{m}_r\, h_4 + (\dot{m}_p - \dot{m}_r)\, h_{ai} - \dot{m}_p\, h_{ao} - \dot{m}_{wa}\, C_{pw}\, E_{ha}\, (T_{ai} - T_{wai}) = 0 \quad (3.21)$$

3.3.1.4–Heat–Exchanger :

A block diagram of the heat–exchanger is shown in fig (3.10). The purpose of the heat–exchanger is to aid the absorption and the boiling processes by cooling the strong solution down to a temperature where absorption can take place and heating the weak solution to a temperature where generation can occur.

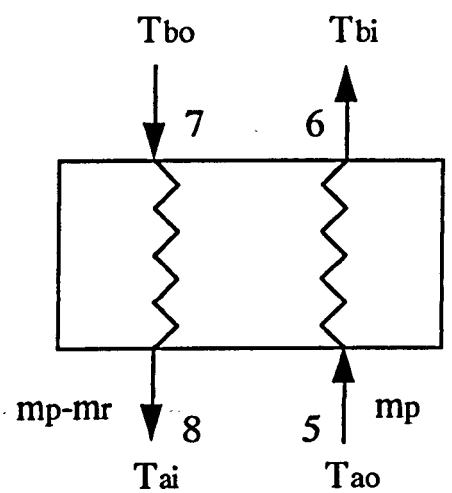

Fig (3.10)

The Heat–Exchanger

The heat balance for the heat–exchanger yields :

$$\dot{m}_p\, (h_{ao} - h_{bi}) + (\dot{m}_p - \dot{m}_r)\, (h_{bo} - h_{ai}) = 0 \quad (3.22)$$

The mass flow rate of the strong solution ($\dot{m}_p - \dot{m}_r$) is smaller than that of the weak solution ($\dot{m}_p$), and the specific heat of the strong solution C_{pss} is less than the specific heat of the weak solution C_{pws}, so

$(\dot{m}_p - \dot{m}_r)\, C_{pss} < \dot{m}_p\, C_{pws}$, and the temperature profiles in the heat–exchanger, therefore, will be as represented in fig (3.11).

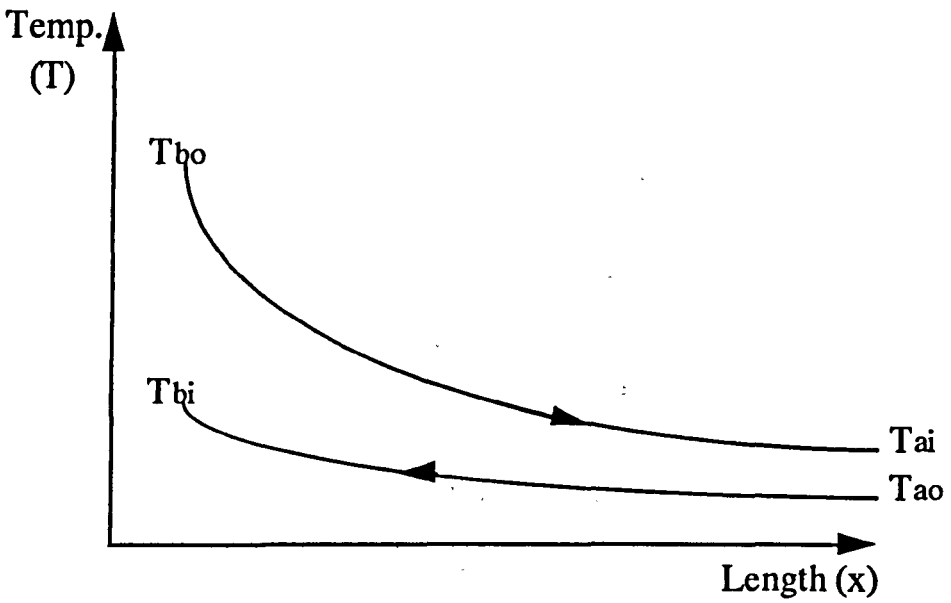

Fig (3.11)

Temperature profiles in the heat–exchanger

In terms of temperature, the heat–exchangers effectiveness is defined by

$$E_X = \frac{T_{bo} - T_{ai}}{T_{bo} - T_{ao}} \qquad (3.23)$$

Alternatively, E_X is also given by eqn (3.18a) as a function of the properties of the heat–exchanger, i.e., $E_X = f(NTU, \frac{(\dot{m}C_p)_{min}}{(\dot{m}C_p)_{max}})$.

From eqn (3.23) the heat–exchanger's equation is written as :

$$E_X (T_{bo} - T_{ao}) - (T_{bo} - T_{ai}) = 0 \quad (3.24)$$

3.3.1.5–Boiler :

Heat is added to the solution in the boiler, shown schematically in fig (3.12), to boil off some of its refrigerant's content.

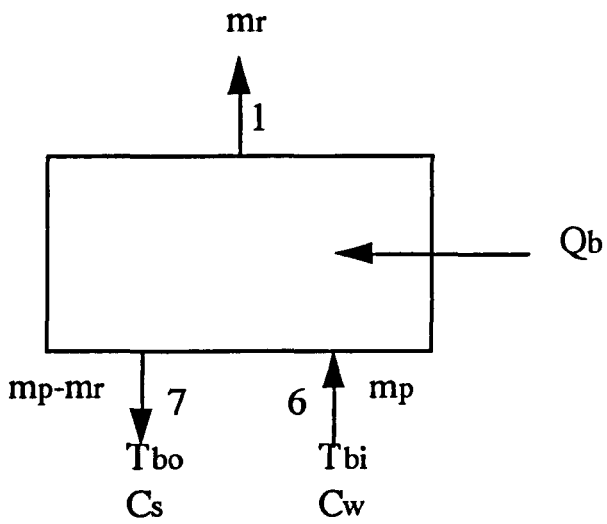

Fig (3.12)

The Boiler

The heat balance for the boiler is written as

$$\dot{Q}_b + \dot{m}_p h_{bi} - \dot{m}_r h_1 - (\dot{m}_p - \dot{m}_r) h_{bo} = 0 \quad (3.25)$$

A mass effectiveness for the boiler similar to that of the absorber is defined as :

$$E_{mb} = \frac{C_s - C_w}{C_b - C_w} \quad (3.26)$$

which, as in the case of the absorber, is a measure of deviation from the equilibrium concentration C_b. Where C_b is the equilibrium concentration of the boiler at the condenser's pressure and the exit bulk temperature of the liquid.

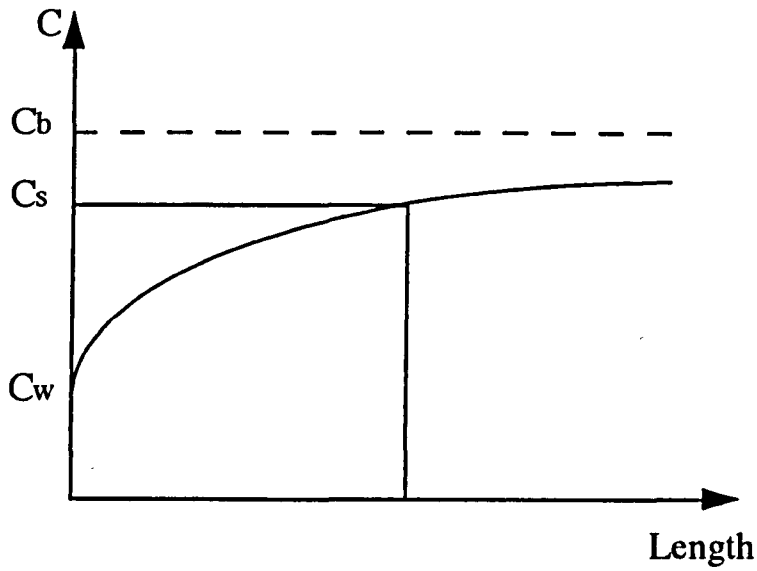

Fig (3.13)

Concentration profile in the boiler

From eqn (3.26)

$$C_s = E_{mb} (C_b - C_w) + C_w \qquad (3.27)$$

Manipulating eqns (3.11) and (3.27), two separate equations in C_w and C_s respectively are obtained

$$C_w(E_{ma}E_{mb} - E_{ma} - E_{mb})+(E_{mb}C_b + E_{ma}C_a - E_{ma}E_{mb}C_b)=0 \quad (3.28)$$

$$C_s(E_{ma}E_{mb} - E_{ma} - E_{mb})+(E_{mb}C_b + E_{ma}C_a - E_{ma}E_{mb}C_a) =0 \quad (3.29)$$

3.3.2–Solution :

Equations (3.4), (3.9), (3.15), (3.21), (3.22), (3.24), (3.25), (3.28), and (3.29) are the nine equations describing the absorption system and should be solved simultaneously to find the system's operational conditions i.e., $\dot{m}_r$, T_e, T_c, T_{ai}, T_{ao}, T_{bi}, T_{bo}, C_s, and C_w for given outside and design conditions i.e., the cooling media flow rates and

temperatures, the cooling load, the heating and pumping capacities of the system and the effectivenesses of its components.

The solution's specific enthalpy and equilibrium concentration can be obtained from the data [50]. However, it is more convenient, from the computational point of view, to find, and use, an accurate fit for this data. It can be shown [51], [52] that the specific enthalpy of the solution can be approximated to a good deal of accuracy by a double quadratic function of its temperature and concentration , i.e.,

$$Hs = A+BC+CC^2+DT+ET^2+FCT+GC^2T+HCT^2+I(CT)^2 \qquad (3.30)$$

The same approximation can be applied to the equilibrium concentration of the solution being a function of the solution and refrigerant temperatures [52], i.e.,

$$C=a+bT_d+cT_d^2+dT_r+eT_r^2+fT_dT_r+gT_d^2T_r+hT_dT_r^2+i(T_dT_r)^2 \qquad (3.31)$$

where $T_d = T_s - T_r$ and A—I and a—i are constants. The use of the reduced temperature T_d gives a more accurate correspondence than using the solution temperature T_s directly.

The data from [50] was used to calculate the enthalpy and concentration constants of eqns (3.30) and (3.31) respectively for $LiBr/H_2O$ and the values obtained are listed in tables (3.1) and (3.2) below.

Constant	Value
A	346.1483
B	-2125.558
C	1917.998
D	2.43394
E	4.832 E-3
F	1.295926
G	-3.8
H	-1.84 E-2
I	2 E-2

Table (3.1)

Enthalpy constants for $LiBr/H_2O$ solution

Constant	Value
a	39.0963
b	.5361985
c	-2.103 E-4
d	-.1335454
e	7.784 E-4
f	4.794 E-3
g	-7.475 E-5
h	-4.526 E-5
i	6.113 E-7

Table (3.2)

Concentration constants for $LiBr/H_2O$ solution

Some of the governing equations are nonlinear which means that an explicit solution is not possible and an iterative method is required. The Newton–Raphson iteration method was used for this purpose. It was coupled with Gauss elimination technique [53] to solve the above system of equations. This method needs solution seed values to start the iteration process and it is imperative that these seed values be chosen carefully because on this choice will depend whether or not the procedure converges into the solution and indeed the speed of this convergence. Fortunately in this case the functions are well behaved and the values of the seed solution are not very critical. They need,

* Pivoting (whether partial or total) is only possible if the pivot elements are nonzeros. Therefore the programme was equiped with a stop statement should this condition is encountered and a new set of seed values is used.

however, to be within the range of typical working conditions of the $LiBr/H_2O$ system.

The partial derivatives used by the iterative method were evaluated numerically using central difference method for more accuracy.

Partial pivoting was used in conjunction with Gauss elimination method to solve the 9 × 9 system of matrices. This saves time and memory as it needs approximately 50% less calculations than the full pivoting. A graphical representation of the procedure and a detailed illustration of the Newton–Raphson method are presented in the appendix.

3.4–Sample Input to Computer:

To illustrate how the method works, a $LiBr/H_2O$ system operating under the typical conditions listed below is considered.

*10 kw input heating power.

* 0.05 kg/s solution pump flow rate (weak solution).

* water having a flow rate of 0.2 kg/s is used to cool the condenser and to provide the cooling load for the evaporator.

* The heat transfer coefficient and the area will be given the typical values of of 1.5 kW/m^2 K and 1 m^2 respectively for the evaporator and condenser. The NTU for these components is calculated to be 1.6 which gives an effectiveness of 0.84. The effectiveness of the heat–exchanger is taken to be the same.

* Using the data produced at chapter 4 it is possible to determine both the heat and mass effectivenesses of the absorber. Taking the same values for the heat transfer coefficient and area as those of the other components and a cooling water mass flow rate of 1.2 kg/s an NTU of 0.3 is calculated. The heat and mass effectivenesses are then calculated as 0.118, and 0.29 respectively. The temperature of the cooling water to the components is taken to be 23 °C, and the mass effectiveness of the boiler is taken to be 0.5.

It is now possible to feed these values into the programme which will produce all the unknowns of the system and compute the capacities of the various components and the system's heat ratio. A copy of the programme output is shown in fig (3.14).

Table (3.3) shows the set of seed values used in the sample calculation introduced above together with the solution values they produced. Two facts are evident from the table ; (1) the seed values were chosen within the range of working conditions of a typical $LiBr/H_2O$ system, and (2) the model was able to converge to the solution despite the differences between the two sets. This shows that, in this case, the process of converging to a solution was not very sensitive to the values of the solution seeds.

```
Refrigerant Mass Flow          =   3.2839091E-03 Kg/S
Evaporator Temp                =    11.87110     C
Condenser Temp                 =    34.32632     C
Absorber Inlet Temp            =    39.66087     C
Absorber Outlet Temp           =    29.73921     C
Boiler Inlet Temp              =    76.46214     C
Boiler Outlet Temp             =    91.74956     C
Strong Mass Ratio              =   0.6177129     Kg/Kg
Weak Mass Ratio                =   0.5771425     Kg/Kg

Heat Ratio =  0.7815158

System Capacity   =   7.815158   KW
Condenser Capacity=   7.953791   KW
Absorber Capacity =   9.861366   KW
Boiler Capacity   =   10.00000   KW

Converged To Solution In          5 Iterations

      The Set Of Conditions For The Above Results Is :

Pump Flow Rate                          =   5.0000001E-02Kg/S
Evaporator Heating Water Flow Rate      =   0.2000000    Kg/S
Condenser  Cooling Water Flow Rate      =   0.2000000    Kg/S
Absorber   Cooling Water Flow Rate      =    1.200000    Kg/S
Evaporator Heating Water Temp.          =    23.00000    C
Condenser  Cooling Water Temp.          =    23.00000    C
Absorber   Cooling Water Temp.          =    23.00000    C
Evaporator Effectiveness                =   0.8400000
Condenser  Effectiveness                =   0.8400000
H.Exchange Effectiveness                =   0.8400000
Absorber Mass Effectiveness             =   0.2900000
Absorber Heat Effectiveness             =   0.1180000
Boiler Mass Effectiveness               =   0.5000000
```

Fig (3.14)

Computer printout of the sample calculation

Quantity	mr	Te	Tc	Tai	Tao	Tbi	Tbo	Cs	Cw
Seed Value	0.05	5	50	50	40	80	100	0.68	0.57
Solution	0.003	11.9	34.3	39.7	29.7	76.5	91.7	0.618	0.577

Table (3.3)

Seed values and solution of the sample calculation

For average working conditions of a $LiBr/H_2O$ water chiller, the code required approximately 4 to 6 iterations and took few seconds, on a main frame computer, to converge to a solution.

3.5–Results and Discussion :

The effects of different inputs on the system's heat ratio (Hr) are shown in figs (3.15) to (3.19) , where Hr is defined by :

$$Hr = \frac{\dot{Q}_e}{\dot{Q}_b}$$

In fig (3.15) Hr increases with the weak solution's mass flow rate (solution pump's flow rate) up to a maximum and drops steadily afterwards. This is explained by the fact that the increased flow rate corresponds to more water being evaporated in the boiler, hence increasing the refrigerant mass flow rate $\dot{m}_r$. The sensible heat required to warm up the solution to the boiling point is increased with the increased flow rate until a point is reached where this starts to reduce the heat available for evaporation, hence reducing $\dot{m}_r$ and

* This low value is attributed to the fact that the difference between the inlet and outlet temperature of the cooling water is smaller than the difference in the absorbent's inlet and outlet temperatures as detailed earlier. The need to keep the absorbent's inlet temperature relatively high, to combat crystalization, also lowers the heat effectiveness of the absorber.

causing Hr to drop. There is, therefore, an optimum flow rate at which the solution pump should be adjusted in order to maximize the system's performance. For the conditions of this exercise this optimum flow rate is approximately 0.007 kg/s.

Fig (3.16) shows the variation of Hr with the absorber's heat effectiveness. Hr rapidly increases with increasing E_{ha}, but shows less response as E_{ha} gets larger which is a typically expected behaviour since absorption diminishes as the equilibrium conditions are approached.

The effects of different component effectivenesses on Hr is shown in fig (3.17). The reason why the curves converge in and diverge out at the point where effectiveness equal to 0.7 is that this is the point chosen to be the design point, i.e., while one of the effectivenesses is been varied all the rest are kept at 0.7. The effect on Hr vary in importance between different effectivenesses, with E_x having the most effect (over the range shown in the figure) followed by E_{ma} then E_e then E_c then E_{mb}.

It is noted that the design point of E_{ha} is 0.3 as this is a more typical value for the heat effectiveness of the absorber.* It is also noted that while it is true that Hr is sensitive to E_x over the range of 0.5 to 1, it is even more sensitive to the variation in E_{ha} over its practical range of values, i.e., between 0.1 and 0.3. It is, therefore, more useful to invest in improving the heat effectiveness of the absorber than in any other component.

Fig (3.18) shows the effect of the cooling water mass flow rates to the condenser, absorber and that of the heating water to the evaporator on Hr. Again the effect vary between the three flow rates with the absorber's flow rate having the most effect followed by the evaporator then the condenser. Increasing the mass flow rates beyond the value of about 0.3 seems to have little effect on Hr, i.e., the water mass flow rates have a diminishing effect on Hr as that of E_{ha}.

The temperature of the cooling water to the absorber and condenser and of the heating water to the evaporator have linear effect on Hr as shown by fig (3.19). Hr is slightly more sensitive to the change in the water temperature of the evaporator than to that of the condenser and absorber. The effect on Hr of the water temperature of the latter two components is very close. Again the design point is 20 °C as can be seen from the figure.

3.6–Conclusion :

In this chapter a computer code to simulate a complete $LiBr/H_2O$ absorption refrigeration system is developed. The performance of the various components was characterized by their effectivenesses. The definition and use of the absorber's heat and mass effectivenesses is an important effort in facilitating the design of absorbers. To complement this work, a method of calculating the heat and mass effectivenesses of the absorber is developed in chapter 4. As was anticipated in the review, there was no need for the temperature constraints used in [4] as the chosen seed values were within the range of physical conditions of the typical $LiBr/H_2O$ water chiller.

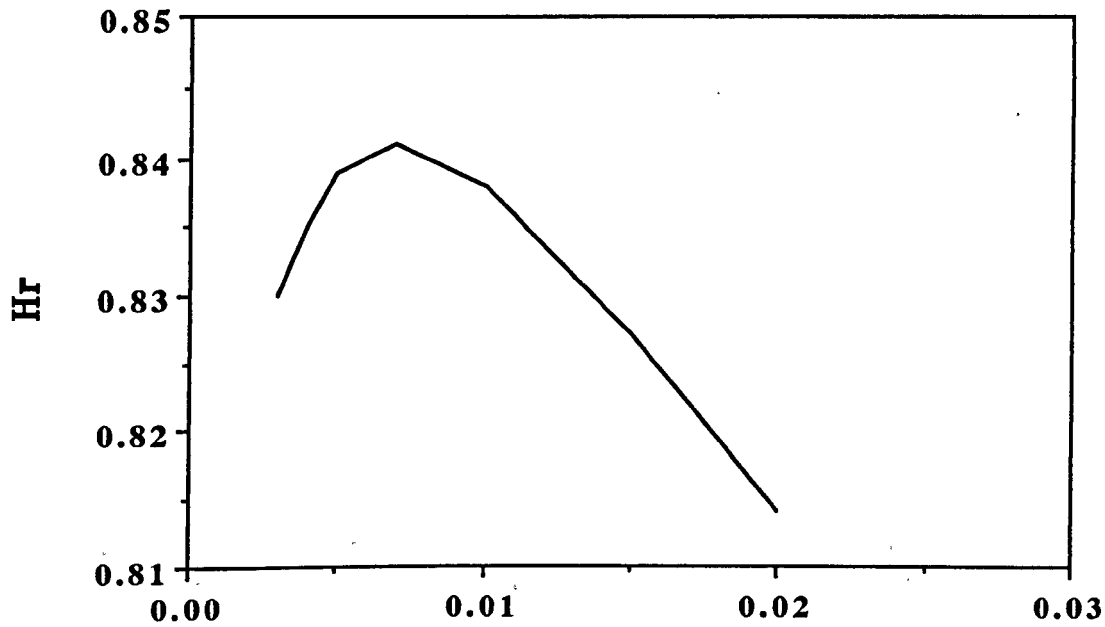

Variation of Hr with the pump flow rate

Fig (3.15)

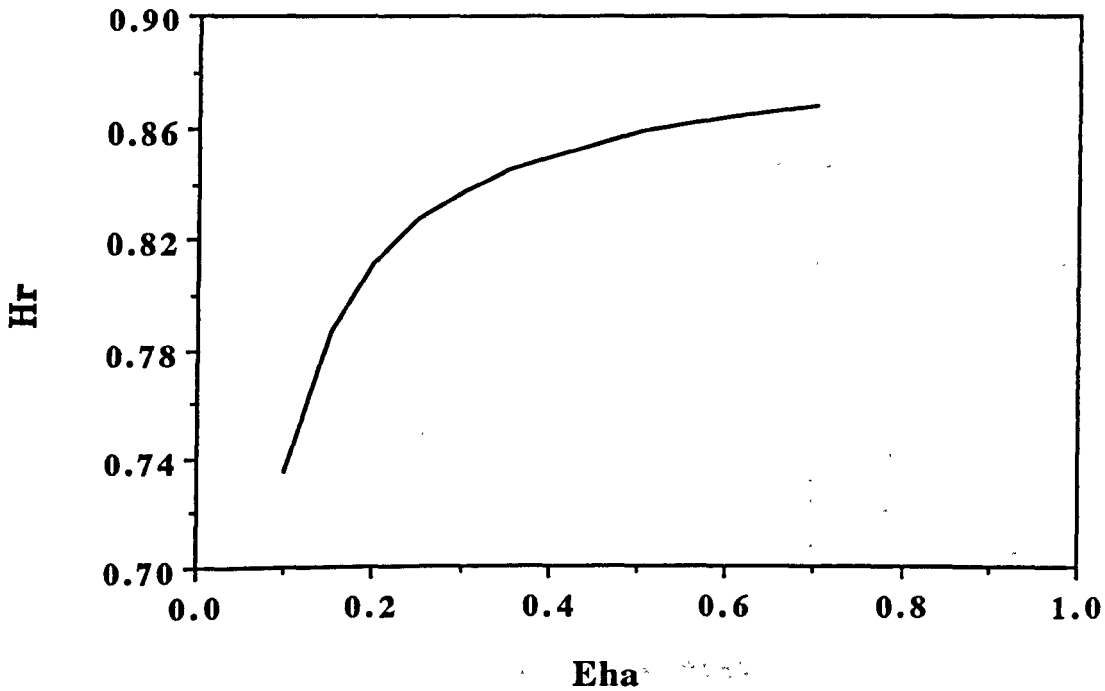

Variation of Hr with the absorber's heat effectiveness

Fig (3.16)

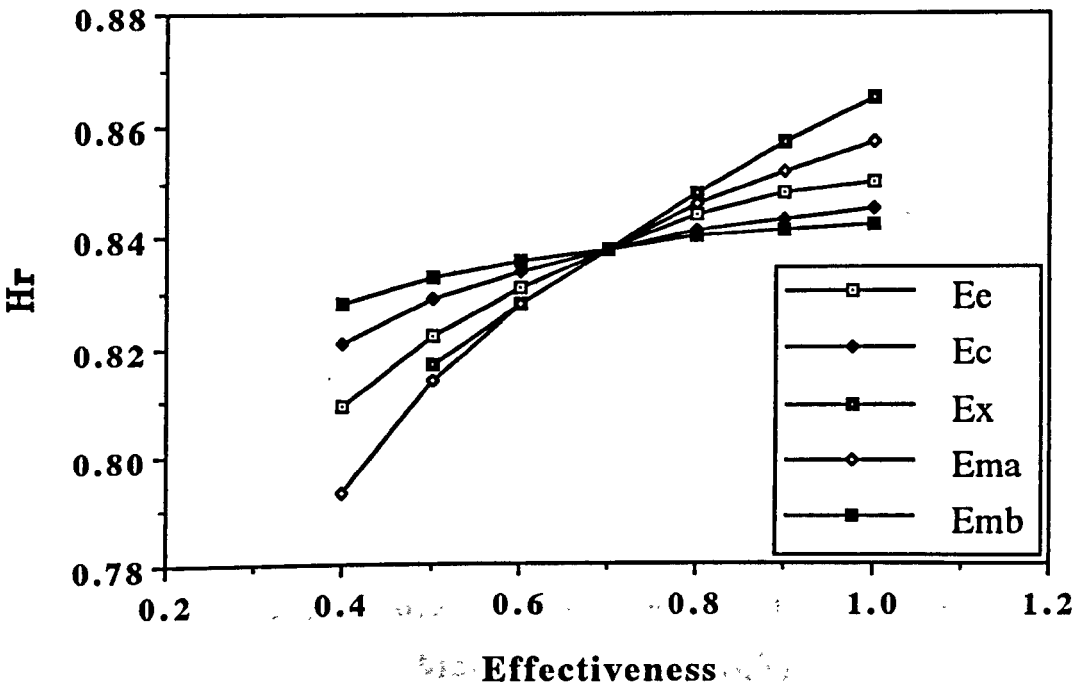

Variation of Hr with different component's effectivenesses

Fig (3.17)

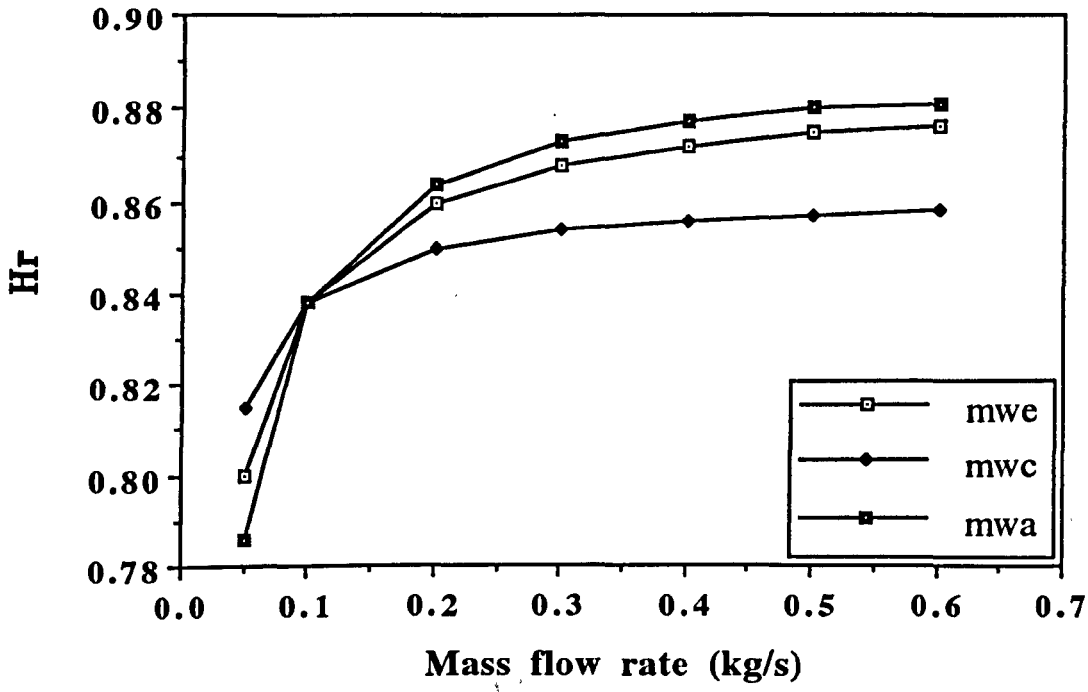

Variation of Hr with different water mass flow rates

Fig (3.18)

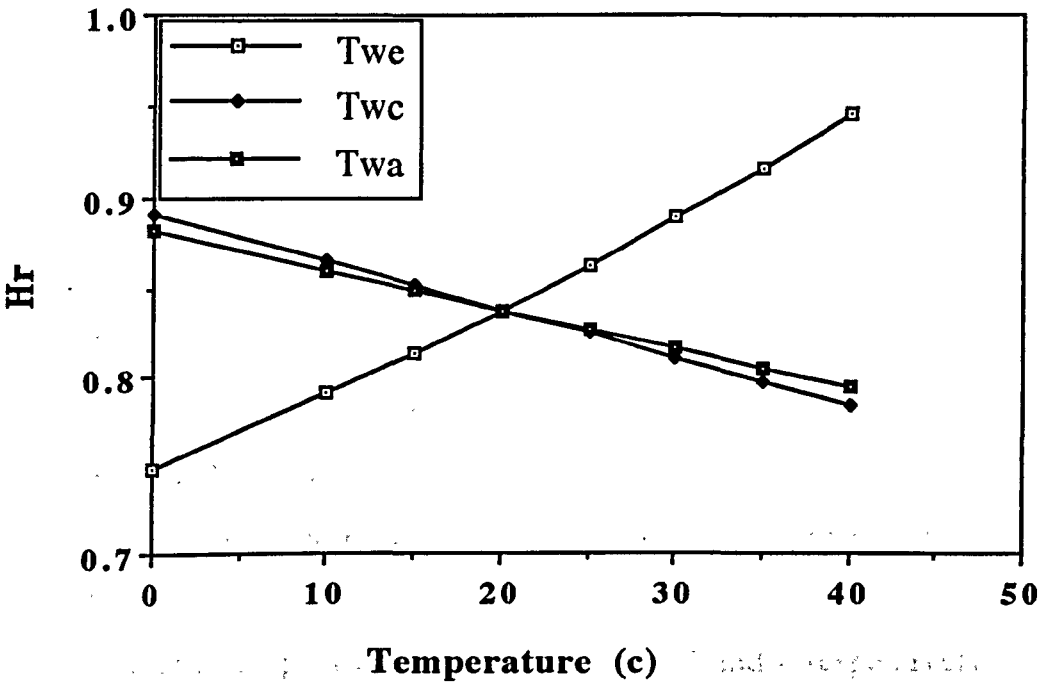

Variation of Hr with inlet water temperatures

Fig (3.19)

Nomenclature :

A	area (m^2).
C_a	absorber's equilibrium concentration.
C_b	boiler's equilibrium concentration.
C_p	heat capacity (kJ/kg °C).
C_s	strong concentration.
C_w	weak concentration.
E	effectiveness.
E_c	condenser's effectiveness.
E_e	evaporator's effectiveness.
E_{ha}	absorber's heat effectiveness.
E_{ma}	absorber's mass effectiveness.
E_{mb}	boiler's mass effectiveness.
h_1, h_2	refrigerant's specific enthalpies at point 1 and 2 respectively (kJ/kg).
h_3, h_4	refrigerant's specific enthalpies at point 3 and 4 respectively (kJ/kg).
h_{ai}	enthalpy of the absorbent at absorber inlet (kJ/kg).
h_{ao}	enthalpy of the absorbent at absorber outlet (kJ/kg).
h_{bi}	enthalpy of the absorbent inlet to the boiler (kJ/kg).
h_{bo}	enthalpy of the absorbent outlet of the boiler (kJ/kg).
Hr	system's heat ratio.
$\dot{m}_l$	mass flow rate of the liquid water in the absorbent (kg/s).
$\dot{m}_p$	absorbent pump flow rate (kg/s).
$\dot{m}_r$	refrigerant's mass flow rate (kg/s).

$\dot{m}_s$	mass flow rate of the LiBr salt (kg/s).
$\dot{m}_{wc}$	mass flow rate of cooling water to condenser (kg/s).
$\dot{m}_{we}$	mass flow rate of water to evaporator (kg/s).
NTU	number of transfer units.
$\dot{Q}_b$	boiler's capacity (kW).
$\dot{Q}_c$	condenser's capacity (kW).
$\dot{Q}_e$	evaporator's capacity (kW).
T_{ai},T_{ao}	absorbent's inlet and outlet temperatures to the absorber (°C).
T_{bi},T_{bo}	absorbent's inlet and outlet temperatures to the boiler (°C).
T_c	condenser's temperature (°C).
T_{ci}	temperature of the cold fluid inlet (°C).
T_{co}	temperature of the cold fluid outlet (°C).
T_e	evaporator's temperature (°C).
T_{hi}	temperature of the hot fluid inlet (°C).
T_{ho}	temperature of the hot fluid outlet (°C).
Twai	temperature of the cooling water inlet to the absorber (°C).
Twao	temperature of the cooling water outlet from the absorber (°C).
Twci	temperature of cooling water inlet to the condenser (°C).
Twco	temperature of cooling water outlet from the condenser (°C).
Twei	temperature of the heating water inlet to the evaporator (°C).
Tweo	temperature of heating water outlet from the evaporator (°C).
U	heat transfer coefficient (kW/m^2 °C).
x	length (m).

4–Simplified Method for the Analysis of Falling Film Absorbers :

4.1–Introduction :

It is seen from the analysis of chapter 3 that the absorber is the single most important device of the absorption refrigeration system. It is complicated in that it must have a free surface of the absorbent in contact with the refrigerant vapour and another surface for cooling the absorbent. The purpose of this chapter is to develop a simplified method of estimating the performance of the film absorbers which, as pointed out earlier, achieve high performance due to the thin film flow of the absorbent. The data used here is of a smooth laminar falling film $LiBr/H_2O$ type absorber. The method, however, is not limited to such condition and can be equally applied to other refrigeration pairs as well as other flow types.

It can be shown [54] that for a smooth and laminar flow of a liquid film down an absorber plate the concentration and temperature are respectively governed by the equations :

$$V_X \frac{\partial C}{\partial X} = D \frac{\partial^2 C}{\partial Y^2} \qquad (4.1)$$

$$V_X \frac{\partial T}{\partial X} = \alpha \frac{\partial^2 T}{\partial Y^2} \qquad (4.2)$$

These equations have been solved using a hybrid technique [26] which consisted of an analytical solution at the entry region and a finite difference method thereafter. However, this requires extensive

* It was found that while the hybrid method needed about 15 minutes on the main frame the simplified method proposed here will take about 3 minutes, i.e., a reduction of $\frac{1}{5}$ in time.

computing time. This chapter provides an alternative simplified method which is much less demanding in terms of computational time and memory hence is more suitable for use on personal computers. However, the method will need a prior data on heat and mass transfer coefficients and is not, therefore, a direct replacement of the hybrid method.

4.2–Analysis :

The essential simplification in this method is that the concentration and temperature of the absorbent bulk at any point, x, along the absorber's length are represented by a single value each and that another pair of values represent the concentration and temperature at the liquid/vapour interface.

The governing equations are produced by performing energy and mass balance for an element along the absorber's length.

4.2.1–Enthalpy Balance for the Absorbent :

Considering fig (4.1), the enthalpy balance for an element dx of the absorbent can be written as :

$$d\dot{H} = (\dot{m}_v h_{fg} - q_w - q_i)\, w\, dx$$

or

$$\frac{d\dot{H}}{dx} = (\dot{m}_v h_{fg} - q_w - q_i)\, w \qquad (4.3)$$

where $\dot{H} = \dot{m}_a h_a$

and w is the absorber's width.

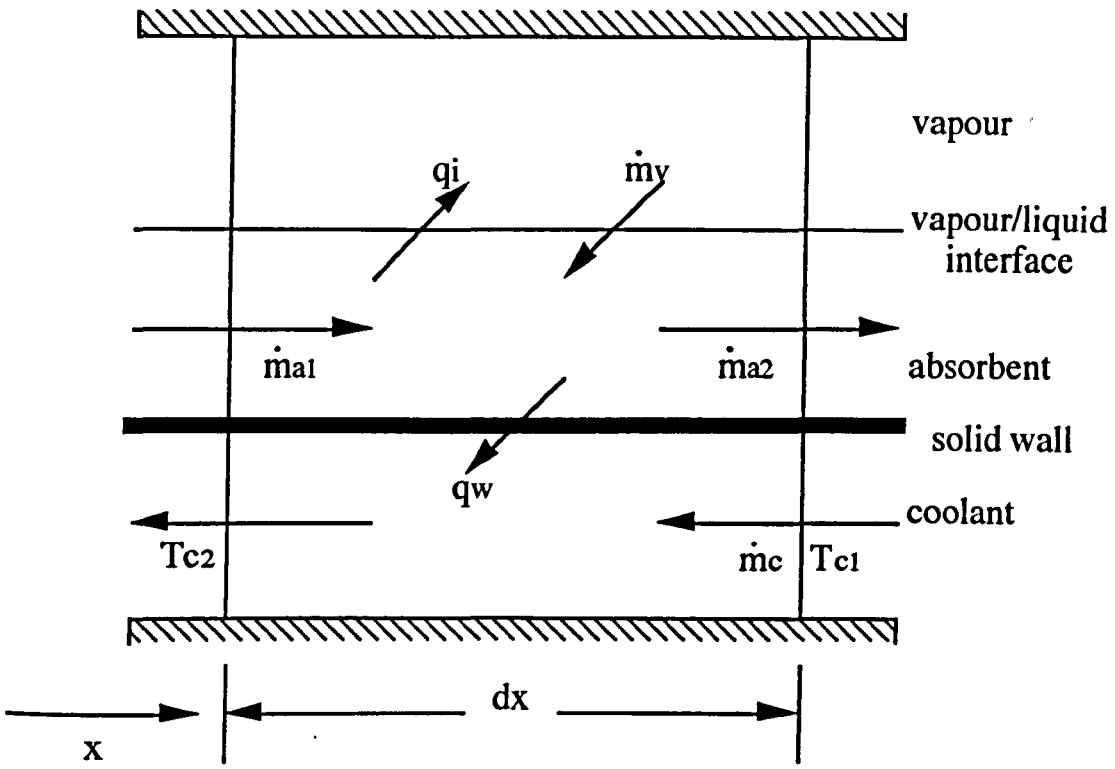

Fig (4.1)

The absorber's element

4.2.2–Mass Balance :

From fig (4.1) the mass balance for the absorbent is written as :

$$\dot{dm}_a = \dot{m}_v \, dx \, w$$

or

$$\frac{d\dot{m}_a}{dx} = \dot{m}_v \, w \qquad (4.4)$$

4.2.3–Enthalpy Balance for the Coolant :

As shown in fig (4.1) the coolant is assumed to be flowing in a counter flow to the absorbent and the enthalpy balance for it can be written as :

$$(\dot{m} \, C_p)_c \, dT_c = q_w \, w \, dx$$

or

$$\frac{dT_c}{dx} = \frac{q_w \, w}{(\dot{m} \, C_p)_c} \qquad (4.5)$$

4.2.4–Transfer Rates :

The mass and heat fluxes are written as :

$$\dot{m}_v = \rho \, G_{li} \, (C_a - C_i) \qquad (4.6)$$

$$q_w = U_w \, (T_a - T_c) \qquad (4.7)$$

$$q_i = U_i (T_i - T_v) \qquad (4.8)$$

where the absorbent's concentration C_a is defined as the mass ratio of the LiBr salt to the liquid absorbent i.e.,

$$C_a = \frac{\dot{m}_s}{\dot{m}_a}$$

- It was found that the heat and mass transfer coefficient obtained from the hybrid method do not vary much with the operating conditions and can be used in the simplified method for varying conditions.

G_{li} is the mass transfer coefficient from the bulk of the liquid to the interface. U_W is the heat transfer coefficient from the bulk of the liquid to the coolant which combines the heat transfer coefficients across the bulk of the liquid (U_a), across the solid wall (U_S), and through the coolant (U_C). U_i is the heat transfer coefficient from the interface to the vapour. These coefficients can be obtained either from experimental data or from analytical results e.g the hybrid method [26] where these coefficients are produced as a part of the analysis. The heat transfer coefficient from the wall to the coolant (U_C) can be obtained, for example, from the Dittus–Boetler equation [49].

4.2.5–Solution :

Equations (4.3), (4.4), and (4.5) can be put into a more convenient non–dimensional form by using the non–dimensional length X and the capacity ratio Cr defined as:

$$X = \frac{x\ U_a\ w}{(\dot{m}\ C_p)_a\ Nu}$$

which is the formula used in [26] and [59],without proof, but had to be used here to be able to compare the two methods at the same points, and X = 0.294 x.

where Nu is the Nusselt Number, based on the heat transfer coefficient across the absorbent, U_a, and

$$Cr = \frac{(\dot{m}\ C_p)_c}{(\dot{m}\ C_p)_a}.$$

Cr is based on the inlet $(\dot{m}\ C_p)_a$

A typical absorber would have a dimensionless length, X, of about 10 and a capacity ratio, Cr, between 40 and 60. The equations then become

$$\frac{d\dot{H}}{dX} = \frac{(\dot{m}\ C_p)_c\ Nu}{Cr\ U_a}\ (\dot{m}_V\ h_{fg} - q_w - q_i) \qquad (4.9)$$

✳ The origins of this equation is found from the replot of the Duhring plot for $LiBr/H_2O$ presented in [26]. The replot represents the Duhring data in axes of solution temperature and solution concentration with the vapour pressure as parameter. This is similar to figures (3.1b) and (3.2) of this work. The actual $LiBr/H_2O$ data shows the vapour pressure lines to be almost straight over a wide range of values which covers the practical working conditions of $LiBr/H_2O$ systems. This suggests an approximately linear dependency of temperature and concentration at equilibrium conditions. This approximation which was adopted by [56], [57], and [26] can be written in the form.

$$T_i = a\,C_i + b \qquad \text{(i)}$$

In order to obtain eqn (4.13), the constants a and b must first be found. This can be done by writing eqn (i) for the initial conditions, i.e.,

$$T_e = a\,C_{in} + b \qquad \text{(ii)}$$

$$T_{in} = a\,C_e + b \qquad \text{(iii)}$$

where T_e is the equilibrium temperature at the initial concentration C_{in} and C_e is the equilibrium concentration at the initial temperature T_{in}. Solving eqns (ii) and (iii) gives:

$$a = -\frac{T_{in} - T_e}{C_{in} - C_e} \quad \text{and} \quad b = \frac{C_{in}\,T_{in} - C_e\,T_e}{C_{in} - C_e}$$

Substituting in eqn (i) and using the definitions (4.14) and (4.15) gives:

$$T_{di}(T_e - T_{in}) + T_{in} = -\frac{T_{in} - T_e}{C_{in} - C_e}(C_{di}(C_e - C_{in}) + C_{in}) + \frac{C_{in}T_{in} - C_eT_e}{C_{in} - C_e} \qquad \text{(iv)}$$

$$\frac{dm_a}{dX} = \frac{(\dot{m}\ C_p)_c\ Nu}{Cr\ Ua}\ m_v \qquad (4.10)$$

$$\frac{dT_c}{dX} = \frac{Nu}{Cr\ Ua}\ q_w \qquad (4.11)$$

Equations (4.9), (4.10), and (4.11) are a set of ordinary differential equations that can be solved numerically by a standard technique. In this case the four point Runge–Kutta method [55] was used for this purpose.

To obtain the rate of absorption from equation (4.6) requires the calculation of the equilibrium interface states from the known bulk states. This is done iteratively by solving the non–linear implicit equation for enthalpy balance at the interface which is :

$$\rho\ h_{fg}\ G_{li}\ (C_a - C_i) + U_a\ (T_i - T_a) = 0 \qquad (4.12)$$

in conjunction with the linear equilibrium state equation of the interface:

$$C_{di} + T_{di} = 1 \qquad (4.13)$$

where, C_{di} and T_{di} are the interface dimensionless concentration and temperature defined respectively by :

$$C_{di} = \frac{C_i - C_{in}}{C_e - C_{in}}, \text{ and} \qquad (4.14)$$

$$T_{di} = \frac{T_i - T_{in}}{T_e - T_{in}} \qquad (4.15)$$

which are the standard forms of dimensionless concentration and temperature respectively as defined for the interface conditions. These forms are used in [23] and [26] as well as in chapter 5 of this work.

The subscripts i, e, and in designate the interface, equilibrium, and initial conditions respectively. The equilibrium concentration and temperature C_e, T_e are in turn obtained respectively from the double quadratic fit of the concentration seen in the previous chapter, i.e., eqn (3.31).

4.3–Comparison with the Hybrid Finite Difference Method :

In order to assess the accuracy of the simplified method it was compared to the hybrid method [26] and for this reason it was necessary to restrict the solution with the same assumptions as the finite difference method. These are :

(a) the specific enthalpy of the absorbent is a linear function of temperature only,

(b) the vapour absorption rate is negligible compared to the absorbent flow rate, i.e., m_a is constant, and

(c) the heat transfer across the vapour/liquid interface is negligible, i.e., $q_i = 0$.

When these assumptions are introduced the only change is that to eqn (4.9) which becomes :

$$\frac{dTa}{dX} = \frac{Nu}{Ua}(m_V h_{fg} - q_w) \qquad (4.16)$$

The comparison between the two methods was conducted as follows : A set of dimensionless bulk concentrations and temperatures along the absorber's length were produced using the hybrid method which at the

same time produced the corresponding heat and mass transfer coefficients. These coefficients together with the conditions that produced them were used to obtain several sets of results from the simplified method for reducing values of the step size dX until a solution independent of the step size was finally obtained. These results were then compared with the original results obtained using the hybrid method. Unfortunately when compared they were found to be different. It was first thought that the method of Runge–Kutta was the source of error so it was replaced by the Predictor–Corrector method [55]. However, the results from the latter method completely agreed with those of the Runge–Kutta. Despite much thought no obvious reason for the discrepancy was found. One possible explanation, however, could be the approximation of the bulk conditions at any location x by a single pair of concentration and temperature while in the finite difference method that bulk was divided into a mesh with large number of elements with corresponding values of concentration and temperature for each element. Typical results are shown in table (4.1) where the concentration and temperature of a $LiBr/H_2O$ absorbent from all three methods are compared. For convenience the concentration and temperature are presented in dimensionless forms defined by :

$$C = \frac{C_a - C_{in}}{C_e - C_{in}}, \quad T = \frac{T_a - T_{in}}{T_e - T_{in}}$$

✳ It must be emphasized however that since the error increases with X, therefore, for typical absorbers (with X≤10 and NTU≤0.1) the error is small and the method can be applied without any correction. This is shown on the figures below where the overall effectiveness of the absorber is plotted for both corrected and uncorrected cases for X of up to10 and NTU values of up to 0.1. Both curves are plotted for Cr=200

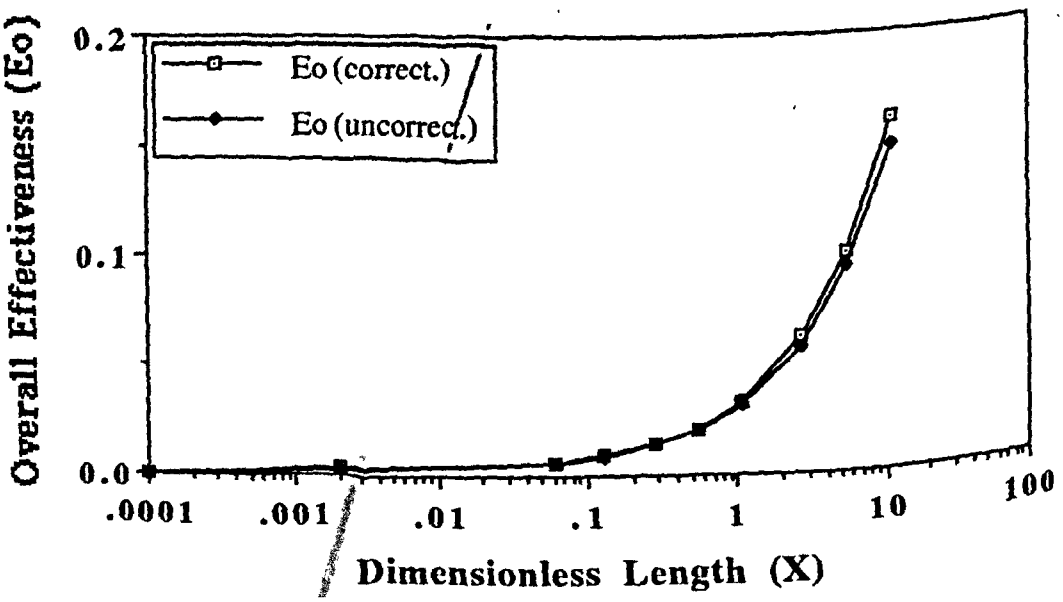

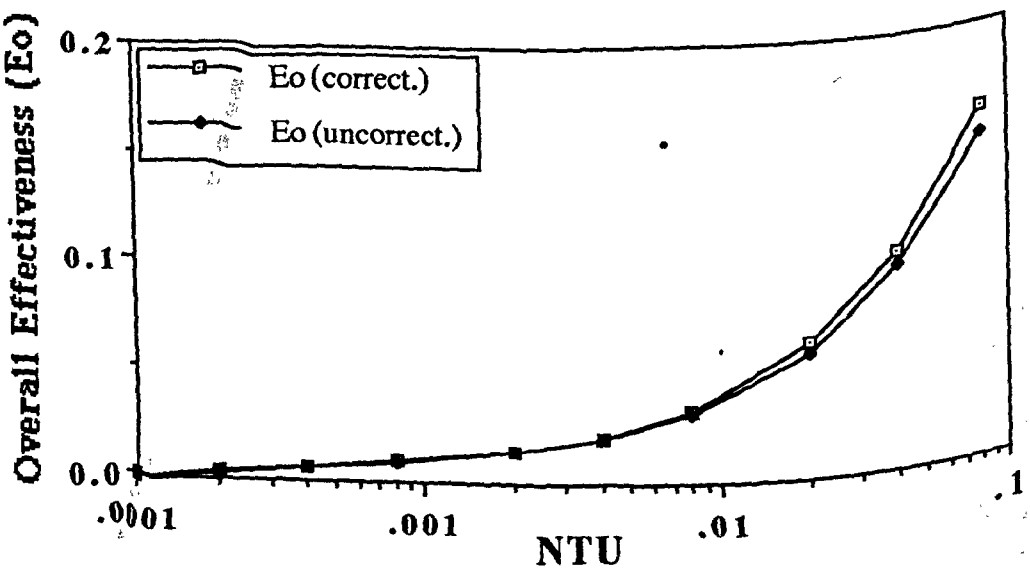

dimenless length (X)	Dimensionless Concentration (C)			Dimensionless Temperature (T)		
	hybrid method	Runge Kutta	predict. correct.	hybrid method	Runge Kutta	predict. correct.
1	.049	.048	.016	.077	.022	.076
10	.274	.240	.234	-.168	-.177	-.170
20	.477	.375	.368	-.230	-.216	-.210
40	.791	.576	.570	-.294	-.253	-.250
60	1.0	.728	.723	-.334	-.278	-.277
80	1.138	.847	.843	-.360	-.299	-.298
100	1.230	.942	.939	-.377	-.314	-.314
200	1.388	1.210	1.210	-.408	-.358	-.361
400	1.413	1.354	1.358	-.413	-.382	-.388

Table (4.1)

Comparison between the results of the three methods at Cr = 200

The persistence of the difference between the solutions was unfortunate but because it appeared to be consistent it was felt that the problem could be circumvented by including a correction factor in the Runge–Kutta method. It was found, by comparative analysis of the results, that a correction factor for the heat and mass transfer coefficients that is a linear function of the absorber's length produced good agreement between the different solutions. This has the form :

$$cf = 1 + .03\,X \qquad (4.17)$$

*

The agreement was found to improve sightly with the capacity ratio. This is illustrated in figures (4.2) and (4.3) where the values of concentration and temperature obtained using both the corrected and uncorrected Runge–Kutta method are compared to those obtained by the finite difference method at Cr = 40 and 200 respectively. Although it is evident that the agreement is better at Cr = 200, the disagreement at Cr = 40 is not very large and considering the large difference between 200 and 40 it is concluded that the correction is largely independent of the capacity ratio and will be used in the rest of this analysis.

Equations (4.6) and (4.7) consequently become :

$$\dot{m}_v = cf\ \rho\ Gli\ (C_a - C_i) \qquad (4.18)$$

$$q_w = cf\ U_w\ (T_a - T_c) \qquad (4.19)$$

and the set of equations that describe the system is :

$$\frac{dT_a}{dX} = \frac{Nu}{Ua}(\dot{m}_v\ h_{fg} - q_w) \qquad (4.20)$$

$$\frac{d\dot{m}_a}{dX} = \frac{(\dot{m}\ C_p)_c\ Nu}{Cr\ Ua}\ \dot{m}_v \qquad (4.21)$$

$$\frac{dT_c}{dX} = \frac{Nu}{Cr\ Ua}\ q_w \qquad (4.22)$$

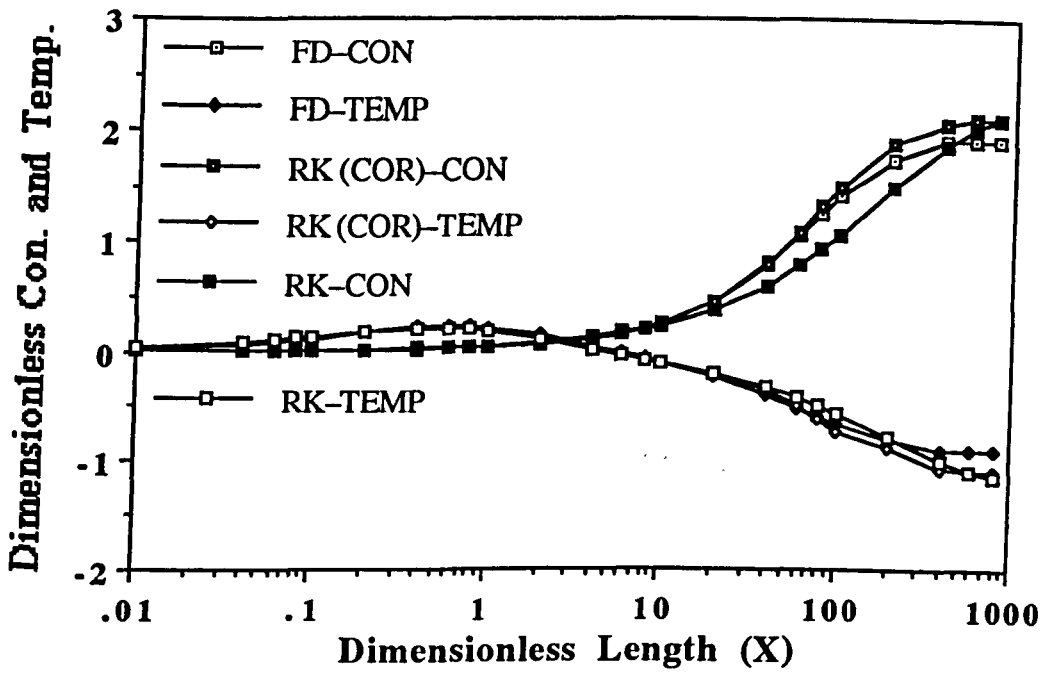

Effect of correction at Cr = 40

Fig (4.2)

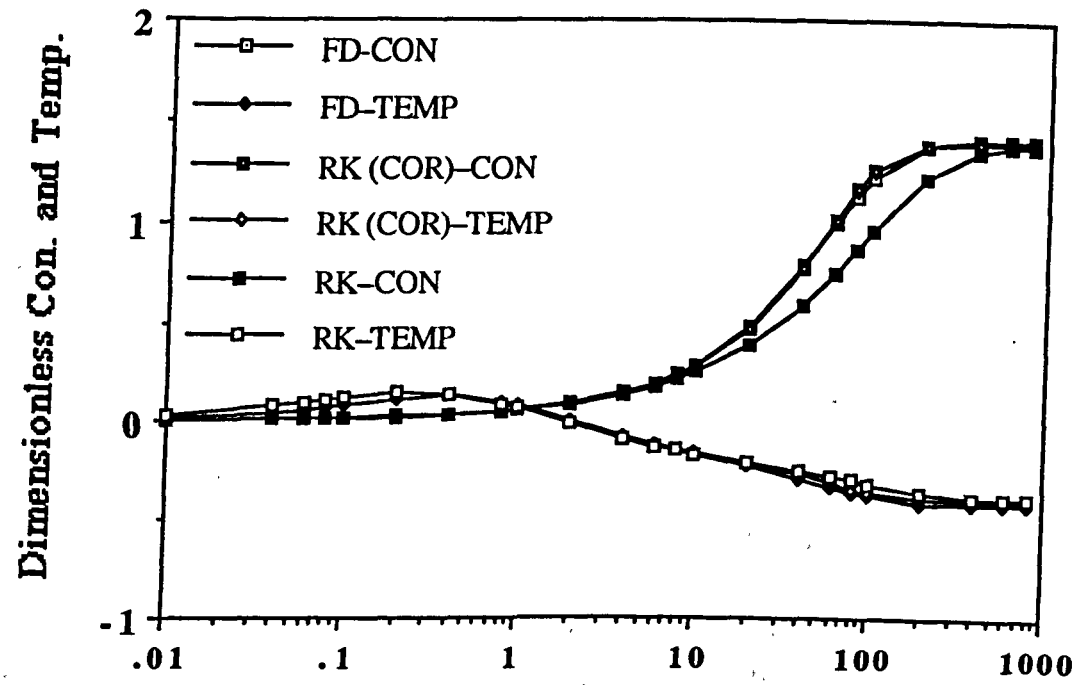

Effect of correction at Cr = 200

Fig (4.3)

4.4–Effect of the Simplifying Assumptions :

Because the simplified method does not need the simplifying assumptions used by the finite difference method it is useful to see their effect on the solution and hence judge the accuracy of the finite difference method.

The effect of the assumption of the specific enthalpy of the absorbent being a function of the temperature only on the solution is shown in table (4.2) where the results obtained using such assumption is compared to the real case. The comparison is made in terms of the overall effectivenesses Eo defined as the ratio of the amount of vapour absorbed by the absorber to that absorbed by an equivalent absorber at equilibrium conditions with the absorbent leaving at the entering coolant's temperature, i.e., $Eo = \frac{m_v}{m_{ve}}$. It is quite evident from the table that the assumption has negligible effect on the solution. This is to be expected since for LiBr/H_2O combination the value of the specific enthalpy is small compared to the heat of absorption hence its contribution to the solution will also be small. In fact, the case can be further simplified by assuming the specific enthalpy to be constant. In this case eqn (4.16) becomes the simple algebraic equation :

$$\dot{m}_v h_{fg} - q_w = 0 \qquad (4.23)$$

Even the introduction of this further simplification made almost no difference to the solution as also shown in table (4.2) where the overall effectiveness obtained for this case is also listed in the table.

	Overall Effectiveness		
Dimensionless Length (X)	ha=f(Ca,Ta)	ha=f(Ta)	ha=Const.
1	.032	.0324	.031
10	.17	.17	.173
20	.288	.29	.291
40	.503	.504	.506
60	.679	.679	.682
80	.808	.808	.810
100	.894	.896	.895
200	.998	.997	.998
400	.9999	.999	.99999

Table (4.2)

Effect of simplifying the absorbent's enthalpy at Cr = 200

The effect of assuming constant absorbent's mass flow rate is presented in table (4.3) where results obtained using constant and variable mass flow rates are compared. Again, the table clearly shows marginal differences between the two sets of results despite the fact that the entry conditions of the absorbent used to obtain these results were set at the somewhat unrealistic values of 66% concentration and 40 °C temperature to maximize the absorption and consequently the change in mass flow rate which amounted to 22.5%. In reality these values would not be possible because it will result in crystallization and a maximum change in mass flow rate would be approximately 10%. However, even

at these unrealistic conditions the solutions remained virtually unchanged.

It can be concluded from this investigation that the finite difference method is accurate and additionally there is no reason for the simplifying assumptions to be used in the simplified method. When using the finite difference method, which may still be used to obtain the heat and mass transfer coefficients, it is of considerable benefit to know that the effects of the assumptions are negligible and so the results are reassuring in that respect.

	Overall Effectiveness	
Dimensionless Length (X)	ma=Const.	ma=Var.
1	.032	.0317
10	.17	.169
20	.288	.286
40	.503	.50
60	.679	.678
80	.808	.808
100	.894	.896
200	.998	.9999
400	.9999	.9999

Table (4.3)

Effect of assuming constant absorbent's mass flow rate at Cr = 200

Following the above discussion the set of equations which will produce acceptable accuracy and good agreement with the finite difference method is :

$$\dot{m}_v \, hfg - q_w = 0 \tag{4.24}$$

$$\frac{d\dot{m}_a}{dX} = \frac{(\dot{m}\, C_p)_c \, Nu}{Cr \, Ua} \dot{m}_v \tag{4.25}$$

$$\frac{dT_c}{dX} = \frac{Nu}{Cr \, Ua} q_w \tag{4.26}$$

where :

$$\dot{m}_v = cf \, \rho \, G_{li} \, (C_a - C_i) \tag{4.27}$$

$$q_w = cf \, U_w \, (T_a - T_c) \tag{4.28}$$

These equations, provided the appropriate heat and mass transfer coefficients are available, can be applied to any type of flow, e.g wavy or turbulent. In fact, the calculation method of the wavy flow introduced in chapter 5 can be used to produce such transfer coefficients which may then be used in them.

4.5–Heat and Mass Effectivenesses :

It was noted in chapter 3 that the simplified method presented here was used to produce the absorber's heat and mass effectivenesses which were used there. Recall that these effectivenesses are defined respectively by :

$$E_h = \frac{T_{co} - T_{ci}}{T_{ai} - T_{ci}}$$

$$E_m = \frac{C_s - C_w}{C_s - C_e}$$

The absorber's heat, mass, and overall effectivenesses should be independent of its entry conditions, i.e., its temperature and concentration, and dependent only on the physical conditions represented by Cr and NTU. NTU represents the area of the absorber for a constant heat capacity and heat transfer coefficient of the coolant and is defined by :

$$NTU = \frac{U_w \; w \; L}{(\dot{m} \; C_p)_c}$$

The independence of the effectivenesses from the entry conditions was confirmed by obtaining solutions for varying inlet conditions of the absorbent ranging between 50 °C and 30 °C for temperature and 0.66 and 0.50 for concentration. It was found that the solution remained unchanged throughout.

In fig (4.4) all three effectivenesses are plotted against NTU for a capacity ratio, Cr, of 200. It is clear from the figure that while both the mass and the overall effectivenesses have a maximum value of unity, the heat effectiveness has a maximum of about 0.25. This is because, as discussed in chapter 3, $\frac{(\dot{m}C_p)_{absorbent}}{(\dot{m}C_p)_{coolant}}$ is less than unity, therefore $\Delta T_{absorbent} > \Delta T_{coolant}$, and at equilibrium $T_{ci} = T_{ao}$ which results in

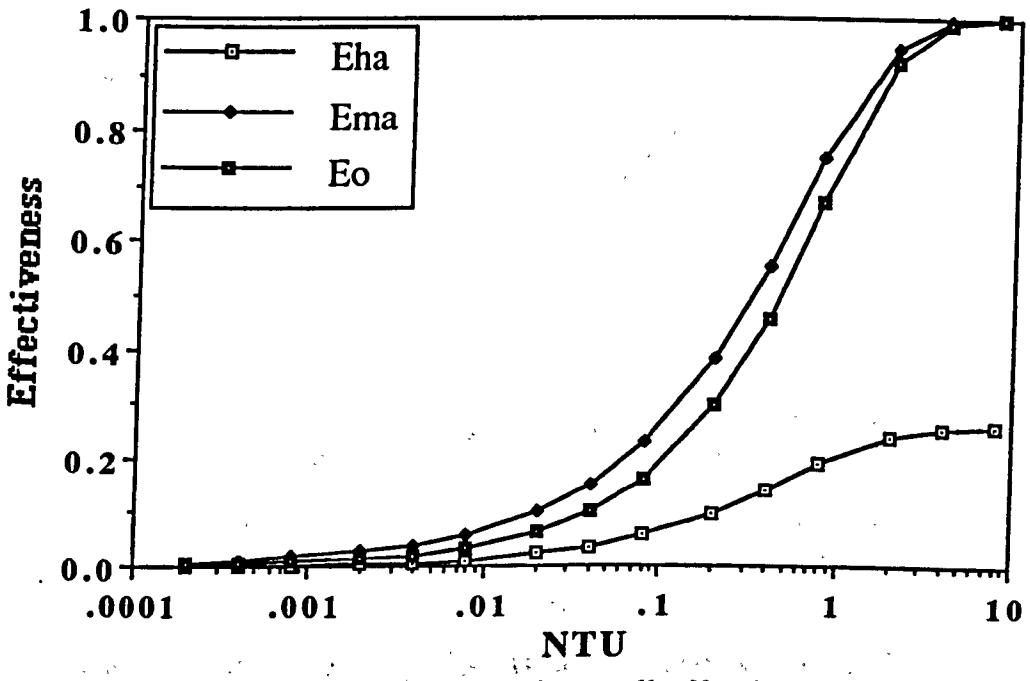

Variation of the heat, mass, and overall effectivenesses with NTU at Cr=200

Fig (4.4)

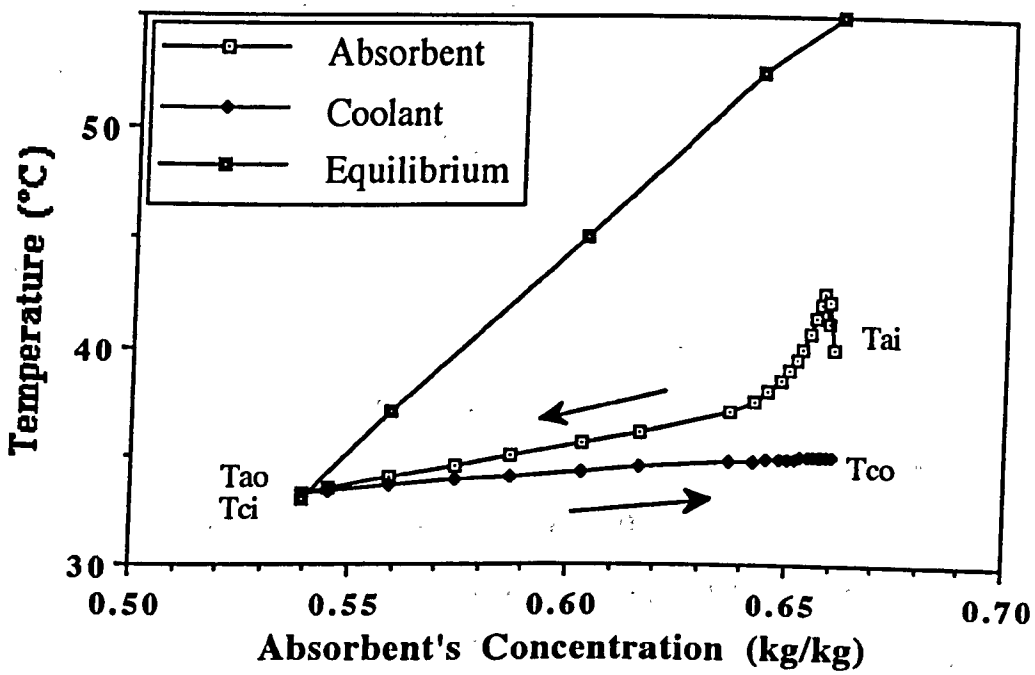

Absorbent and coolant paths inside the absorber at Cr=200 and inlet conditions of Tai=40 °C, Tci=33.3 °C, and Cs=0.66 kg/kg.

Fig (4.5)

a maximum effectiveness of less than unity. The actual changes in the absorbent's concentration and temperature and in the temperature of the coolant, as they flow counter to each other, are shown in fig (4.5). The absorbent enters the absorber at temperature T_{ai} and concentration C_s and leaves, if it reaches equilibrium, at temperature and concentration of T_{ci} and C_e respectively. In practice, the absorbent will leave the absorber at temperature and concentration of T_{ao} and C_w respectively which are higher than the equilibrium conditions. The heat and mass effectivenesses will be measures of the deviation of the actual temperature and concentration from those at equilibrium. The initial surge in the absorbent's temperature in the entry region is due to the sudden release of the heat of absorption which, at this particular conditions, is such that the cooling effect is not enough to keep the temperature down. It must be noted that the plotting of the coolant's temperature curve on the diagram of fig (4.5) is not entirely appropriate since the figure is a Temperature–Concentration diagram and the coolant does not undergo a concentration change. The points on the coolants curve are temperature points that correspond to the temperature/concentration points on the absorbent's curve. However, this was done to illustrate the typical behaviour of the absorbent and the coolant in relation to each other.

4.6–Effect of the Step Size :

Earlier in this chapter it was mentioned that a solution independent of the step size was obtained. Now the effect of step size on the solution

can be discussed in greater detail. In table (4.4) the overall effectiveness obtained using different non–dimensional step size (dX) is

	Overall Effectiveness				
X	dX=0.0035	dX=0.035	dX=0.175	dX=0.35	dX=0.7
.1	.00831	.00825			
1	.03205	.0320	.0324	.0346	.0350
10	.1687	.1687	.1690	.1729	.1770
100	.8940	.8950	.8950	.8951	.8967
200	.9981	.9982	.9983	.9983	1.050

Table (4.4)

Effect of the step size on the accuracy at Cr = 200

listed to show the effect on accuracy of varying the step size. It is seen that the solution is consistent up to a step size of 0.175, and is still acceptable at dX = 0.35. At step size of 0.7 the solution is still stable but less accurate. Further increase in the step size causes instability and the code fails to output any solution after a short length. In this analysis a step size of 0.035 is used throughout.

4.7–Results and Discussion :

4.7.1–Transfer Area and Cooling Rate :

The absorber's performance can be improved by increasing the areas of heat and mass transfer and by increasing the rate of flow of the

coolant at a given inlet temperature. In the following analysis the contribution of each factor to the overall effectiveness of the absorber is discussed based on the results obtained for LiBr/H_2O combination.

In fig (4.6) the overall effectiveness for different capacity ratios is plotted against the number of transfer units NTU. As expected the effectiveness improves with the increased NTU. However, this improvement diminishes as NTU is increased by, for example, increasing the absorber's area. For example, at Cr = 60 doubling NTU from 4 to 8 only increases the effectiveness by a mere 10% from 0.89 to 0.99. It is noted the values of Cr are much greater than those common in heat exchangers. This is to cater for the heat of absorption of the refrigerant.

In fig (4.7) the effectiveness is plotted against the capacity ratio for different area ratios (Ar), where Ar is the ratio of the absorber's area (A) to that corresponding to equilibrium conditions (A_∞) i.e., $Ar = \frac{A}{A_\infty}$, and is a measure of the relative size of the absorber i.e., the area of heat and mass transfer. In this case A_∞ was taken at X = 1000 and is equal to 170 m^2. The figure combines the effects of both the coolant's flow rate and the absorber's area on the effectiveness, but does not give information as to what Cr–Ar combination is best to achieve certain effectiveness. It does, however, show what combinations are to be considered. For example at Ar = 0.2 there is little point of increasing the coolant's flow rate beyond a capacity ratio of 80, whereas for smaller areas e.g. at Ar = 0.03 increasing Cr beyond 60 is even less useful. The improvement of effectiveness with capacity ratio increases

steadily with Ar as the curves grow more steeper up to Ar = 0.2 then the curves start to flatten out again until an area ratio of 0.7 where the equilibrium conditions are reached for all capacity ratios and the curves become straight flat lines. This means that at Ar = 0.2 the effectiveness responds more strongly to the change in Cr than to any other smaller or larger area ratio. This is because at Ar < 0.2 the small area limits the benefit of large cooling flow rates, and at Ar > 0.2 the equilibrium conditions are approached and the effectiveness becomes less sensitive to changes in Cr.

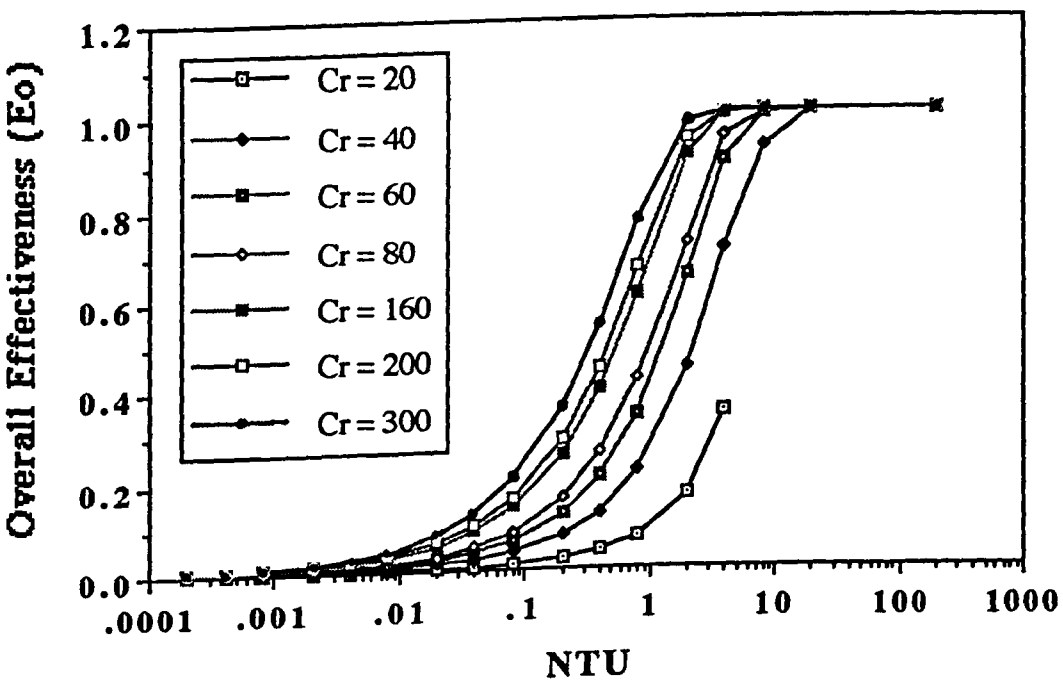

Variation of the overall effectiveness with NTU

Fig (4.6)

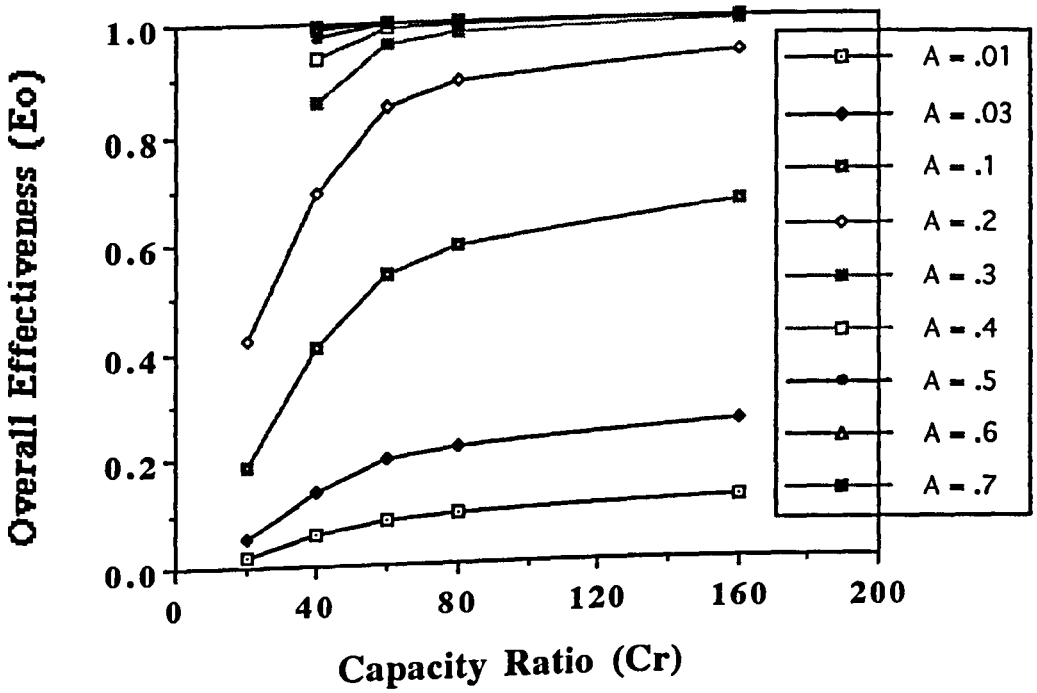

Variation of the overall effectiveness with Cr at various area ratios

Fig (4.7)

4.7.2–Temperature Variation :

In heat exchangers the only point where the temperatures of the hot and cold fluids are equal is at infinite length. This is seen in fig (4.8) where the two temperature curves will only touch at $x = \infty$ and nowhere can the two curves cross each other because this will mean that the cold fluid is heated to a temperature higher than that of the heating source (and vice versa).

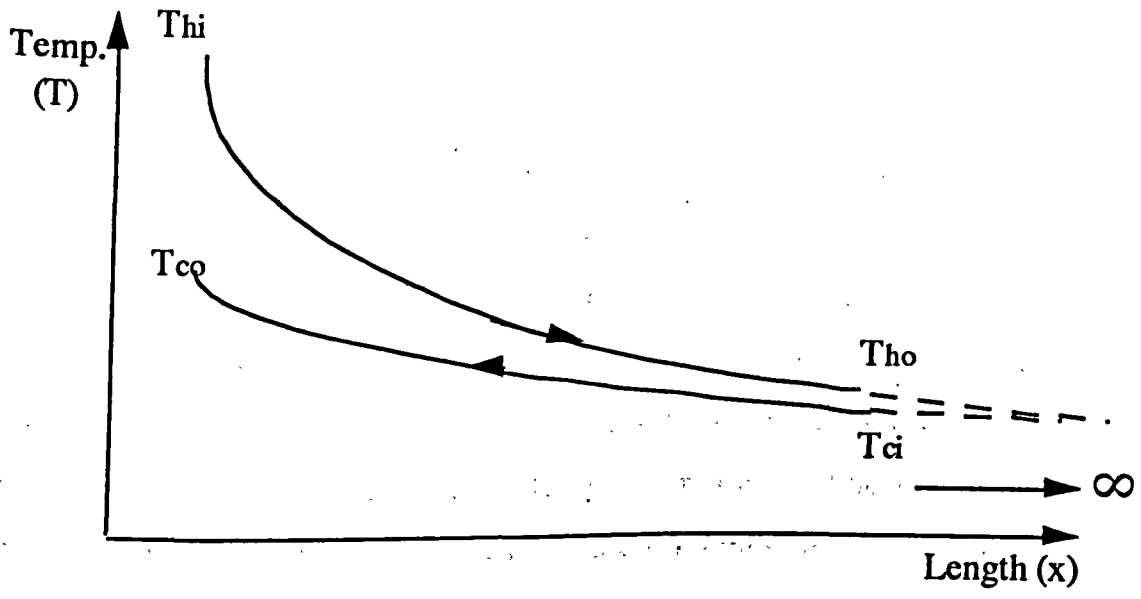

Fig (4.8)

Temperature curves in counterflow heat–exchangers

Surprisingly, such a crossing of the temperature profiles can occur in absorbers and results to illustrate this are displayed in fig (4.9) to (4.12).

This phenomenon seems to be exclusive to absorbers and happens because the phase change occurs at varying temperature. The release of the heat of absorption causes the absorbent's temperature to rise before decreasing again due to the cooling effect of the coolant. This creates a hump in the absorbent's temperature curve and, because the coolant flows in the opposite direction to the absorbent, its temperature curve can cross that of the absorber. This is an interesting phenomenon but is unlikely to happen in practice because it needs high temperatures of the coolant and/or low capacity ratios. Either of these conditions are unlikely in reality.

4.8–Conclusion :

In this chapter a simplified method of predicting the performance of the absorber has been developed. The method is simpler than the existing finite difference methods but requires the knowledge of the heat and mass transfer coefficients which can be obtained from either analytical or experimental data. The method was corrected to give better agreement with the finite difference method. The performance was found to improve with increasing the coolant's mass flow rate and the absorber's area. It was also found that the temperature of the coolant can exceed the absorbent's temperature at the same point of the absorber's length. This is due to the fact that in the absorber the phase change occurs at varying temperature. However, this is only likely to happen at high coolant's temperature and/or low Cr.

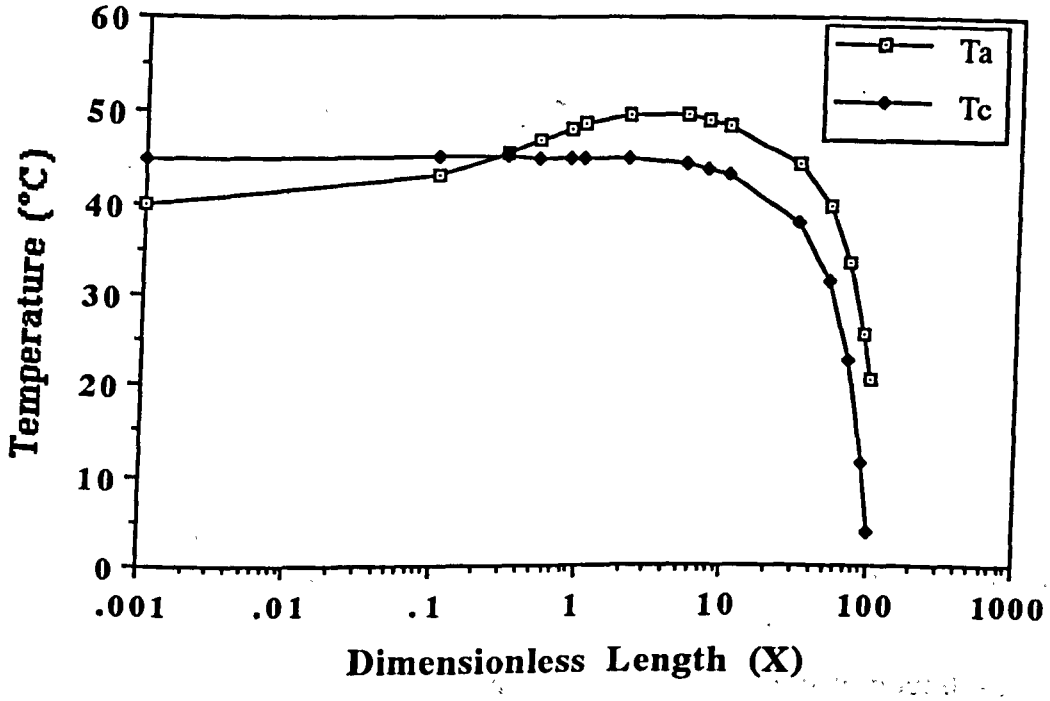

Temperature curves with cooling water outlet temperature of 45 °C at Cr = 40

Fig (4.9)

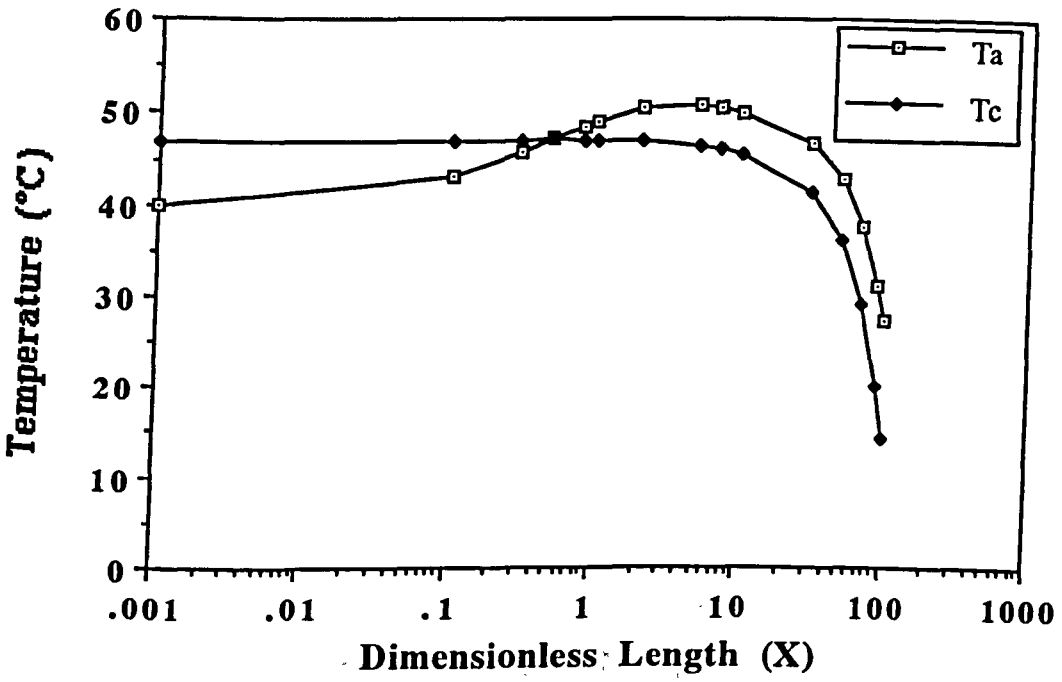

Temperature curves with cooling water outlet temperature of 47 °C at Cr = 40

Fig (4.10)

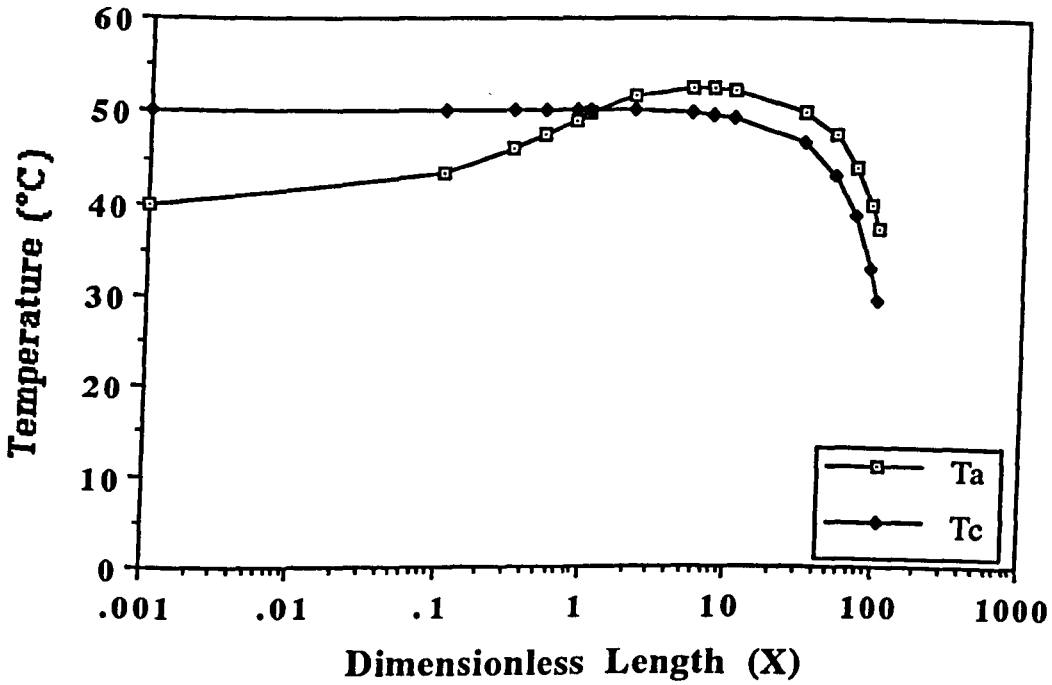

Temperature curves with cooling water outlet temperature of 50 °C at Cr = 40

Fig (4.11)

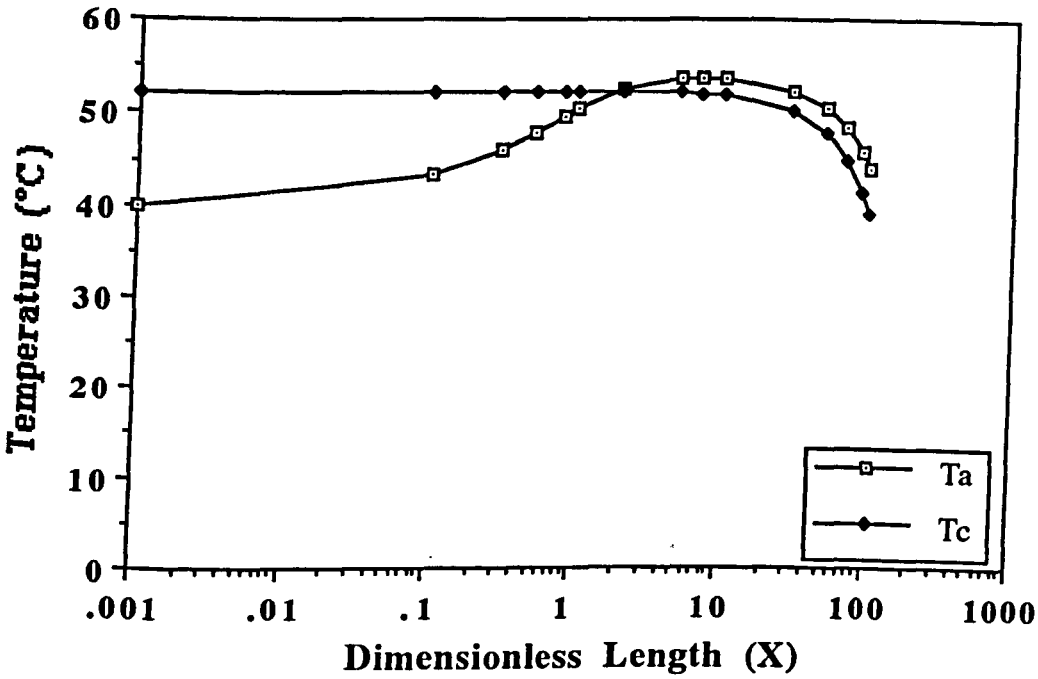

Temperature curves with cooling water outlet temperature of 52 °C at Cr = 40

Fig (4.12)

Nomenclature:

A	absorber's area (m^2).
A_∞	absorber's area at equilibrium (m^2).
Ar	area ratio.
V_X	dimensionless velocity of absorbent in the x–direction.
C	dimensionless concentration of LiBr in $LiBr/H_2O$ absorbent.
C_a	concentration of the absorbent.
C_{di}	dimensionless concentration at the interface.
C_e	equilibrium concentration.
cf	correction factor.
C_i	interface concentration.
C_{in}	initial concentration.
C_{pa}	heat capacity of absorbent (kJ/kg °C).
C_{pc}	heat capacity of cooling water (kJ/kg °C).
C_s	strong concentration.
C_w	weak concentration.
Cr	capacity ratio.
D	diffusion coefficient (m^2/s).
dx	absorber's element length (m).
dX	non–dimensional element length.
Eo	absorber's overall effectiveness.
G_{li}	mass transfer coefficient (m/s).
H	total enthalpy of the absorbent (kJ).
h_a	specific enthalpy of absorbent (kJ/kg).
h_{fg}	Specific heat of vaporization (kW/kg).
L	absorber's total length (m).

$\dot{m}_a$ mass flow rate of liquid absorbent (kg/s).

$\dot{m}_c$ mass flow rate of cooling water (kg/s).

$\dot{m}_s$ mass flow rate of LiBr salt (kg/s).

m_v total amount of vapour absorbed (kg).

$\dot{m}_v$ vapour absorption rate per unit absorber's area (kg/s m^2).

m_{ve} total amount of vapour absorbed at equilibrium conditions (kg).

NTU number of transfer units.

Nu Nusselt number.

q_i heat flux to vapour (kW/m^2).

q_w heat flux to coolant (kW/m^2).

T dimensionless temperature.

T_a temperature of absorbent (°C).

T_{ai} temperature of absorbent at inlet to absorber (°C).

T_{ao} temperature of absorbent at outlet from absorber (°C).

T_c temperature of coolant (°C).

T_{ci} temperature of coolant at inlet to absorber (°C).

T_{co} temperature of coolant at outlet from absorber (°C).

T_{di} dimensionless temperature at the interface

T_e equilibrium temperature (°C).

T_i temperature at the interface (°C).

T_{in} initial temperature (°C).

T_v temperature of vapour (°C).

U_a heat transfer coefficient across the bulk of the absorbent (kW/m^2 °C).

U_c heat transfer coefficient across the coolant (kW/m^2 °C).

U_i heat transfer coefficient from absorbent to vapour($kW/m^2\,°C$).

U_s heat transfer coefficient across the solid wall ($kW/m^2\,°C$).

U_w heat transfer coefficient from absorbent to coolant($kW/m^2°C$).

w absorber's width (m).

X dimensionless longitudinal dimension.

x longitudinal dimension (m).

Y dimensionless vertical dimension.

Greek:

α thermal diffusivity (m^2/s).

ρ density of absorbent (kg/m^3).

* It must be emphasized that the role of Penev et al [24] was to find the velocity profile of the wavy flow under the conditions of uniform and two dimensional waves. The use of this profile to obtain the concentration and temperature distributions for the combined heat and mass transfer problem is a unique contribution of this work to this area of research.

5–Effect of Waves on the Absorber's Performance :

5.1–Introduction :

It is concluded from the literature survey that for wavy flows with sufficiently high Reynold's Number, Re, the improvements of heat and mass transfer are explainable by the mixing effect of the waves. However, it was felt that at low Re, the explanation of the improvement by the convection associated with the vertical component of the velocity needed to be investigated further and to be verified in the combined problem of heat and mass transfer. Therefore the data of Penev et al [24], who devised a velocity profile that denies the possibility of mixing, as quoted by Beschkov and Boyadjiev [23], is used in this chapter to evaluate the heat and mass transfer processes associated with the absorption of a vapour by a thin wavy laminar film flowing downwards under the action of gravity. ✳

5.2–Analysis :

For a thin wavy liquid film flowing down a vertical (or inclined) surface under the system of coordinates shown in fig (5.1), the diffusion and energy equations can be written respectively as [54]

$$\frac{\partial c}{\partial t} + v_x \frac{\partial c}{\partial x} + v_y \frac{\partial c}{\partial y} = D \left(\frac{\partial^2 c}{\partial x^2} + \frac{\partial^2 c}{\partial y^2} \right) \qquad (5.1)$$

$$\frac{\partial T}{\partial t} + v_x \frac{\partial T}{\partial x} + v_y \frac{\partial T}{\partial y} = \alpha \left(\frac{\partial^2 T}{\partial x^2} + \frac{\partial^2 T}{\partial y^2} \right) \qquad (5.2)$$

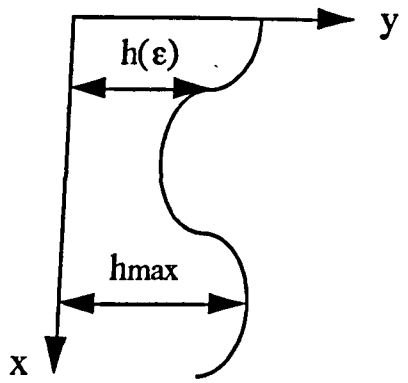

Fig (5.1)

The wavy domain

5.2.1–Boundary Conditions :

To solve equations (5.1) and (5.2), the initial and boundary conditions must first be obtained. The initial distributions of concentration and temperature are assumed to be of smooth flow i.e.,

at $t = 0$ $\quad c = c_0(x,y)$ (5.3)

$T = T_0(x,y)$ (5.4)

The boundary conditions at entry assume well mixed uniform inlet properties i.e.,

at $x = 0$ $\quad c = c_i$ (5.5)

$T = T_i$ (5.6)

For the y coordinate the concentration boundary condition at the wall reflects the impermiability of the solid wall i.e.,

at $y = 0$ $\quad \frac{\partial c}{\partial y} = 0$ (5.7)

and the temperature is assumed to be equal that of the wall i.e.,

$$T = T_w \tag{5.8}$$

At the vapour/liquid interface the boundary conditions assume that the absorbent is saturated, which from [56], [57], and [26] can be approximated by the linear dependency of concentration and temperature as shown below :

$$\text{at } y = h(\varepsilon) \qquad T = a\,c + b \tag{5.9}$$

Also at the interface, and if the sensible heat transfer is neglected, the heat flux is proportional to the rate of vapour absorption [26], i.e.,

$$\text{at } y = h(\varepsilon) \qquad \frac{\partial \theta}{\partial y} = Ha \frac{\partial \gamma}{\partial y} \tag{5.10}$$

where θ and γ are the dimensionless temperature and concentration defined respectively by :

$$\gamma = \frac{c - c_i}{c_{eq} - c_i} \tag{5.11}$$

$$\theta = \frac{T - T_i}{T_{eq} - T_i} \tag{5.12}$$

Ha is the dimensionless heat of absorption defined by :

$$Ha = \frac{\rho\, D\, \Delta h}{K} \frac{c_{eq} - c_i}{T_{eq} - T_i} \tag{5.13}$$

5.2.1.1–Smooth Flow (Initial Distribution) :

It is necessary to find the initial distributions of concentration $c_0(x,y)$ and temperature $T_0(x,y)$ defined by eqns (5.3) and (5.4) not only to

obtain the time dependant wavy distributions, but also because both distributions (smooth and wavy) will be compared to each other to assess the relative improvements in heat and mass transfer brought about by the actions of waves.

The diffusion and energy equations for a smooth flow under the same conditions and system of coordinates as those of the wavy flow described earlier in this chapter, can be written as :

$$v_x \frac{\partial c}{\partial x} = D \frac{\partial^2 c}{\partial y^2} \tag{5.14}$$

$$v_x \frac{\partial T}{\partial x} = \alpha \frac{\partial^2 T}{\partial y^2} \tag{5.15}$$

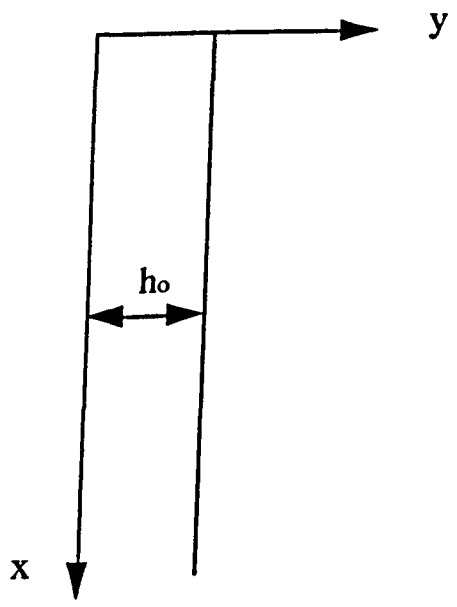

Fig (5.2)

The smooth flow

To proceed with the analysis, the following dimensionless properties are defined

$$X = \frac{x}{Pe\ h_0}$$

$$Y = \frac{y}{h_0}$$

$$V_x = \frac{v_x}{v_0}$$

It is now possible to non–dimensionalise the terms of eqns (5.14) and (5.15) as follows :

$$\frac{\partial c}{\partial x} = (c_{eq} - c_i)\frac{\partial \gamma}{\partial x} = (c_{eq} - c_i)\frac{\partial \gamma}{\partial X}\frac{\partial X}{\partial x} = \frac{(c_{eq} - c_i)}{Pe\ h_0}\frac{\partial \gamma}{\partial X} \qquad (5.16a)$$

$$\frac{\partial c}{\partial y} = (c_{eq} - c_i)\frac{\partial \gamma}{\partial y} = (c_{eq} - c_i)\frac{\partial \gamma}{\partial Y}\frac{\partial Y}{\partial y} = \frac{(c_{eq} - c_i)}{h_0}\frac{\partial \gamma}{\partial Y} \qquad (5.16b)$$

$$\frac{\partial^2 c}{\partial y^2} = \frac{\partial}{\partial Y}\left(\frac{(c_{eq} - c_i)}{h_0}\frac{\partial \gamma}{\partial Y}\right)\frac{\partial Y}{\partial y} = \frac{(c_{eq} - c_i)}{h_0^2}\frac{\partial^2 \gamma}{\partial Y^2} \qquad (5.16c)$$

Similarly

$$\frac{\partial T}{\partial x} = \frac{(T_{eq} - T_i)}{Pe\ h_0}\frac{\partial \theta}{\partial X} \qquad (5.17a)$$

$$\frac{\partial T}{\partial y} = \frac{(T_{eq} - T_i)}{h_0}\frac{\partial \theta}{\partial Y} \qquad (5.17b)$$

$$\frac{\partial^2 T}{\partial y^2} = \frac{(T_{eq} - T_i)}{h_0^2}\frac{\partial^2 \theta}{\partial Y^2} \qquad (5.17c)$$

Substituting eqns (5.16) and (5.17) in eqns (5.14) and (5.15) and using the definitions of the dimensionless variables X, Y,and V_x gives

$$\frac{V_x\ v_0}{Pe\ h_0}\frac{\partial \gamma}{\partial X} = \frac{D}{h_0^2}\frac{\partial^2 \gamma}{\partial Y^2}$$

$$\frac{V_x\ v_0}{Pe\ h_0}\frac{\partial\theta}{\partial X}=\frac{\alpha}{h_0^{\,2}}\frac{\partial^2\theta}{\partial Y^2}$$

and multiplying by $\frac{h_0^{\,2}}{D}$ to obtain

$$V_x\frac{\partial\gamma}{\partial X}=\frac{\partial^2\gamma}{\partial Y^2} \tag{5.18}$$

$$V_x\frac{\partial\theta}{\partial X}=\frac{1}{Le}\frac{\partial^2\theta}{\partial Y^2} \tag{5.19}$$

where Le is Lewis Number defined by : $Le=\frac{D}{\alpha}$.

Equations (5.18) and (5.19) are the diffusion and energy equations of the smooth film flow in dimensionless form.

The liquid domain, shown in fig (5.3), is divided into a mesh of small elements with the grid points designated by i and j along the x and y axes respectively, where i = 1,2,3,..... M, and j = 1,2,3,..... N.

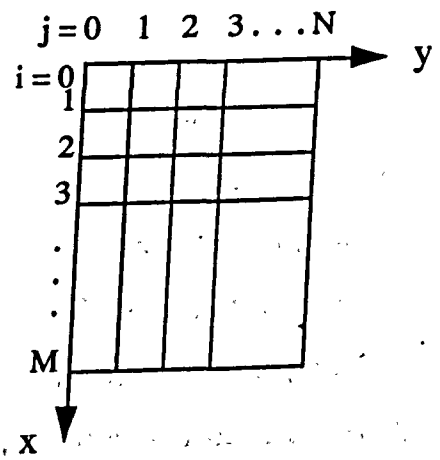

Fig (5.3)
The finite difference mesh

An explicit finite difference scheme was used to approximate the differential equations (5.18) and (5.19), which accordingly become

$$V_x \frac{\gamma_{i+1j} - \gamma_{ij}}{\Delta X} = \frac{1}{(\Delta Y)^2} (\gamma_{ij+1} + \gamma_{ij-1} - 2 \gamma_{ij}) \qquad (5.20)$$

$$V_x \frac{\theta_{i+1j} - \theta_{ij}}{\Delta X} = \frac{1}{Le\ (\Delta Y)^2} (\theta_{ij+1} + \theta_{ij-1} - 2 \theta_{ij}) \qquad (5.21)$$

Rewriting as

$$\gamma_{i+1j} = Rc\ (\gamma_{ij+1} + \gamma_{ij-1} - (2 - \frac{1}{Rc}) \gamma_{ij}) \qquad (5.22)$$

$$\theta_{i+1j} = RT\ (\theta_{ij+1} + \theta_{ij-1} - (2 - \frac{1}{RT}) \theta_{ij}) \qquad (5.23)$$

where

$$Rc = \frac{\Delta X}{V_x\ (\Delta Y)^2} \qquad (5.24)$$

$$RT = \frac{\Delta X}{Le\ V_x\ (\Delta Y)^2} \qquad (5.25)$$

Explicit finite difference schemes, are simple to construct and solve, but have the drawback that ΔX and ΔY have to be chosen to satisfy the stability criterion that Rc and RT must everywhere be no greater than 0.5 which means smaller mesh size than in the case of implicit methods, hence more calculations. This is not a disadvantage in this particular problem because, as mentioned earlier, the smooth distributions of concentration and temperature will be used as the initial condition for the wavy distribution and will be compared to it to obtain the relative improvement, thus the mesh size has to be the same in both cases, and

with the complicated stability of the wavy problem, its mesh size is very small anyway. Therefore using the implicit method to increase the mesh size of the smooth flow domain would not be of any benefit.

Now from eqns (5.24) and (5.25) it is seen that

$$RT = \frac{Rc}{Le}$$

and since Le is less than unity, then

$$RT > Rc \qquad (5.26)$$

and, consequently if RT is no greater than 0.5 neither will Rc. To calculate the mesh size it is noted that since : $Y = \frac{y}{h_0}$ and since in the non–wavy flow : $y_{max} = h_0$.

then $Y_{max} = \frac{y_{max}}{h_0} = 1$

and so

$$\Delta Y = \frac{1}{N}$$

and if a half–parabolic velocity profile is assumed, which is reasonable following Penev et al [24], then

$$v_x = \frac{3}{2} v_0 \left(2\left(\frac{y}{h_0}\right) - \left(\frac{y}{h_0}\right)^2 \right)$$

and so

$$V_x = \frac{v_x}{v_0} = \frac{3}{2}(2Y - Y^2) \qquad (5.27)$$

From eqn (5.25) it is clear that RT has a maximum value at $V_{x\,min}$ which occurs at the element adjacent to the solid wall i.e at $Y = \Delta Y$. Therefore

$$V_{x\,min} = \frac{3}{2}\left(2\Delta Y - (\Delta Y)^2 \right) \tag{5.28}$$

and the maximum possible value of RT is given by

$$RT_{max} = \frac{\Delta X}{Le\ V_{x\,min}\ (\Delta Y)^2} \tag{5.29}$$

Equating RT_{max} to 0.5 enables the calculation of ΔX which produces a stable solution. Thus from eqns (5.28) and (5.29), i.e.,

$$\Delta X = 0.75\ Le\ \left(2(\Delta Y)^3 - (\Delta Y)^4 \right) \tag{5.30}$$

5.2.1.1.1–Boundary Conditions for the Smooth Flow :

The boundary conditions for he non–wavy flow are the same as those of the wavy flow. They are written for the dimensionless domain as follows :

$$\text{at } x = 0,\ X = 0,\ c = c_i,\ \gamma_{0j} = 0 \tag{5.31a}$$

$$\text{and } T = T_i,\ \theta_{0j} = 0 \tag{5.31b}$$

$$\text{at } y = 0,\ Y = 0,\ \frac{\partial c}{\partial y} = \frac{(c_{eq} - c_i)}{h_0}\frac{\partial \gamma}{\partial Y} = 0,\ \text{i.e.,}\ \frac{\partial \gamma}{\partial Y} = 0$$

in finite difference form

$$\frac{\gamma_{i1} - \gamma_{i0}}{\Delta Y} = 0$$

$$\gamma_{i1} = \gamma_{i0} \qquad (5.32a)$$

Earlier in the chapter it was mentioned that the temperature of the liquid element at y = 0 is taken to be equal to the wall (T_w). For the sake of simplicity T_w was assumed to be constant and equal to T_i, i.e isothermal cooling. The cooling mode makes no difference to the relative result as it is applied to both fields, i.e. smooth and wavy. So

at $Y = 0$, $\theta_{i0} = \theta_{0j} = \theta_w$

and since : $\theta_{0j} = \dfrac{T_i - T_i}{T_{eq} - T_i} = 0$, then

$$\theta_{i0} = 0 \qquad (5.32b)$$

and at $y = h_0$, $Y = 1$ eqn (5.9) states that

$$T = a\,c + b$$

This equation translates into the dimensionless form [26] :

$$\gamma + \theta = 1$$

and is written for the interface as :

$$\gamma_{iN} + \theta_{iN} = 1 \qquad (5.36)$$

Also at the interface

$$\frac{\partial \theta}{\partial Y} = Ha \frac{\partial \gamma}{\partial Y}$$

which can be written in dimensionless interface notation as :

$$\theta_{iN} - \theta_{iN-1} = Ha\,(\gamma_{iN} - \gamma_{iN-1}) \qquad (5.37)$$

Solving the finite difference equations (5.22) and (5.23) gives the distribution of concentration and temperature in the smooth film which will be used as the initial distribution (t = 0) for the wavy problem. Both solutions of smooth and wavy will later be compared to see the improvement to the heat and mass transfer brought about by the waves.

5.2.2– Wavy Distribution :

The main difficulty in solving the problem of the wavy flow is that the film surface is rippled (fig (5.1)), so the film thickness h(ε) varies with time and along the film length. This difficulty can be overcome by introducing a new variable Z, where

$$Z = \frac{y}{h(\varepsilon)} \quad , 0 \le Z \le 1$$

therefore replacing the rippled boundary in the y direction by a flat one in the Z direction

Hence the wavy domain (x, y, t) could be transformed into, in effect, the smooth domain (x, Z, t).

To facilitate the transformation of the equations into the smooth domain (x, Z, t), the following notations are made for any arbitrary function f(x,y,t)

$$\frac{\partial f}{\partial x}(x,y,t) = \frac{\partial f}{\partial x}$$

and the same for y and t

and for the transformed function f(x, Z, t)

$$\frac{\partial f}{\partial x}(x,Z,t) = f'_x$$

and the same for Z and t

Now

$$df = \frac{\partial f}{\partial x} dx + \frac{\partial f}{\partial y} dy + \frac{\partial f}{\partial t} dt \qquad (5.38)$$

also

$$df = f'_x\, dx + f'_Z\, dZ + f'_t\, dt \qquad (5.39)$$

where

$$dZ = \frac{\partial Z}{\partial x} dx + \frac{\partial Z}{\partial y} dy + \frac{\partial Z}{\partial t} dt \qquad (5.40)$$

Substituting eqn (5.40) in eqn (5.39) gives

$$df = f'_x\, dx + f'_Z \left(\frac{\partial Z}{\partial x} dx + \frac{\partial Z}{\partial y} dy + \frac{\partial Z}{\partial t} dt \right) + f'_t\, dt \qquad (5.41)$$

and rearranging as

$$df = \left(f'_x + f'_Z \frac{\partial Z}{\partial x}\right) dx + f'_Z \frac{\partial Z}{\partial y} dy + \left(f'_t + f'_Z \frac{\partial Z}{\partial t}\right) dt \qquad (5.42)$$

Equating the coefficients of eqns (5.38) and (5.42) it is seen that :

$$\frac{\partial f}{\partial x} = f'_x + f'_Z \frac{\partial Z}{\partial x} \qquad (5.43)$$

$$\frac{\partial f}{\partial y} = f'_Z \frac{\partial Z}{\partial y} \qquad (5.44)$$

$$\frac{\partial f}{\partial t} = f'_t + f'_Z \frac{\partial Z}{\partial t} \qquad (5.45)$$

Using eqn (5.43) the second derivative w.r.t. x is evaluated as

$$\frac{\partial^2 f}{\partial x^2} = \frac{\partial}{\partial x} \left(f'_x + f'_Z \frac{\partial Z}{\partial x} \right) \qquad (5.46)$$

$$= (f'_x + f'_Z \frac{\partial Z}{\partial x})_x + (f'_x + f'_Z \frac{\partial Z}{\partial x})_Z \frac{\partial Z}{\partial x}$$

$$= f''_{xx} + f''_{Zx} \frac{\partial Z}{\partial x} + f'_Z (\frac{\partial Z}{\partial x})_x + (f''_{xZ} + f''_{ZZ} \frac{\partial Z}{\partial x} + f'_Z (\frac{\partial Z}{\partial x})_Z) \frac{\partial Z}{\partial x} \qquad (5.47)$$

and from eqn (5.44) the second derivative w.r.t. y is evaluated as

$$\frac{\partial^2 f}{\partial y^2} = \frac{\partial}{\partial y} (f'_Z \frac{\partial Z}{\partial y}) = (f'_Z \frac{\partial Z}{\partial y})_y + (f'_Z \frac{\partial Z}{\partial y})_Z \frac{\partial Z}{\partial y} \qquad (5.48)$$

but $(f'_Z \frac{\partial Z}{\partial y})_y = 0$ because neither f'_Z nor $\frac{\partial Z}{\partial y}$ is function of y, so eqn (5.48) becomes

$$\frac{\partial^2 f}{\partial y^2} = (f'_Z \frac{\partial Z}{\partial y})_Z \frac{\partial Z}{\partial y}$$

$$= (f''_{ZZ} \frac{\partial Z}{\partial y} + f'_Z (\frac{\partial Z}{\partial y})_Z) \frac{\partial Z}{\partial y} \qquad (5.49)$$

and since $(\frac{\partial Z}{\partial y})_Z = 0$, because $\frac{\partial Z}{\partial y}$ is a function of x and t only, eqn (5.49) becomes

$$\frac{\partial^2 f}{\partial y^2} = f''_{ZZ} (\frac{\partial Z}{\partial y})^2$$

Eqns (5.1) and (5.2) can both be written in the general form :

$$\frac{\partial f}{\partial t} + v_x \frac{\partial f}{\partial x} + v_y \frac{\partial f}{\partial y} = \text{const.} (\frac{\partial^2 f}{\partial x^2} + \frac{\partial^2 f}{\partial y^2}) \qquad (5.50)$$

where f = c and const. = D in the diffusion equation, and

f = T and const. = α in the energy equation

Substituting for the derivatives, the left hand side becomes

$$\frac{\partial f}{\partial t} + v_x \frac{\partial f}{\partial x} + v_y \frac{\partial f}{\partial y} = f'_t + f'_Z \frac{\partial Z}{\partial t} + v_x (f'_x + f'_Z \frac{\partial Z}{\partial x}) + v_y f'_Z \frac{\partial Z}{\partial y}$$

and rearranging as

$$\frac{\partial f}{\partial t} + v_x \frac{\partial f}{\partial x} + v_y \frac{\partial f}{\partial y} = f'_t + v_x f'_x + f'_Z (\frac{\partial Z}{\partial t} + v_x \frac{\partial Z}{\partial x} + v_y \frac{\partial Z}{\partial y}) \qquad (5.51)$$

Dividing eqn (5.40) by dt gives

$$\frac{dZ}{dt} = \frac{\partial Z}{\partial x}\frac{dx}{dt} + \frac{\partial Z}{\partial y}\frac{dy}{dt} + \frac{\partial Z}{\partial t}$$

$$\frac{dZ}{dt} = \frac{\partial Z}{\partial x} v_x + \frac{\partial Z}{\partial y} v_y + \frac{\partial Z}{\partial t} \qquad (5.52)$$

Substituting in the last term of eqn (5.51) the equation becomes

$$\frac{\partial f}{\partial t} + v_x \frac{\partial f}{\partial x} + v_y \frac{\partial f}{\partial y} = f'_t + v_x f'_x + \frac{dZ}{dt} f'_Z \qquad (5.53)$$

Using eqns (5.47) and (5.49) to substitute for the right hand side of eqn (5.50) gives

$$\frac{\partial^2 f}{\partial x^2} + \frac{\partial^2 f}{\partial y^2} = f''_{xx} + f''_{Zx}\frac{\partial Z}{\partial x} + f'_Z (\frac{\partial Z}{\partial x})_x + (f''_{xZ} + f''_{ZZ}\frac{\partial Z}{\partial x} + f'_Z (\frac{\partial Z}{\partial x})_Z)\frac{\partial Z}{\partial x} + f''_{ZZ}(\frac{\partial Z}{\partial y})^2$$

and since $f''_{xZ} = f''_{Zx}$ the above equation can be written as

$$\frac{\partial^2 f}{\partial x^2} + \frac{\partial^2 f}{\partial y^2} = f''_{xx} + 2f''_{xZ}\frac{\partial Z}{\partial x} + f''_{ZZ}(\frac{\partial Z}{\partial x})^2 + f''_{ZZ}(\frac{\partial Z}{\partial y})^2 + f'_Z (\frac{\partial Z}{\partial x})_x + f'_Z (\frac{\partial Z}{\partial x})_Z \frac{\partial Z}{\partial x}$$

However, the last term : $f'_Z (\frac{\partial Z}{\partial x})_Z \frac{\partial Z}{\partial x}$ is equal to zero because

$$(\frac{\partial Z}{\partial x})_Z = \frac{\partial^2 Z}{\partial x \partial Z} = \frac{\partial}{\partial x}(\frac{\partial Z}{\partial Z}) = 0$$

so the equation becomes

$$\frac{\partial^2 f}{\partial x^2}+\frac{\partial^2 f}{\partial y^2}=f''_{xx}+2f''_{xZ}\frac{\partial Z}{\partial x}+f''_{ZZ}\left(\frac{\partial Z}{\partial x}\right)^2+f''_{ZZ}\left(\frac{\partial Z}{\partial y}\right)^2+f'_Z\left(\frac{\partial Z}{\partial x}\right)_x \qquad (5.54)$$

Equating the right hand sides of eqns (5.53) and (5.54) will produce the general diffusion and energy equation in the transformed domain (x,Z,t)

$$f'_t+v_x f'_x+\frac{dZ}{dt}f'_Z=\text{const.}\left(f'_{xx}+2f''_{xZ}\frac{\partial Z}{\partial x}+f''_{ZZ}\left(\frac{\partial Z}{\partial x}\right)^2+f''_{ZZ}\left(\frac{\partial Z}{\partial y}\right)^2+f'_Z\frac{\partial^2 Z}{\partial x^2}\right)$$

or

$$\frac{\partial f}{\partial t}+v_x\frac{\partial f}{\partial x}+\frac{dZ}{dt}\frac{\partial f}{\partial Z}=\text{const.}\left(\frac{\partial^2 f}{\partial x^2}+2\frac{\partial^2 f}{\partial x\partial Z}\frac{\partial Z}{\partial x}+\frac{\partial^2 f}{\partial Z^2}\left(\frac{\partial Z}{\partial x}\right)^2+\frac{\partial^2 f}{\partial Z^2}\left(\frac{\partial Z}{\partial y}\right)^2+\frac{\partial f}{\partial Z}\frac{\partial^2 Z}{\partial x^2}\right) \qquad (5.55)$$

As before this equation has to be non–dimensionalised. This is achieved by defining the dimensionless time τ as

$$\tau=\frac{D\ t}{h_0^{\ 2}} \qquad (5.56)$$

and using this definition together with the other non–dimensional variables, to write

$$\frac{\partial f}{\partial t}=\frac{\partial f}{\partial \tau}\frac{\partial \tau}{\partial t}=\frac{D}{h_0^{\ 2}}\frac{\partial f}{\partial \tau} \qquad (5.57)$$

$$\frac{\partial f}{\partial x}=\frac{\partial f}{\partial X}\frac{\partial X}{\partial x}=\frac{1}{Peh_0}\frac{\partial f}{\partial X} \qquad (5.58)$$

$$\frac{\partial^2 f}{\partial x^2}=\frac{\partial}{\partial X}\left(\frac{\partial f}{\partial x}\right)\frac{\partial X}{\partial x}=\frac{\partial}{\partial X}\left(\frac{\partial f}{\partial X}\frac{1}{Peh_0}\right)\frac{1}{Peh_0}=\frac{1}{(Peh_0)^2}\frac{\partial^2 f}{\partial X^2} \qquad (5.59)$$

$$\frac{\partial Z}{\partial y}=\frac{1}{h(\varepsilon)} \qquad (5.60)$$

$$\frac{\partial Z}{\partial t} = \frac{\partial Z}{\partial \tau}\frac{\partial \tau}{\partial t} = \frac{D}{h_0^2}\frac{\partial Z}{\partial \tau} \tag{5.61}$$

$$\frac{\partial^2 f}{\partial x \partial Z} = \frac{1}{Peh_0}\frac{\partial^2 f}{\partial X \partial Z} \tag{5.62}$$

$$\frac{\partial Z}{\partial x} = \frac{1}{Peh_0}\frac{\partial Z}{\partial X} \tag{5.63}$$

$$\frac{\partial^2 Z}{\partial x^2} = \frac{1}{(Peh_0)^2}\frac{\partial^2 Z}{\partial X^2} \tag{5.64}$$

Substituting eqns (5.57) —— (5.64) and the definition : $V_x = \frac{v_x}{v_0}$ in eqn (5.55) gives

$$\frac{\partial f}{\partial \tau}\frac{D}{h_0^2} + \frac{V_x v_0}{Peh_0}\frac{\partial f}{\partial X} + \frac{dZ}{d\tau}\frac{\partial f}{\partial Z}\frac{D}{h_0^2} = \text{const.}\left(\frac{1}{(Peh_0)^2}\frac{\partial^2 f}{\partial X^2} + 2\frac{\partial^2 f}{\partial X \partial Z}\frac{\partial Z/\partial X}{(Peh_0)^2}\right.$$
$$\left. + \frac{\partial^2 f}{\partial Z^2}\left(\frac{\partial Z/\partial X}{Peh_0}\right)^2 + \frac{\partial^2 f}{\partial Z^2}\frac{1}{h(\varepsilon)^2} + \frac{\partial f}{\partial Z}\frac{\partial^2 Z/\partial X^2}{(Peh_0)^2}\right)$$

Multiplying by $\frac{h_0^2}{D}$ and using the definition : $Pe = \frac{h_0 v_0}{D}$ one obtains

$$\frac{\partial f}{\partial \tau} + V_x\frac{\partial f}{\partial X} + \frac{dZ}{d\tau}\frac{\partial f}{\partial Z} = \frac{\text{const.}}{D}\left(\frac{1}{Pe^2}\frac{\partial^2 f}{\partial X^2} + 2\frac{\partial^2 f}{\partial X \partial Z}\frac{\partial Z/\partial X}{Pe^2} + \frac{\partial^2 f}{\partial Z^2}\right.$$
$$\left.\left(\frac{\partial Z/\partial X}{Pe}\right)^2 + \frac{\partial^2 f}{\partial Z^2}\frac{1}{H(\varepsilon)^2} + \frac{\partial f}{\partial Z}\frac{\partial^2 Z/\partial X^2}{Pe^2}\right) \tag{5.65}$$

where $H(\varepsilon)$ is the non–dimensional film thickness defined by :

$$H(\varepsilon) = \frac{h(\varepsilon)}{h_0}.$$

Rearranging eqn (5.65) and putting $B = \frac{\text{const.}}{D}$ gives

$$\frac{\partial f}{\partial \tau}+V_x\frac{\partial f}{\partial X}+\left(\frac{dZ}{d\tau}-B\left(\frac{\partial^2 Z/\partial X^2}{Pe^2}\right)\right)\frac{\partial f}{\partial Z}=B\left(\frac{1}{Pe^2}\frac{\partial^2 f}{\partial X^2}+\left(\frac{1}{H(\varepsilon)^2}+\left(\frac{\partial Z/\partial X}{Pe}\right)^2\right)\frac{\partial^2 f}{\partial Z^2}+2\frac{\partial^2 f}{\partial X\partial Z}\frac{\partial Z/\partial X}{Pe^2}\right) \qquad (5.66)$$

In this problem Pecklet Number, Pe, is large, and terms containing Pe^2 in the denominator are justifiably neglected from the equation above (in this case $Pe^2 = 25.10^8$). Equation (5.66) hence becomes

$$\frac{\partial f}{\partial \tau}+V_x\frac{\partial f}{\partial X}+\left(\frac{dZ}{d\tau}\right)\frac{\partial f}{\partial Z}=B\left(\frac{1}{H(\varepsilon)^2}\frac{\partial^2 f}{\partial Z^2}\right)$$

However, to confirm the neglegibility of such terms a solution for the complete equation (5.66) (applied for both concentration and temperature) was obtained and compared to that of the above equation. The difference between the two solutions was found to be negligible.

The diffusion equation can be obtained by substituting γ for f and putting $B=\frac{D}{D}=1$ giving

$$\frac{\partial \gamma}{\partial \tau}+V_x\frac{\partial \gamma}{\partial X}+\frac{dZ}{d\tau}\frac{\partial \gamma}{\partial Z}=\frac{1}{H(\varepsilon)^2}\frac{\partial^2 \gamma}{\partial Z^2} \qquad (5.67)$$

Similarly, the energy equation is obtained by substituting θ for f and putting $B=\frac{\alpha}{D}=\frac{1}{Le}$ to give

$$\frac{\partial \theta}{\partial \tau}+V_x\frac{\partial \theta}{\partial X}+\frac{dZ}{d\tau}\frac{\partial \theta}{\partial Z}=\frac{1}{Le}\frac{1}{H(\varepsilon)^2}\frac{\partial^2 \theta}{\partial Z^2} \qquad (5.68)$$

Eqns (5.67) and (5.68) are the final non–dimensional equations for which solution is sought. To do so, first the quantities V_x, $\frac{dZ}{d\tau}$, and $H(\varepsilon)$ should be evaluated.

V_x is calculated from the velocity profile of Penev et al (24) :

$$V_x = a_1(\varepsilon)Y + a_2(\varepsilon)Y^2 \qquad \text{or,}$$

$$V_x = \sum_{k=1}^{2} a_k(\varepsilon)\ Y^k \tag{5.69}$$

where,

$$a_1(\varepsilon)=a_{10}+a_{11}\sin(n\varepsilon)+\tilde{a}_{11}\cos(n\varepsilon)+a_{12}\sin(2n\varepsilon)+\tilde{a}_{12}\cos(2n\varepsilon) \tag{5.70a}$$

$$a_2(\varepsilon)=a_{20}+a_{21}\sin(n\varepsilon)+\tilde{a}_{21}\cos(n\varepsilon)+a_{22}\sin(2n\varepsilon)+\tilde{a}_{22}\cos(2n\varepsilon) \tag{5.70b}$$

$$\varepsilon = (x - \omega\ v_0 t) / h_0$$

non–dimensionalising the last equation as

$$\varepsilon = \left(X\ Pe\ h_0 - \frac{\omega\ v_0\ h_0^2 \tau}{D} \right) / h_0$$

$$\varepsilon = (X - \omega\ \tau)\ Pe \tag{5.71}$$

Substituting $a_1(\varepsilon)$, $a_2(\varepsilon)$ in eqn (5.69), after calculating ε, will give the V_x profile across the Y axis. Pe is calculated from the relation :

$$Pe = Re\ Sc$$

To calculate $\frac{dZ}{dt}$, eqn (5.52) is quoted

$$\frac{dZ}{dt} = \frac{\partial Z}{\partial t} + v_x \frac{\partial Z}{\partial x} + v_y \frac{\partial Z}{\partial y} \tag{5.72}$$

Defining V_y, the non–dimensional velocity in the direction of y, as :

$$V_y = \frac{Pe}{v_0} v_y$$

and substituting into eqn (5.72) together with the other non–dimensional quantities gives

$$\frac{dZ}{d\tau}\frac{D}{h_0^2} = \frac{\partial Z}{\partial \tau}\frac{D}{h_0^2} + V_x \frac{v_0}{Pe\ h_0}\frac{\partial Z}{\partial X} + V_y \frac{v_0}{Pe\ h_0}\frac{\partial Z}{\partial Y}$$

multiplying by $\frac{h_0^2}{D}$ one obtains

$$\frac{dZ}{d\tau} = \frac{\partial Z}{\partial \tau} + V_x \frac{\partial Z}{\partial X} + V_y \frac{\partial Z}{\partial Y} \qquad (5.73)$$

and since

$$Z = \frac{y}{h(\varepsilon)}$$

and

$$Y = \frac{y}{h_0}$$

then

$$Z = \frac{Y}{H(\varepsilon)} \qquad (5.74)$$

therefore

$\frac{\partial Z}{\partial Y} = \frac{1}{H(\varepsilon)}$, and

$$\frac{\partial Z}{\partial \tau} = \frac{-Y\frac{\partial H(\varepsilon)}{\partial \tau}}{H(\varepsilon)^2} \qquad (5.75)$$

From Penev et al (24) :

$$h(\varepsilon)=h_0(1+A\ \sin(n\varepsilon)+b_2\sin(2n\varepsilon)+d_2\cos(2n\varepsilon)+...+b_j\ \sin(jn\varepsilon)+d_j\ \cos(jn\varepsilon))$$

which when divided by h_0 and truncated at j = 2, following Penev et al (24), H(ε) is obtained, i.e.,

$$H(\varepsilon) = 1 + A\ \sin(n\varepsilon) + b_2\ \sin(2n\varepsilon) + d_2\ \cos(2n\varepsilon) \qquad (5.76)$$

where $A = (h_{max} - h_0)/\ h_0$

differentiating with respect to τ gives

$$\frac{\partial H(\varepsilon)}{\partial \tau} = nA\cos(n\varepsilon)\frac{\partial \varepsilon}{\partial \tau} + 2nb_2\cos(2n\varepsilon)\frac{\partial \varepsilon}{\partial \tau} - 2nd_2\sin(2n\varepsilon)\frac{\partial \varepsilon}{\partial \tau} \qquad (5.77)$$

and differentiating eqn (5.71) gives

$$\frac{\partial \varepsilon}{\partial \tau} = -\omega\ Pe \qquad (5.78)$$

substituting eqns (5.77) and (5.78) into eqn (5.75) one obtains

$$\frac{\partial Z}{\partial \tau} = \frac{Y\ n\ \omega\ Pe}{H(\varepsilon)^2}(A\cos(n\varepsilon) + 2b_2\cos(2n\varepsilon) - 2d_2\sin(2n\varepsilon)) \qquad (5.79)$$

The partial derivative $\frac{\partial Z}{\partial X}$ is evaluated by differentiating eqn (5.74) with respect to X, i.e.,

$$\frac{\partial Z}{\partial X} = \frac{-Y\frac{\partial H(\varepsilon)}{\partial X}}{H(\varepsilon)^2} \qquad (5.80)$$

Following the same procedure, a final expression for the derivative is obtained as

$$\frac{\partial Z}{\partial X} = \frac{-Y\ n\ Pe}{H(\varepsilon)^2}(A\cos(n\varepsilon) + 2b_2\cos(2n\varepsilon) - 2d_2\sin(2n\varepsilon)) \qquad (5.81)$$

The normal component of the velocity V_y is computed by first writing the continuity equation :

$\frac{\partial v_x}{\partial x} + \frac{\partial v_y}{\partial y} = 0$ in the dimensionless form :

$$\frac{-v_0}{Pe\ h_0}\frac{\partial V_x}{\partial X} = \frac{v_0}{Pe\ h_0}\frac{\partial V_y}{\partial Y}$$, therefore

$$V_y = -\int \frac{\partial V_x}{\partial X}\,\partial Y$$

using eqn (5.69) and integrating gives

$$V_y = -\sum_{k=1}^{2} \frac{\acute{a}_k(\varepsilon)}{K+1} Y^{k+1} \qquad (5.82)$$

The coefficients $\acute{a}_1$ and $\acute{a}_2$ are obtained by differentiating eqns (5.70a) and (5.70b). Substituting the partial derivatives of Z, and V_x, and V_y in eqn (5.73) will enable the evaluation of $\frac{dZ}{d\tau}$. H(ε) is calculated from eqn (5.76).

The constants of eqns (5.70a), (5.70b), and (5.76) together with the wave parameters n, ω, and A as calculated by Penev et al and quoted by Beschkov and Boyadjiev [23] are used in this work.

The boundary conditions remain the same as in the case of smooth flow, while, as mentioned before, the solution to the smooth flow problem becomes the initial distribution of the wavy flow problem.

5.2.2.1–The Finite Difference Method :

As in the case of the smooth flow, a finite difference method was used to approximate the partial differential equations (5.67) and (5.68). However, in this case, because of the size of the problem an implicit method is used to reduce the computational work. This was chosen to be the Alternating Direction Implicit (ADI) method of Peaceman–Rachford [58]. This method amounts to taking a half time step $\frac{\Delta\tau}{2}$ using backward difference approximation which is implicit in the X–direction only using the past values in the Z–direction along the grid line $X = X_i$. The next step of the ADI method counters the bias introduced above by using a backwards difference approximation that is implicit in the Z–direction only, using the past values in the X–direction along the grid line $Z = Z_j$ to advance the final half step in time. Thus a full time step is completed.

Considering eqn (5.67) and putting

$$F_1 = V_x$$

$$F_2 = \frac{dZ}{d\tau}$$

$$F_3 = \frac{1}{H(\varepsilon)^2}$$

eqn (5.67) becomes

$$\frac{\partial\gamma}{\partial\tau} + F_1\frac{\partial\gamma}{\partial X} + F_2\frac{\partial\gamma}{\partial Z} = F_3\frac{\partial^2\gamma}{\partial Z^2} \qquad (5.83)$$

Denoting the intermediate values calculated at $\tau = \tau_k + \frac{\Delta\tau}{2}$ with * (asterisk), and applying the ADI method to eqn (5.83) one obtains

$$\frac{\gamma^*_{ij} - \gamma^{\kappa}_{ij}}{\Delta\tau/2} + \frac{F_1}{2\Delta X}(\gamma^*_{i+1j} - \gamma^*_{i-1j}) + \frac{F_2}{2\Delta Z}(\gamma^{\kappa}_{ij+1} - \gamma^{\kappa}_{ij-1}) = \frac{F_3}{(\Delta Z)^2}(\gamma^{\kappa}_{ij-1} - 2\gamma^{\kappa}_{ij} + \gamma^{\kappa}_{ij+1}) \quad (5.84)$$

Putting

$$F_4 = -\frac{F_1}{2\Delta X}$$

$$F_5 = \frac{2}{\Delta\tau}$$

$$F_6 = -F_4$$

$$F_7 = \frac{F_2}{2\Delta Z} + \frac{F_3}{(\Delta Z)^2}$$

$$F_8 = \frac{2}{\Delta\tau} - \frac{2F_3}{(\Delta Z)^2}$$

$$F_9 = \frac{F_3}{(\Delta Z)^2} - \frac{F_2}{2\Delta Z}$$

and rearranging eqn (5.84) becomes

$$F_4\gamma^*_{i-1j} + F_5\gamma^*_{ij} + F_6\gamma^*_{i+1j} = F_7\gamma^{\kappa}_{ij-1} + F_8\gamma^{\kappa}_{ij} + F_9\gamma^{\kappa}_{ij+1} \quad (5.85a)$$

Eqn (5.85a) is the first step of the ADI method and is used to calculate all the intermediate values γ^*. The procedure by which this is accomplished is referred to as the "horizontal sweep". In particular for each fixed index, j, $1 \le j \le N-1$ the tri–diagonal system (5.85a) is solved for $\gamma^*_{1j}, \gamma^*_{2j}, \ldots\ldots, \gamma^*_{M-1j}$. Thus in order to complete a horizontal

sweep an N-1 tri–diagonal systems each of the size M-1 is solved obtaining (N-1) (M-1) intermediate values.

Upon completion, the second and final step of the ADI method known as the "vertical sweep" could be executed. Equation (5.83) can be written as :

$$\frac{\gamma^{\kappa+1}_{ij} - \gamma^{*}_{ij}}{\Delta\tau/2} + \frac{F_1}{2\Delta X}(\gamma^{*}_{i+1j} - \gamma^{*}_{i-1j}) + \frac{F_2}{2\Delta Z}(\gamma^{\kappa+1}_{ij+1} - \gamma^{\kappa+1}_{ij-1}) =$$

$$\frac{F_3}{(\Delta Z)^2}(\gamma^{\kappa+1}_{ij-1} - 2\gamma^{\kappa+1}_{ij} + \gamma^{\kappa+1}_{ij+1})$$

which is rewritten as

$$-F_7\gamma^{\kappa+1}_{ij-1} + F_{10}\gamma^{\kappa+1}_{ij} - F_9\gamma^{\kappa+1}_{ij+1} = -F_4\gamma^{*}_{i-1j} + F_5\gamma^{*}_{ij} - F_6\gamma^{*}_{i+1j} \qquad (5.85b)$$

where

$$F_{10} = \frac{2}{\Delta\tau} + \frac{2F_3}{(\Delta Z)^2}$$

Eqn (5.85b) is an M-1 tri–diagonal systems each having N-1 equations. So for each index i, $1 \le i \le M-1$ eqn (5.85b) is solved for the final values at $\tau = \tau+\Delta\tau$, $\gamma^{\kappa+1}_{i1}, \gamma^{\kappa+1}_{i2}, \ldots\ldots, \gamma^{\kappa+1}_{iN-1}$.

The same procedure is applied to the energy equation whereby the final pair of equations is reached

$$Ft_4\theta^{*}_{i-1j} + Ft_5\theta^{*}_{ij} + Ft_6\theta^{*}_{i+1j} = Ft_7\theta^{\kappa}_{ij-1} + Ft_8\theta^{\kappa}_{ij} - Ft_9\theta^{\kappa}_{ij+1} \qquad (5.86a)$$

and

$$-Ft_7\theta^{\kappa+1}_{ij-1} + Ft_{10}\theta^{\kappa+1}_{ij} - Ft_9\theta^{\kappa+1}_{ij+1} = -Ft_4\theta^{*}_{i-1j} + Ft_5\theta^{*}_{ij} - Ft_6\theta^{*}_{i+1j} \qquad (5.86b)$$

where

$$Ft_4 = F_4$$

$$Ft_5 = F_5$$

$$Ft_6 = - F6$$

$$Ft_7 = \frac{Ft_2}{2\Delta Z} + \frac{Ft_3}{(\Delta Z)^2}$$

$$Ft_8 = \frac{2}{\Delta\tau} - \frac{2Ft_3}{(\Delta Z)^2}$$

$$Ft_9 = \frac{Ft_3}{(\Delta Z)^2} - \frac{Ft_2}{2\Delta Z}$$

$$Ft_{10} = \frac{2}{\Delta\tau} + \frac{2Ft_3}{(\Delta Z)^2}$$

and

$$Ft_2 = \frac{dZ}{d\tau}$$

$$Ft_3 = \frac{F_3}{Le}$$

Gauss elimination technique was used to solve the tri–diagonal systems (5.85a), (5.85b), (5.86a), and (5.86b).

At a given location, X, both γ and θ oscillate with time at a fixed amplitude and with the same frequency as that of the wave. The amplitude of oscillation diminishes with increasing X as the driving forces $c_{eq} - c_i$ and $T_{eq} - T_i$ decrease with the length. The amplitude of the concentration variation is larger than that of the temperature as the

effect of waves on mass transfer is larger than their effect on heat transfer.

The results are presented as non–dimensional concentration (γ) and temperature (θ) averaged over the film thickness ($h(\varepsilon)$ in the case of wavy flow and h_0 in the smooth film) and over one complete periodical time. The latter is calculated from the following sequence :

The wavelength, $\lambda = \dfrac{2\ \pi\ h_0}{n}$

the wave velocity, $v_w = \omega\, v_0$

the periodical time, $t_w = \dfrac{\lambda}{v_w} = \dfrac{2\ \pi\ h_0}{n\ \omega\ v_0}$

the non–dimensional periodical time, $\tau_w = \dfrac{D\ t_w}{h_0^{\,2}} = \dfrac{2\ \pi}{n\ Pe\ \omega}$

This non–dimensional periodical time, τ_w, was divided into a one hundred small $\Delta\tau$'s and as mentioned above the solution was averaged over the whole period.

Due to the limitations of the resource sharing on the computing facility, the solution could not be obtained as a continuous field and the X, Z, τ domain had to be broken into segments along the X–axis with only the values at the end of each segment stored and used as inlet conditions to the next one. The segment configuration is illustrated by fig (5.4).

In this analysis ΔZ and ΔX were typically 0.01 and 2E-8 respectively and the solution needed, on average, 24 hours of process time on the VAX main frame computer.

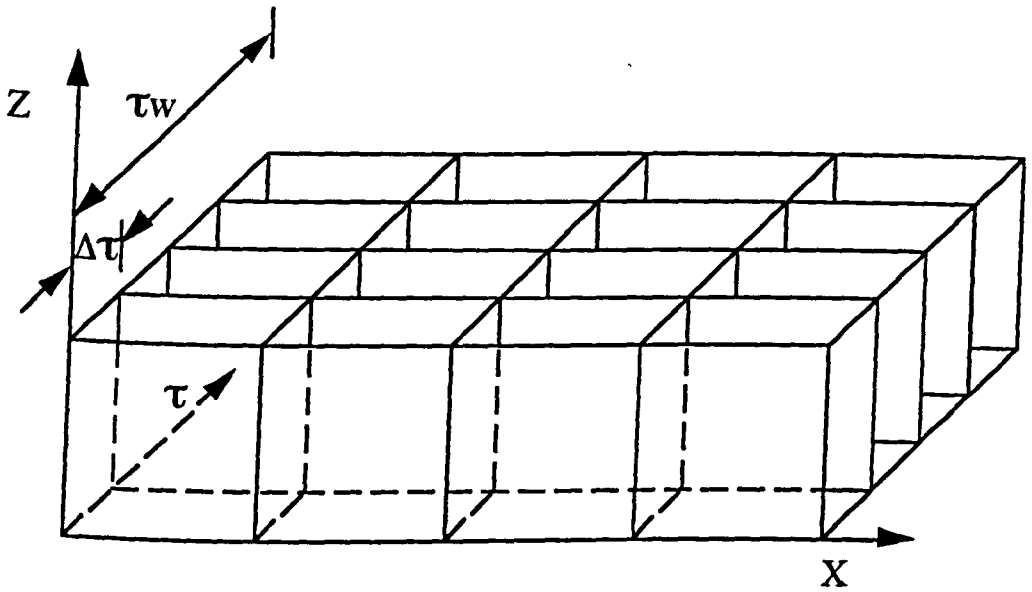

Fig (5.4)

The segment configuration

5.3–Results and Discussion :

5.3.1–Improvement of Concentration and Temperature :

The results present a comparison between the smooth and wavy flows in terms of the average γ and θ defined above. The Reynold's Number and the Schmidt Number were taken to be 100 and 500 respectively.

Figs (5.5) and (5.6) show the relative improvements of mass and heat transfer of the wavy flow over the smooth one, i.e., a higher comparative concentration and lower comparative temperature. The improvement is greater in concentration than in temperature, which agrees with the published data [13], [36]. This is explained by the fact that the mass is transferred across the gas liquid interface where the

waves have greater effect, while heat is transferred across the solid wall from the solution to the cooling medium where the effect of waves is at minimum. The concentration curves rise gradually towards equilibrium while the temperature curves rise steeply at the beginning due the rapid absorption and the heat release associated with it, then they start to cool down after reaching a maximum and decay gradually towards the equilibrium.

5.3.2–Effect of the Heat of Absorption and Lewis Number :

It is evident from figs (5.7) to (5.10) that the concentration improves when decreasing the heat of absorption, Ha, and increasing the Lewis Number, Le. The figures also show that while the temperature increases with increasing Ha, it reacts in a mixed way to Le. The low Le curves rise sharply to high temperature peaks before falling rapidly to low values. This is explainable by the fact that low Le means higher thermal diffusivity which means that the change in temperature travels quicker across the absorbent's film, therefore resulting in sharp slopes. In practice higher concentrations and lower temperatures are desirable which suggests the desirability of lower Ha and higher Le. However, in context of the scope of this work, the effect on the refrigeration capacity needs to be addressed. Ibrahim and Vinnicombe [59] stated that the refrigeration capacity is more strongly proportional to Ha than it is to Le and it is dependant on Le only by the dependency of Le on the concentration variation. They concluded that although increasing Ha will decrease the concentration variation its net effect will be to increase the refrigeration capacity.

The effect of Ha and Le on smooth flows is the same as their effect on wavy flows. This is illustrated by figs (5.11) to (5.14) where the concentration and temperature are plotted for varying Ha and Le in a smooth flow condition.

The independent increase and decrease of Ha and Le is not, in fact, possible as they are both properties of the absorbent at given conditions and are, therefore, interrelated. Eqn (5.11) states that

$$Ha = \frac{\rho\ D\ \Delta h}{K}\ \frac{c_{eq} - c_i}{T_{eq} - T_i}$$

and from the definition of thermal diffusivity

$$\alpha = \frac{k}{\rho\ C_p}$$

so it can be written that

$$Ha = \frac{\Delta h}{C_p}\ \frac{c_{eq} - c_i}{T_{eq} - T_i}\ Le$$

i.e., Ha = f(Le)

This direct proportionality, which means that a higher Le will produce a higher Ha, is fortunate from the refrigeration point of view since, in the light of the findings of Ibrahim and Vinnicombe [59] and the findings of this work, a higher Ha and a higher Le are desirable.

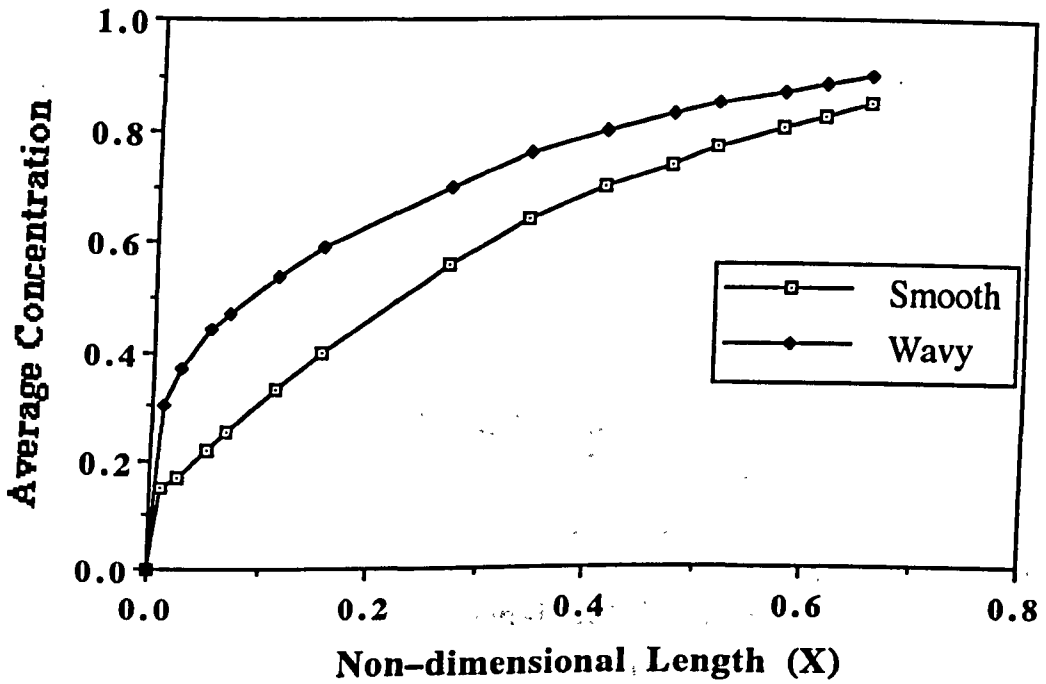

Comparison of wavy and smooth concentration
Re = 100, Ha = 0.1, Le = 0.01

Fig (5.5)

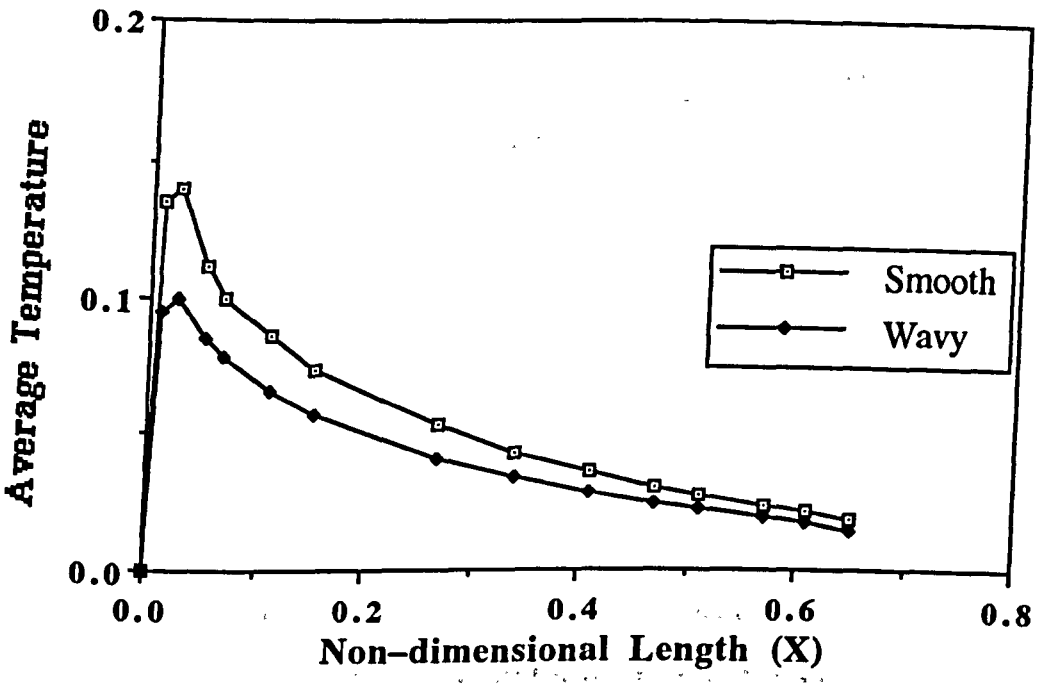

Comparison of wavy and smooth temperature
Re = 100, Ha = 0.1, Le = 0.01

Fig (5.6)

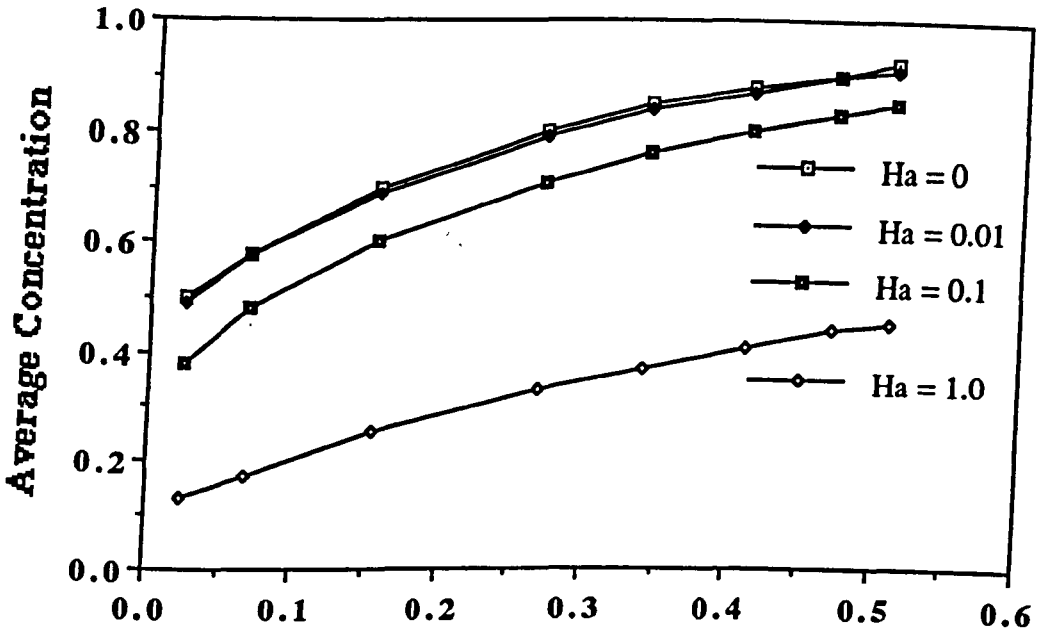

Variation of concentration with Ha for wavy flow
Re = 100, Le = 0.01

Fig (5.7)

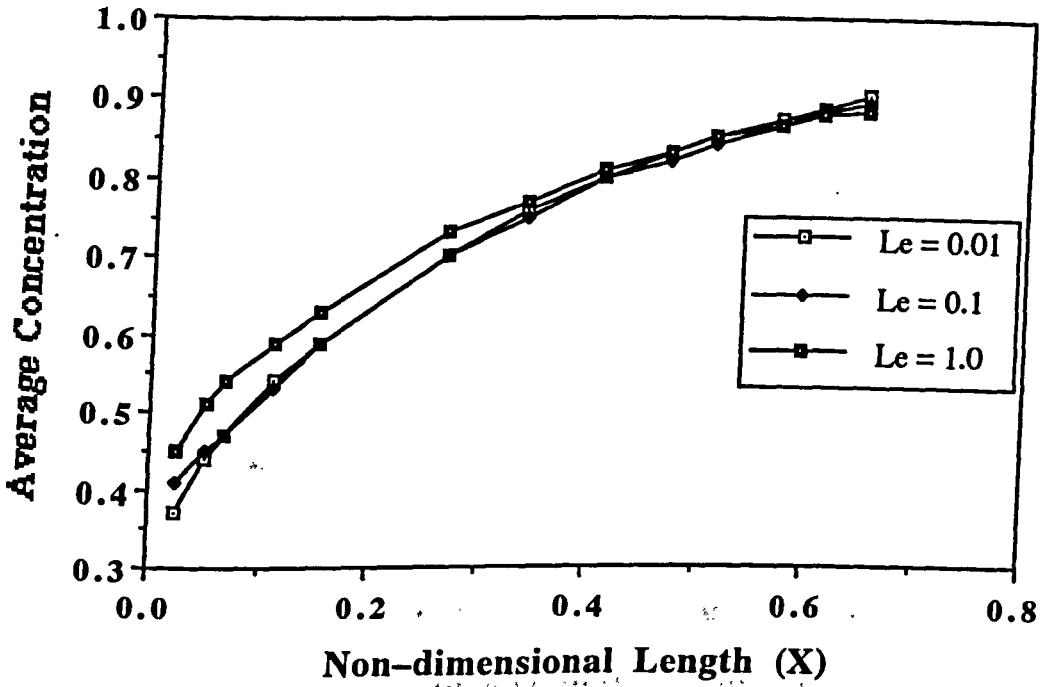

Variation of concentration with Le for wavy flow
Re = 100, Ha = 0.1

Fig (5.8)

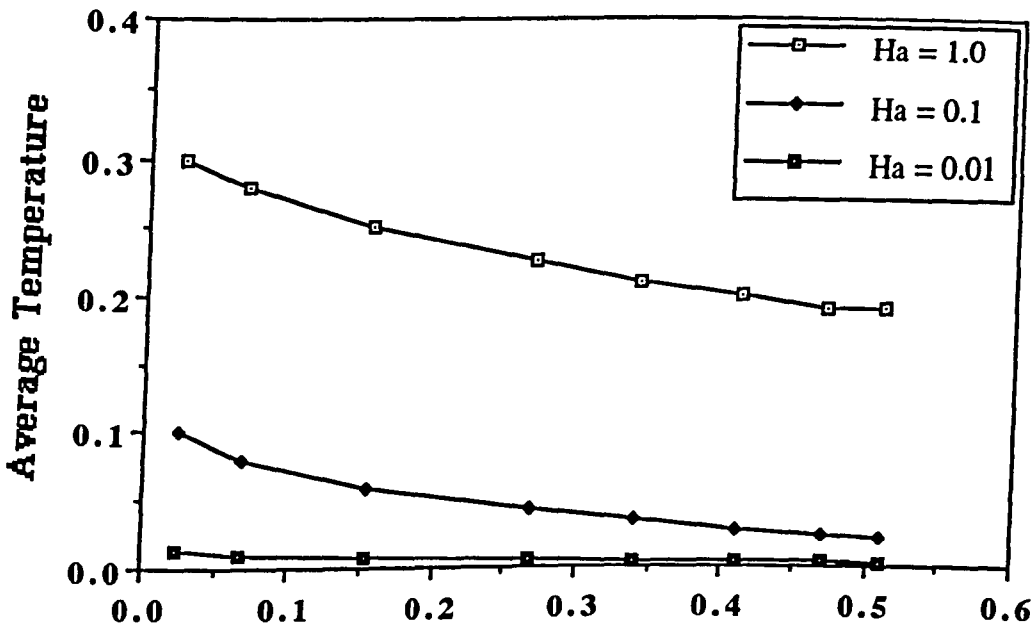

Variation of temperature with Ha for wavy flow
Re = 100, Le = 0.01

Fig (5.9)

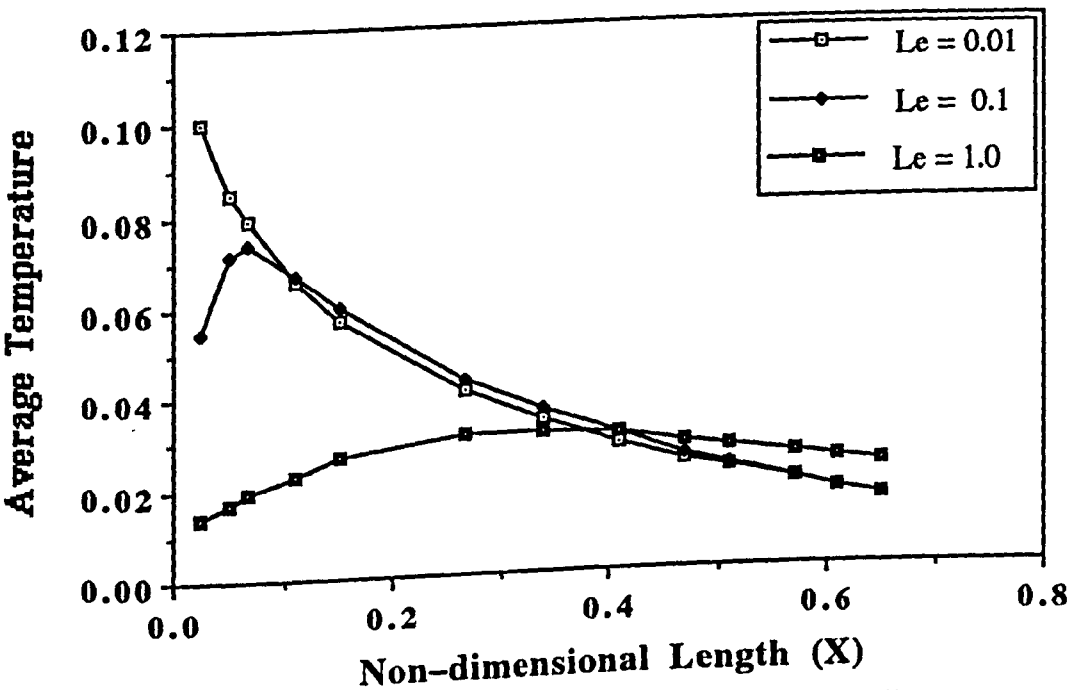

Variation of temperature with Le for wavy flow
Re = 100, Ha = 0.1

Fig (5.10)

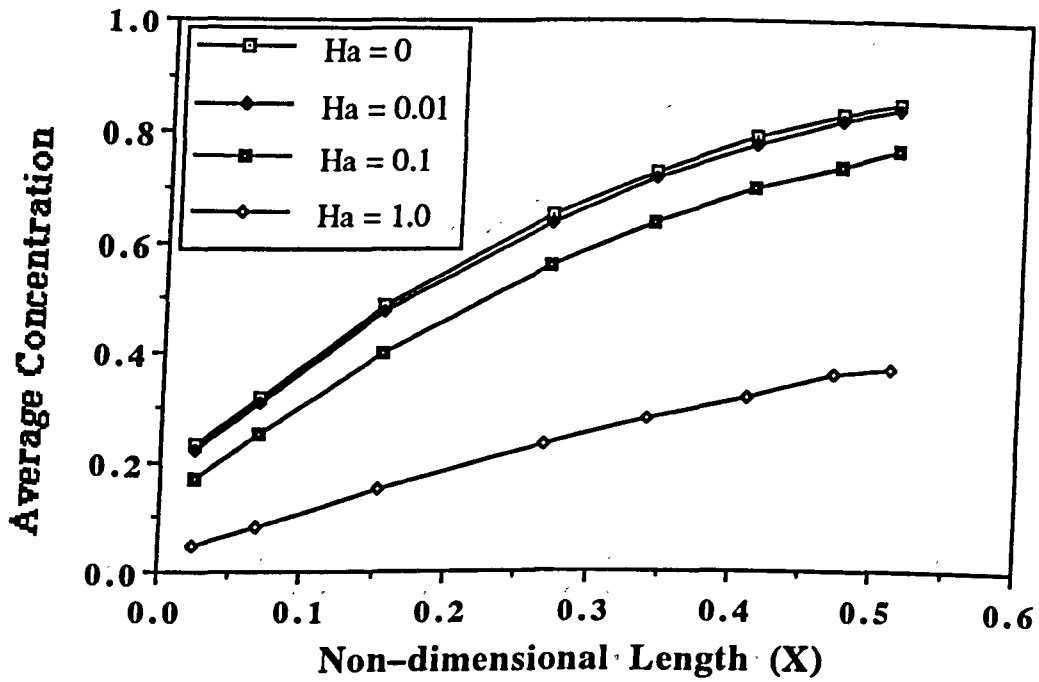

Variation of concentration with Ha for smooth flow
Re = 100, Le = 0.01

Fig (5.11)

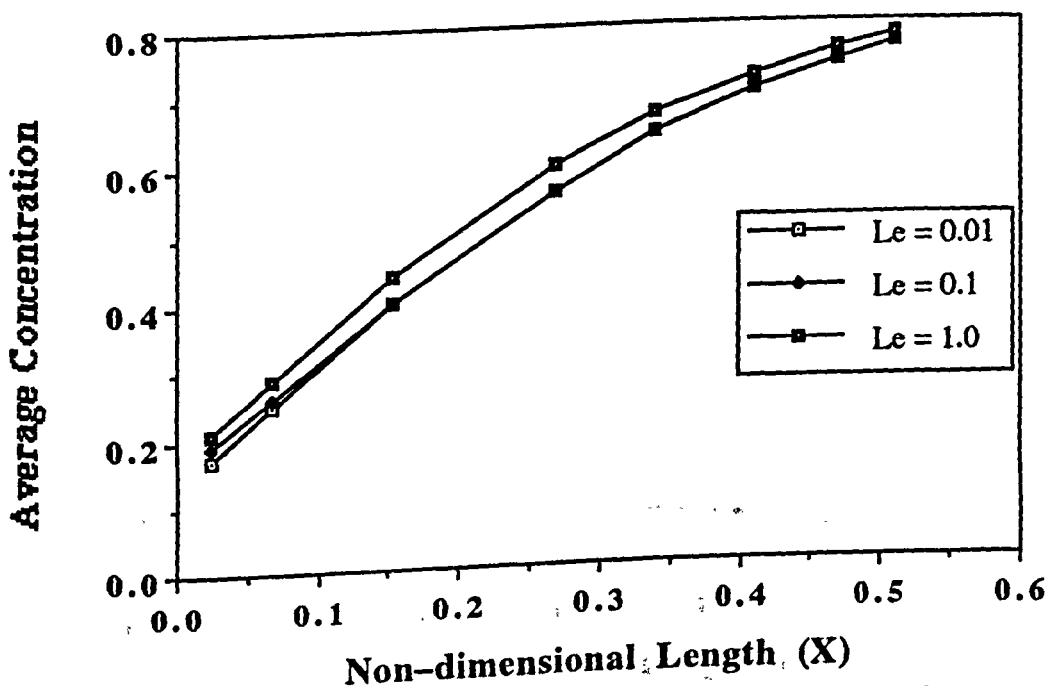

Variation of concentration with Le for smooth flow
Re = 100, Ha = 0.1

Fig (5.12)

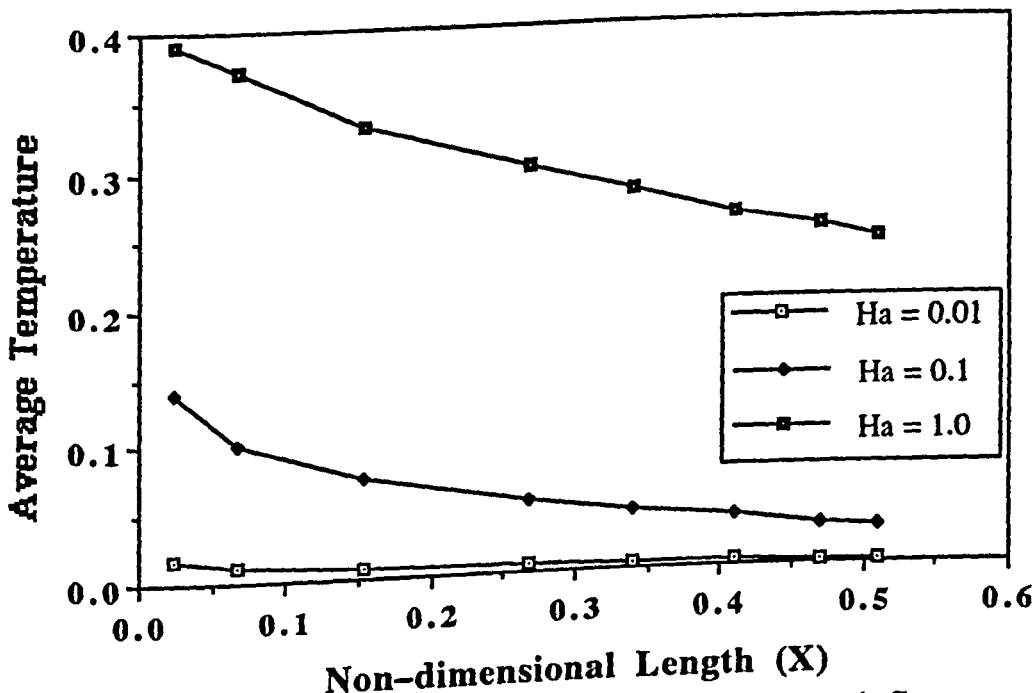

Variation of temperature with Ha for smooth flow
Re = 100, Le = 0.01

Fig (5.13)

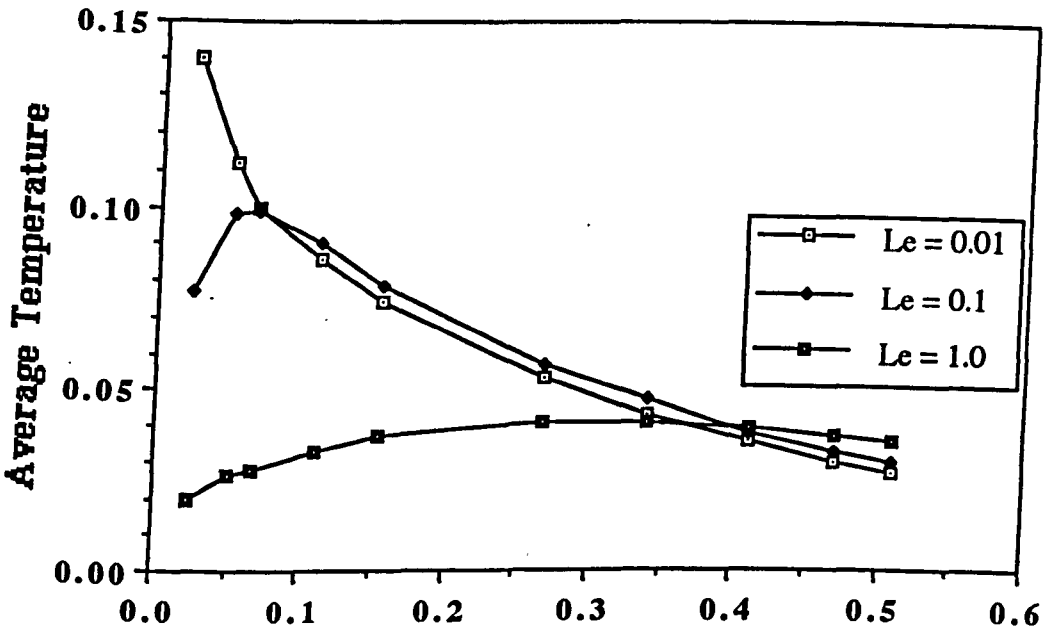

Variation of temperature with Le for smooth flow
Re = 100, Ha = 0.1

Fig (5.14)

5.3.3–Velocity Profile :

To investigate the possibility of the existence of circulation currents under the assumption of uniform, two dimensional waves, Penev et al [24] found the trajectories of the liquid element in a coordinate system travelling downstream at the velocity of the flow. Under this system of coordinates the differential equation of the trajectories is

$$\frac{1}{h_0}\frac{dy}{d\varepsilon} = [\acute{a}_1(\varepsilon)\frac{1}{2}(\frac{y}{h_0})^2 + \acute{a}_2(\varepsilon)\frac{1}{3}(\frac{y}{h_0})^3]/[\omega - a_1(\varepsilon)\frac{y}{h_0} - a_2(\varepsilon)(\frac{y}{h_0})^2] \qquad (5.87)$$

and when integrated gives :

$$a_1(\varepsilon)\frac{1}{2}(\frac{y}{h_0})^2 + a_2(\varepsilon)\frac{1}{3}(\frac{y}{h_0})^3 - \omega(\frac{y}{h_0}) = \text{constant} \qquad (5.88)$$

which is a family of tortuous unclosed curves rarefying under the crests of the wave and condensing in the dents, i.e., no circulation hence no mixing or surface renewal. See fig (5.15).

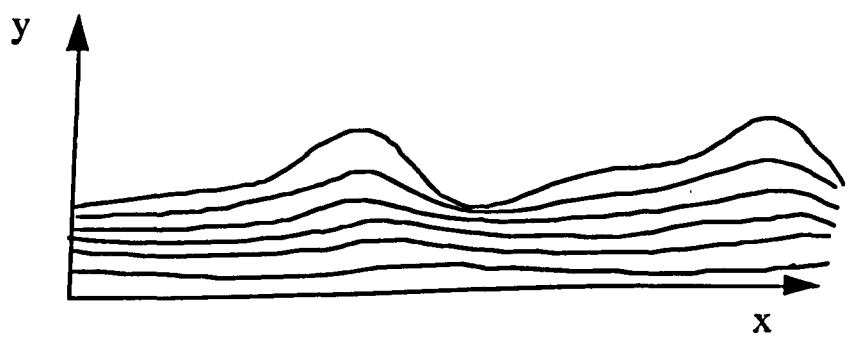

Fig (5.15)

Trajectories of liquid elements

5.4 Conclusion :

The analysis of the effect of absorbent's waves on the heat and mass transfer carried out in this chapter supports the hypothesis that at low Reynold's Number the improvement of concentration and temperature is not due to the mixing effect of waves, since the velocity profile used denies such possibility, but rather due to the vertical component of velocity (which is absent in smooth flows) and the convection associated with it. The effects of Ha and Le on the mass and heat transfer were studied and it was found that a lower Ha and a higher Le result in a better concentration variation. However, for a higher refrigeration capacity a higher Ha is recommended.

5.4 Conclusion :

The analysis of the effect of absorbent's waves on the heat and mass transfer carried out in this chapter supports the hypothesis that at low Reynold's Number the improvement of concentration and temperature is not due to the mixing effect of waves, since the velocity profile used denies such possibility, but rather due to the vertical component of velocity (which is absent in smooth flows) and the convection associated with it. The effects of Ha and Le on the mass and heat transfer were studied and it was found that a lower Ha and a higher Le result in a better concentration variation. However, for a higher refrigeration capacity a higher Ha is recommended.

Nomenclature :

A	dimensionless wave amplitude ; $A = (h_{max} - h_0) / h_0$
a_k	function of ε
c	mass concentration of the liquid (kg/kg)
c_{eq}	equilibrium concentration (kg/kg)
c_i	inlet concentration (kg/kg)
c_0	initial concentration (kg/kg)
C_p	heat capacity (kJ/kg °C)
D	diffusion coefficient (m^2/s)
Ha	dimensionless heat of absorption
h_0	average film thickness (m)
$h(\varepsilon)$	local film thickness (m)
$H(\varepsilon)$	dimensionless film thickness ; $H(\varepsilon) = \frac{h(\varepsilon)}{h_0}$
K	thermal conductivity (W/m °C)
Le	Lewis Number ; $Le = \frac{D}{\alpha}$
n	dimensionless wave number ; $n = 2 \pi h_0 / \lambda$
Pe	Pecklet Number ; $Pe = \frac{v_0 \, h_0}{D}$
t	time (s)
t_w	periodical time (s)
T	local temperature (°C)
T_{eq}	equilibrium temperature (°C)
T_i	inlet temperature (°C)
T_0	initial temperature (°C)
T_w	wall temperature (°C)
v_0	average velocity of the liquid (m/s)

v_x	local velocity of the liquid along the x axis (m/s)
V_x	dimensionless velocity of the liquid in the direction of x
v_y	local velocity of the liquid along the y axis (m/s)
V_y	dimensionless velocity of the liquid in the direction of y
X, Y	dimensionless x and y coordinates respectively
Z	dimensionless vertical coordinate in the wavy field

Greek :

α	thermal diffusivity (m^2/s)
γ, θ	dimensionless concentration and temperature respectively
Δh	vapour's specific heat of absorption (kJ/kg)
ε	parameter ; $\varepsilon = (x - w\, u_0 t) / h_0$
λ	wave length (m)
ν	kinematic viscosity of the liquid (m^2/s)
τ	dimensionless time ; $\tau = \frac{D\, t}{h_0^2}$
τ_w	dimensionless periodical time
ρ	density (kg/m^3)
ω	dimensionless phase velocity

6–Effect of Air Entrainment on the Absorber's Performance:

6.1–Introduction :

It is generally believed that vapour absorption systems must be "air tight", especially systems with sub–atmospheric working pressure e.g $LiBr/H_2O$ systems where air entrainment is a risk and the performance is seriously affected by the inward leakage [41]. In this chapter the effect of such a leakage on the performance of the system's absorber is analyzed.

6.2–Analysis :

To understand the mechanism by which the presence of a non–condensable gas affects the performance of a falling film type absorber, an element of such absorber is shown in fig (6.1).

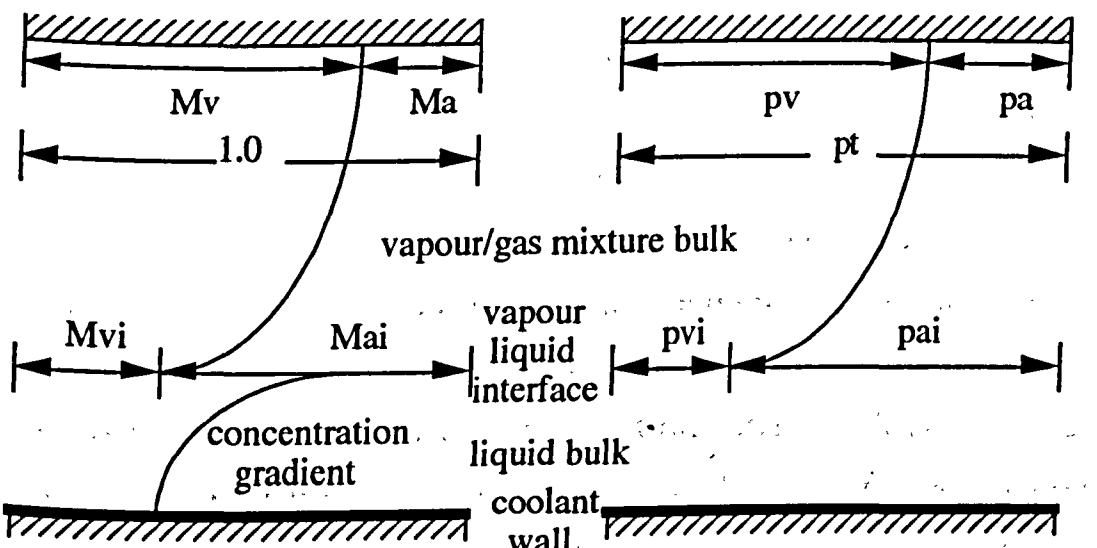

Fig (6.1) Absorber's element

Fig (6.1a) shows the gas and refrigerant vapour mass fractions at the bulk of the vapour/gas mixture and at the vapour/liquid interface and the concentration gradient of the liquid refrigerant in the absorbent. Fig (6.1b) shows the partial pressures of the gas and refrigerant vapour at the same zones.

When no gas is present then $p_a = 0$ and p_v is constant every where at the evaporator condition. In this case there is no resistance in the vapour to absorption and the only resistance is that in the actual absorbent. However, when a gas is present there will be resistance in the vapour and in the absorbent and the total resistance to absorption will be the sum of these two. Thus it is expected that the presence of a non–condensable gas will reduce the performance

Initially, and before any absorption takes place no mass or partial pressure gradients exist in the bulk of the vapour/gas mixture and the values of the mass fractions and partial pressures in the bulk equal those at the interface. Once the first quantity of vapour is absorbed (at the interface), the mass fraction of the refrigerant vapour at the interface (M_{vi}) and its partial pressure (p_{vi}) drop and mass and pressure gradients develop, and the amount of absorption will depend on these gradients. As the liquid travels downstream it becomes more concentrated with refrigerant and its capacity to absorb more vapour decreases, so the vapour's mass fraction at the interface (M_{vi}) increases and so does its partial pressure (p_{vi}), provided that the refrigerant vapour is constantly replenished. This continues until the solution reaches the equilibrium state and the values of M_{vi} and p_{vi} are restored once again to their initial values.

In this chapter a method of calculating the effect of air entrainment on the performance of the absorber of a $LiBr/H_2O$ refrigeration system is undertaken. The procedure consists of solving the simultaneous equations obtained from the mass and energy balance of an absorber's element and the equilibrium state assumed at the vapour/liquid interface.

6.2.1–Mass Balance :

The mass flow rate of the water vapour from the bulk of the vapour/gas mixture to the interface is proportional to the gradient of the mass fraction that exists in the vapour mixture i.e.,

$$\dot{m}_V = \rho_V G_V (M_V - M_{Vi}) \qquad (6.1)$$

where G_V is the mass transfer coefficient of the vapour, and the mass fractions M_V and M_{Vi} are found from the equations :

$$M_V = \frac{p_V N_V}{p_V N_V + p_a N_a} \qquad (a)$$

$$M_{Vi} = \frac{p_{Vi} N_V}{p_{Vi} N_V + p_{ai} N_a} \qquad (b)$$

The same mass flow is absorbed by the absorbent and is proportional to the concentration gradient that exists across the liquid film i.e.,

$$\dot{m}_V = \rho_l G_{li} (C_a - C_i) \qquad (6.2)$$

where G_{li} is the mass transfer coefficient of the liquid at the interface and the concentrations C_a and C_i are defined as the mass ratios of the LiBr in the absorbent in the liquid bulk and at the interface respectively. Equating the two vapour mass flow rates gives the first equation i.e.,

$$\rho_v G_v (M_v - M_{vi}) = \rho_l G_{li} (C_a - C_i) \quad (6.3)$$

6.2.2–Energy Balance :

The enthalpy balance for an element at the interface yields

$$F_v (T_v - T_i) + \dot{m}_v h_{fg} = F_{li} (T_i - T_a)$$

where F_{li} and F_v are the heat transfer coefficients from the bulk of the solution to the interface and from the interface to the bulk of the vapour/gas mixture respectively. The free convection term $F_v(T_v - T_i)$ is very small compared to the enthalpy of phase change [60]. In fact, for the particular case of $LiBr/H_2O$ absorber under consideration the ratio of the two terms does not exceed 1%. The free convection term is therefore ignored and the enthalpy balance consequently becomes :

$$\dot{m}_v h_{fg} = F_{li} (T_i - T_a) \quad (6.4)$$

6.2.3–Interface Equilibrium :

Assuming equilibrium state at the interface the saturated vapour pressure will be related to the temperature by [50]

$$\log p_{vi} = 7.05 - \frac{1596.5}{T_{vi}} - \frac{104095.5}{T_{vi}^2} \quad (6.5)$$

where ; p_{vi} is in units of kPa and T_{vi} is in units of K.

Also at the interface

$$T_{vi} = f(C_i, T_i) \quad (6.6)$$

which is the double quadratic fit of eqn (3.31).

* These equations together with equations (a) and (b) of page 149 and the fact that $P_{vi} + P_{ai} = P_t$ enable the calculation of the unknowns: M_v, M_{vi}, C_i, T_i, P_{vi}, P_{ai}, T_{vi},

6.2.4–Calculation of the Transfer Coefficients :

The heat and mass transfer coefficients can be obtained from the appropriate analytical or experimental data. In this case the free convection heat transfer rate in the vapour Fv was found from the Rayleigh equation [49] and from it the vapour's mass transfer coefficient G_V was calculated using the Lewis analogy. G_{li} and F_{li} were respectively calculated from Sherwood and Nusselt Numbers taken from [26].

6.2.5–Solution :

The set of governing equations is :

$$\rho_v G_V (M_V - M_{vi}) = \rho_l G_{li} (C_a - C_i)$$

$$\dot{m}_V h_{fg} = F_{li} (T_i - T_a)$$

$$\log p_{vi} = 7.05 - \frac{1596.5}{T_{vi}} - \frac{104095.5}{T_{vi}^2}$$

$$T_{vi} = f(C_i, T_i)$$

These governing equations were incorporated and solved by the programme simulation of the smooth falling film type absorber described in chapter 4. The solution enabled the assessment of the effect of different values of air partial pressure (p_a) and mass transfer coefficient of the vapour (G_V) on the performance of the absorber characterized in the following discussion by the overall effectiveness already introduced in chapter 4 and defined by :

$$E_O = \frac{m_V}{m_{Ve}}$$

where m_V is the total amount of vapour absorbed in the absorber, and m_{Ve} is the maximum possible amount of absorption.

6.3–Results and Discussion :

6.3.1–Absorber's Performance :

In this analysis the effect of the partial pressure of air (p_a) and the mass transfer coefficient of the vapour (G_V) on the performance of the absorber is discussed.

Typical value of the partial pressure of air (p_a) in absorption refrigeration systems is about 0.1 mm Hg (0.013 kPa) [61]. The mass transfer coefficient of the vapour (G_V) for this case, which is representative of the average working conditions in LiBr/H_2O systems, is calculated [49] at 0.006 m/s. The results shown in the following discussion are obtained for values of p_a and G_V at and around those values to cover a realistic range of working conditions.

The effect of p_a on the performance of the absorber is shown in fig (6.2) where the partial pressure of air is varied around the value of 0.013 kPa (which is typical for refrigeration systems [61]) between 0 and 1 kPa (the corresponding values of air mass fraction are shown in brackets) and the overall effectiveness is plotted along the NTU axis. The effect is immediately evident from the figure where the presence of only 2% air (Ma = 0.02) causes a remarkable reduction in effectiveness, and further increase in p_a decreases the effectiveness further.

As for the effect of G_V on the performance, this is shown in fig (6.3) where the overall effectiveness is calculated and plotted for three values of G_V starting with a low value of 0.002 m/s and ending with a high 0.04 m/s which is calculated [49] for a forced convection condition assuming the vapour is circulated by a fan at a speed of 10 m/s. The 0.006 m/s value in between these two extremes is the value calculated for the natural convection conditions of this case. As expected, the figure clearly shows that the effectiveness is improved with the increase in G_V with a very significant improvement due to the introduction of the forced convection mass transfer in the vapour/gas mixture region.

It can be seen that the performance of the absorber could be improved by : (a) decreasing the amount of air, i.e., decreasing p_a by creating and maintaining higher levels of vacuum, or (b) increasing the mass transfer coefficient of the vapour G_V by introducing a forced convection device in the absorber chamber e.g. a fan. This means that the same values of effectiveness could be achieved by different p_a–G_V combinations. This is illustrated in figures (6.4), (6.5), (6.6), and (6.7) where the overall effectiveness is plotted against p_a for the three different values of G_V at NTU = 1, 10, 40, and 80 respectively. The choice of any particular p_a–G_V combination to achieve certain effectiveness will depend on the optimum economy and design. For example it is evident from the figures that the values of effectiveness obtained in the presence of air at partial pressure of 1 kPa and G_V of 0.006 m/s are comparable to those obtained at an air partial pressure of 0.013 kPa and a mass transfer coefficient of 0.002 m/s. The choice of which combination will be a matter of optimization since, on one hand, the harder the vacuum the higher the cost of creating and maintaining it,

and on the other hand increasing the vapour's mass transfer coefficient will involve the extra cost of mounting and operating an extra device (a fan) inside the absorber's chamber.

It must be emphasized that the presence of air, or any non–condensable gas, will also affect the performance of the rest of the refrigeration system's components i.e., the evaporator, condenser, and boiler. Thus the effect on the overall performance of the whole system will be larger than that obtained here.

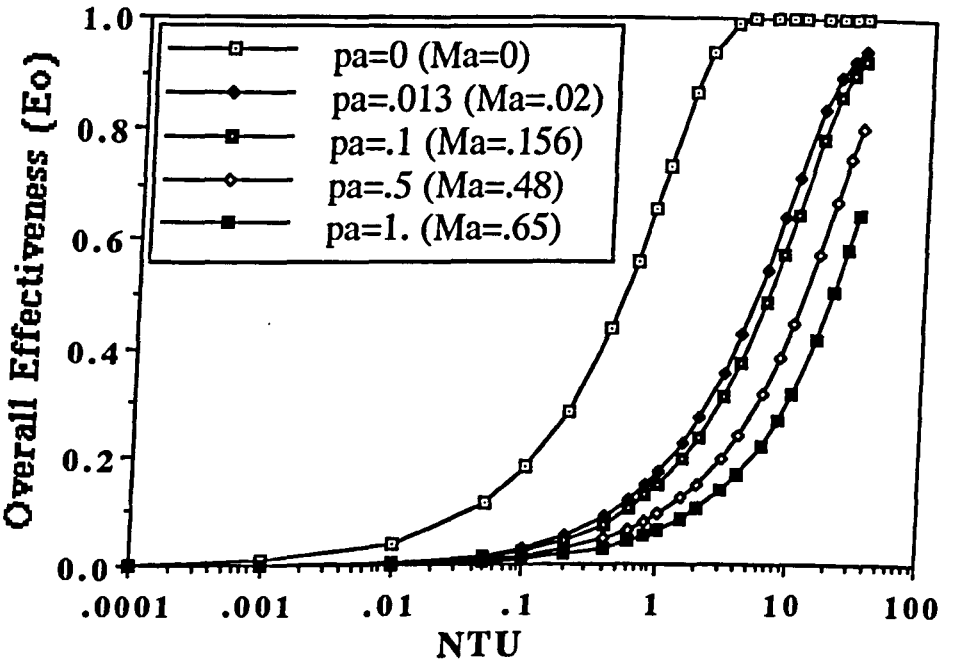

Effect of air on the absorber's performance, Gv = 0.006 m/s

Fig (6.2)

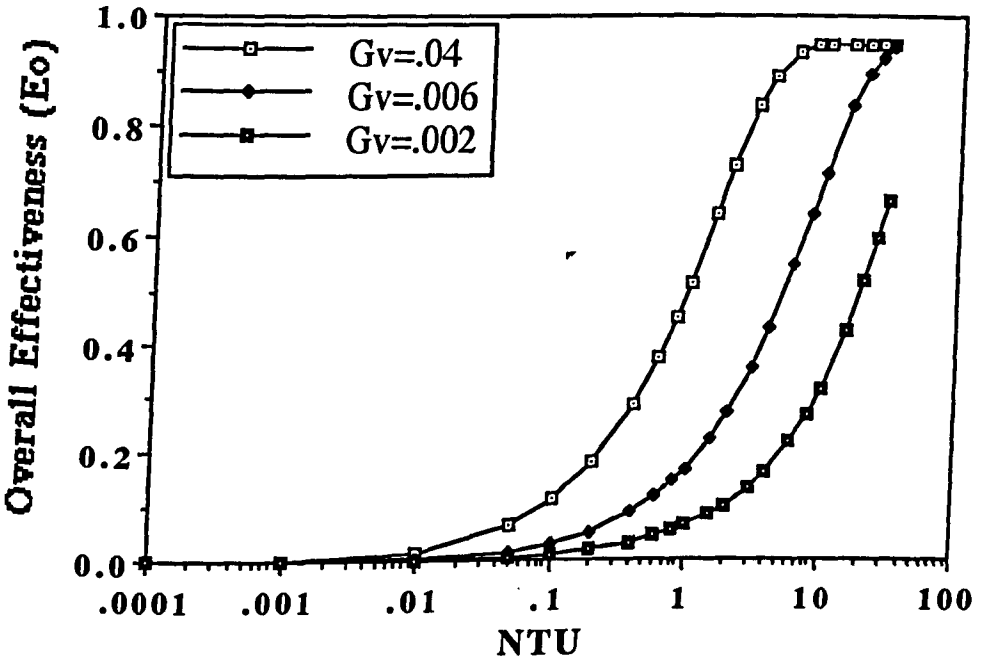

Effect of vapour's mass transfer coefficient on the absorber's performance, pa = 0.013 kPa

Fig (6.3)

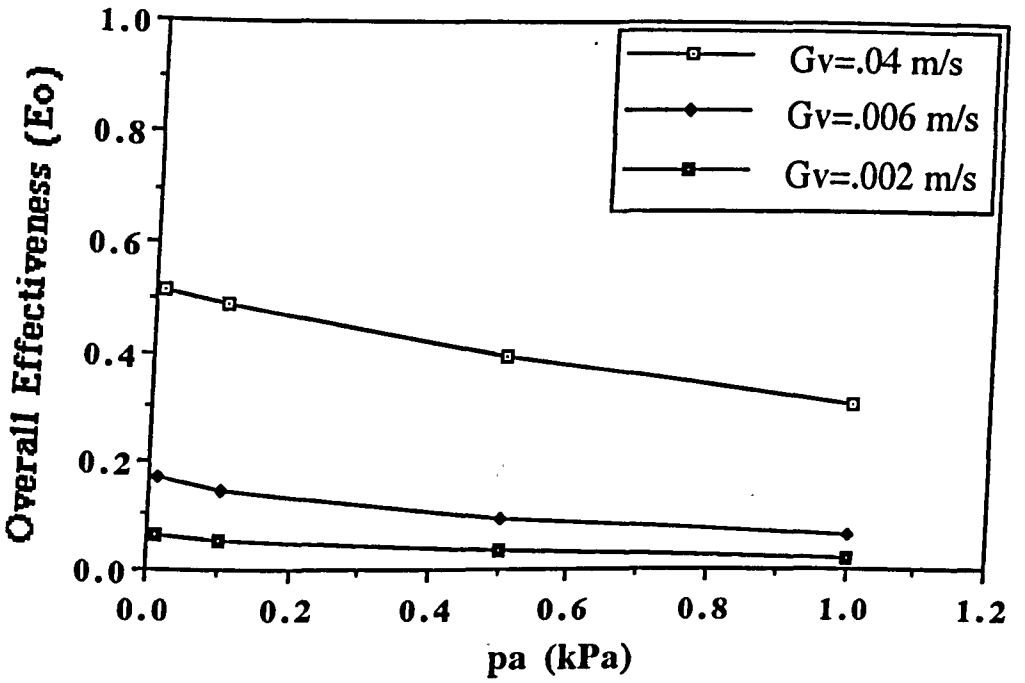

Effect of various pa/Gv combinations on the absorber's performance at NTU=1.

Fig (6.4)

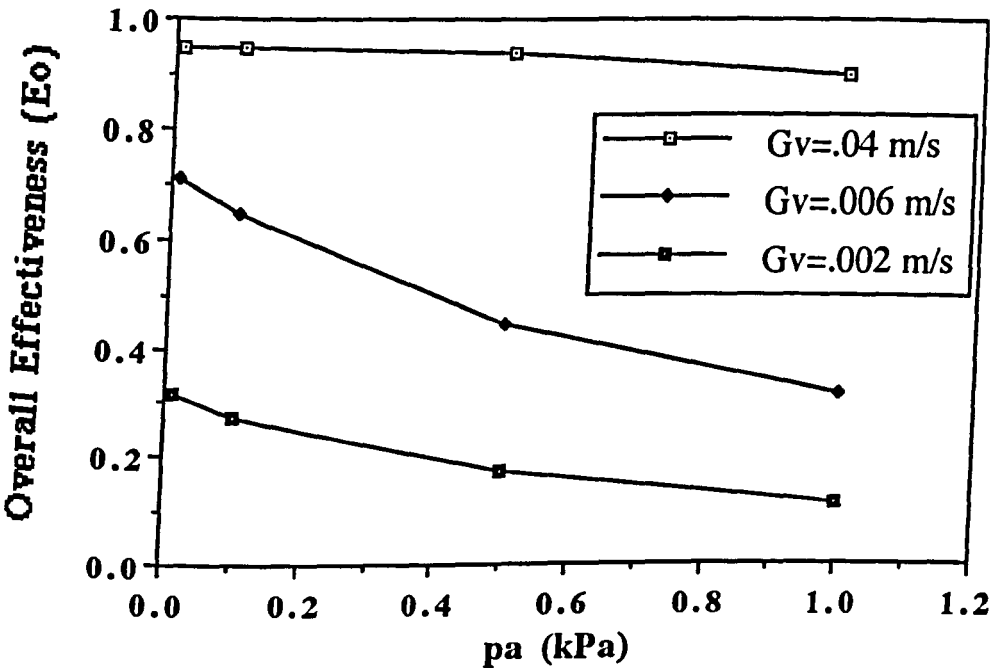

Effect of various pa/Gv combinations on the absorber's performance at NTU=10.

Fig (6.5)

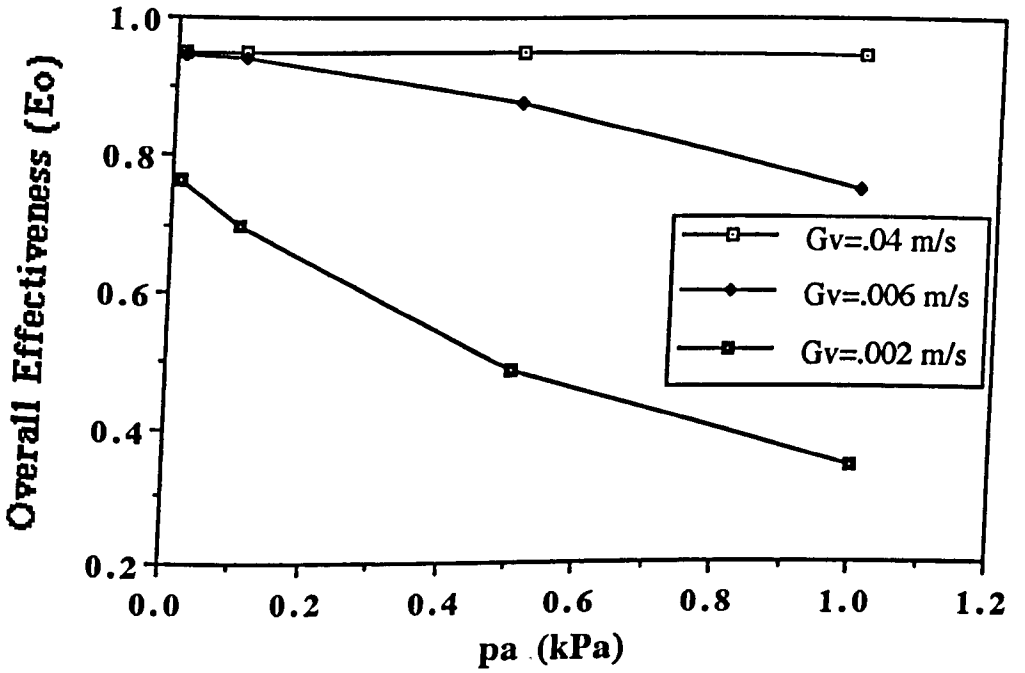

Effect of various pa/Gv combinations on the absorber's performance at NTU=40

Fig (6.6)

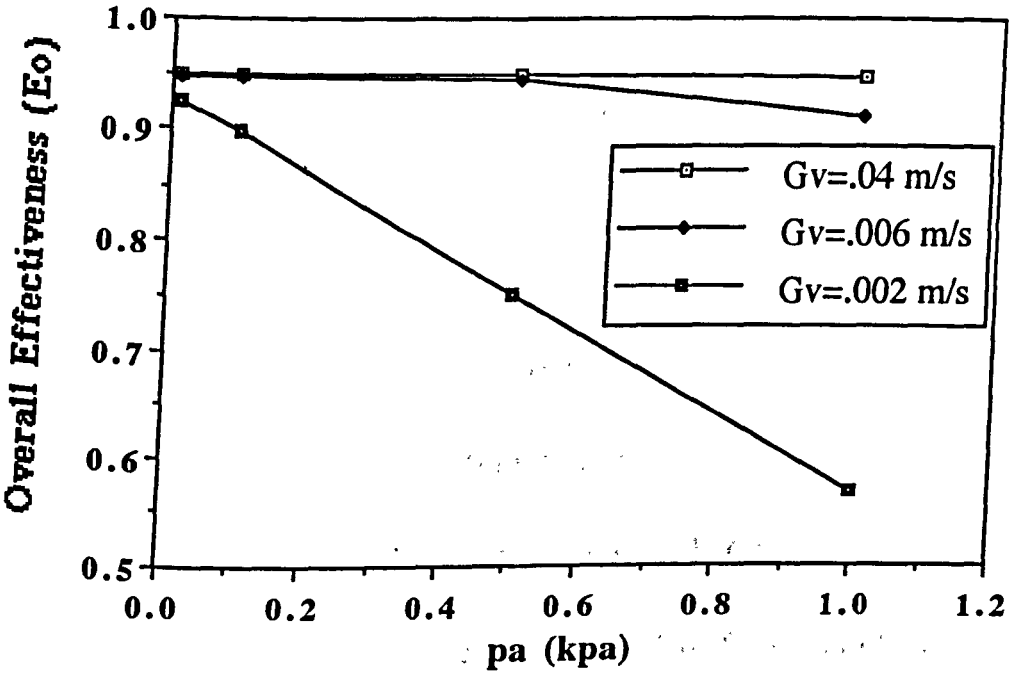

Effect of various pa/Gv combinations on the absorber's performance at NTU=80.

Fig (6.7)

6.3.2–Vacuum Considerations :

Air free absorbers are practically impossible, not only because 100% air tight joints and sealants are nonexistent, but also because an *absolute* vacuum is impossible to create initially, however a pressure of 0.1 mm Hg (0.013 kPa) absolute is considered to be sufficient initial vacuum in the field of refrigeration [61]. Vacuum systems are classified according to their working pressures. One method of classifying that is widely accepted is the following [62] :

Rough vacuum	760 to 1 mm Hg (100 to 0.13 kPa)
Fine vacuum	1 to 1E-3 mm Hg (0.13 to 0.13E-3 kPa)
High vacuum	1E-3 to 1E-6 mm Hg (0.13E-3 to 0.13E-6 kPa)
Very high vacuum	1E-6 to 1E-9 mm Hg (0.13E-6 to 0.13E-9 kPa)
Ultra high vacuum	1E-9 mm Hg and less (0.13E-9 kPa and less)

There are several means by which vacuum is created. Perhaps the most common is the oil sealed rotary pump, this has a vacuum range of about 2E-5 to 5 mm Hg. This was the one used in the experimental part of this work where a vacuum of about 0.1 mbar was achieved. Other devices include vapour pumps where hot vapour is used to eject gases from the system. These have a vacuum level of up to about 1E-7 mm Hg. There is also the molecular pumps with a vacuum capacity of about 1E-6 mm Hg, and there are other types of vacuum pumps beside those mentioned here.

Along with the problem of creating the initial vacuum and keeping air from leaking into the system, there is also the problem of the materials used in the absorber releasing various gases into the absorber's chamber due to chemical reactions, diffusion, etc. which have the same effect as entrained air.

The harder the initial vacuum the more expensive the vacuum pump needs to be and the more costly the operation will be since it requires more power to remove an air molecule at a lower pressure than to remove it at a higher pressure. This limits the degree of the initial vacuum in the absorber and a small amount of air and/or gases will have to be tolerated. Typically, a value of about 0.1 mm Hg (0.013 kPa) is allowed.

6.4–The Platen–Munters System :

This analysis, though concentrated on the effect of air in a $LiBr/H_2O$ system, can in fact be used to assess the effect of any other non–condensable gas in any other absorption system by using the appropriate properties of the gas, refrigerant, and absorbent.

One particular, very interesting, system is the Platen–Munters system where a non–condensable gas is required in the system to satisfy its functionality.

The system was invented by Baltzar Von Platen and Carl Munters in the 1920s. It used hydrogen gas in the evaporator and the absorber of an Aqua–Ammonia absorption cycle to equalize the pressure throughout

the cycle thus eliminating the expansion valves and the solution pump [63].

The system's vertical generator combines the effect of a boiler and a stripping section. The vapour produced in the generator is fed into a combined rectifier and a reflux condenser where it partially condenses to further enrich it before it condenses. The condensate then passes to the evaporator through a U–tube liquid seal. The seal prevents the uncondensed ammonia from getting into the evaporator and increasing its pressure and consequently its evaporating temperature. The seal is protected from being blown off by a rising condenser pressure by a pressure equalising vessel. In the evaporator the liquid ammonia evaporates, rather than boil, into an atmosphere of hydrogen and the vapour is carried away from the surface by diffusion, therefore the name diffusion–absorption system is sometimes used to describe the system. The mixture of ammonia vapour and hydrogen passes through a gas heat exchanger where it cools down the hydrogen coming from the absorber. The ascending vapour mixture counterflows the descending weak solution in the absorber and most of the ammonia vapour is washed away by the solution. The hydrogen passes back to the evaporator, while the strong solution is carried to the top of the generator by the bubble pump.

Obviously, because of the presence of the non–condensable gas, part of the efficiency of the cycle is compromised to satisfy the principle of operation, and to indicate the amount of reduction in the performance of such a system a $LiBr/H_2O$ system with hydrogen gas present in it is considered in the following analysis.

Taking an evaporation temperature of 5 °C and a condensing temperature of 40 °C, the difference of pressure that need to be compensated for by hydrogen is about 6.5 kPa. This value was used in the programme together with the hydrogen properties to obtain the values of the absorber's mass and heat effectivenesses. These were in turn used in the programme that solves for the overall output (described in chapter 3) to obtain the final effect on the heat ratio and compare it to that of the same system with no hydrogen. The results are presented in table (6.1) for two absorber lengths. However, the absorber's length of a real Platen–Munters system will be much less than 10 m.

Absorber's length (m)	Heat ratio	
	H_2 at 6.5 kpa	No H_2
10	.414	.76
20	.550	.79

Table (6.1)

Effect of hydrogen presence on the heat ratio

It is noted that this analysis takes into consideration the effect on the absorber's performance only without regard to the effects on the performance of the evaporator where hydrogen is also present thus the values in the table overestimates the actual heat ratio of the system. The table already shows that there is, in this system, a price to pay for the simplification engendered by using the non–condensable gas.

6.5-Conclusion :

As noted in the literature review, the main body of literature in this area is concerned with the effects of non–condensable gases on pure condensation rather than absorption [42], [43], [44], [45], and [46]. Therefore, it is hoped that the work done in this chapter will provide a suitable analytical approach to understand the problem and to predict the absorber's performance under various levels of vacuum and to optimize this performance by introducing forced convection in the vapour/gas mixture. However, there is much need for experimental validation of the analysis to cover the gap in the literature.

Nomenclature :

C_a	concentration of LiBr at the liquid bulk.
C_i	interface concentration of LiBr.
E_o	absorber's overall effectiveness.
F_v	free convection heat transfer coefficient in the bulk of the vapour/gas mixture ($W/m^2\,°C$).
F_{li}	heat transfer coefficient from the bulk of liquid to the interface ($W/m^2\,°C$).
G_{li}	mass transfer coefficient of the liquid water at the interface (m/s).
G_v	mass transfer coefficient of vapour (m/s).
h_{fg}	specific heat of phase change (kJ/kg).
M_a	mass fraction of air in the bulk of the vapour/gas mixture.
M_{ai}	mass fraction of air at the interface.
M_v	mass fraction of the vapour in the vapour/gas mixture bulk.
$\dot{m}_v$	mass density of the vapour (kg/m^2s).
m_v	total mass of vapour absorbed (kg).
m_{ve}	total mass of vapour absorbed at equilibrium conditions (kg).
M_{vi}	mass fraction of the vapour at the interface.
N_a	molecular mass of air (kmol/kg).
NTU	number of transfer units.
N_v	molecular mass of vapour (kmol/kg).
p_a	partial pressure of air in the bulk of the vapour/gas mixture (N/m^2).
p_{ai}	partial pressure of air at the interface (N/m^2).

p_t	total pressure of the vapour/gas mixture (N/m^2).
p_v	partial pressure of vapour in the bulk of the vapour/gas mixture (N/m^2).
p_{vi}	partial pressure of vapour at the interface (N/m^2).
T_a	temperature of liquid at the bulk (°C).
T_i	temperature of liquid at the interface (°C).
T_v	temperature of vapour in the bulk of the vapour/gas mixture (°C).
T_{vi}	temperature of vapour at the interface (°C).

Greek :

ρ_l	density of liquid (kg/m^3).
ρ_v	density of vapour (kg/m^3).

p_t total pressure of the vapour/gas mixture (N/m^2).

p_v partial pressure of vapour in the bulk of the vapour/gas mixture (N/m^2).

p_{vi} partial pressure of vapour at the interface (N/m^2).

T_a temperature of liquid at the bulk (°C).

T_i temperature of liquid at the interface (°C).

T_v temperature of vapour in the bulk of the vapour/gas mixture (°C).

T_{vi} temperature of vapour at the interface (°C).

Greek :

ρ_l density of liquid (kg/m^3).

ρ_v density of vapour (kg/m^3).

7–The Experimental Work :

7.1–Introduction :

The experimental work was undertaken to further the understanding of vapour absorption systems and to test the validity of the overall simulation described in chapter 3. The work involved building and testing of a complete LiBr/H_2O refrigeration system.

The system, shown photographically in fig (7.1) and schematically in fig (7.2), was built and equipped with various control and measurement devices. It consisted of a boiler, condenser, evaporator, absorber, heat exchanger, and a solution pump, along with two throttle valves, several regulating and shut-off valves, different measuring devices, and pipeworks of different sizes.

Three flow meters were fitted in the three water circuits (condenser, evaporator, and absorber water circuits). Thermocouples were used to measure temperatures around the absorption cycle and the water circuits. The boiler was fitted with an electrical heating element which was connected to a power variac and a voltmeter to control and measure the heat input to the system. The solution concentration was measured at the inlet and outlet of the absorber i.e., at the strong and weak solution points. Pressure was measured at the two pressure levels of the cycle by two vacuum gauges. Detailed description of the components and the measurement devices is given below.

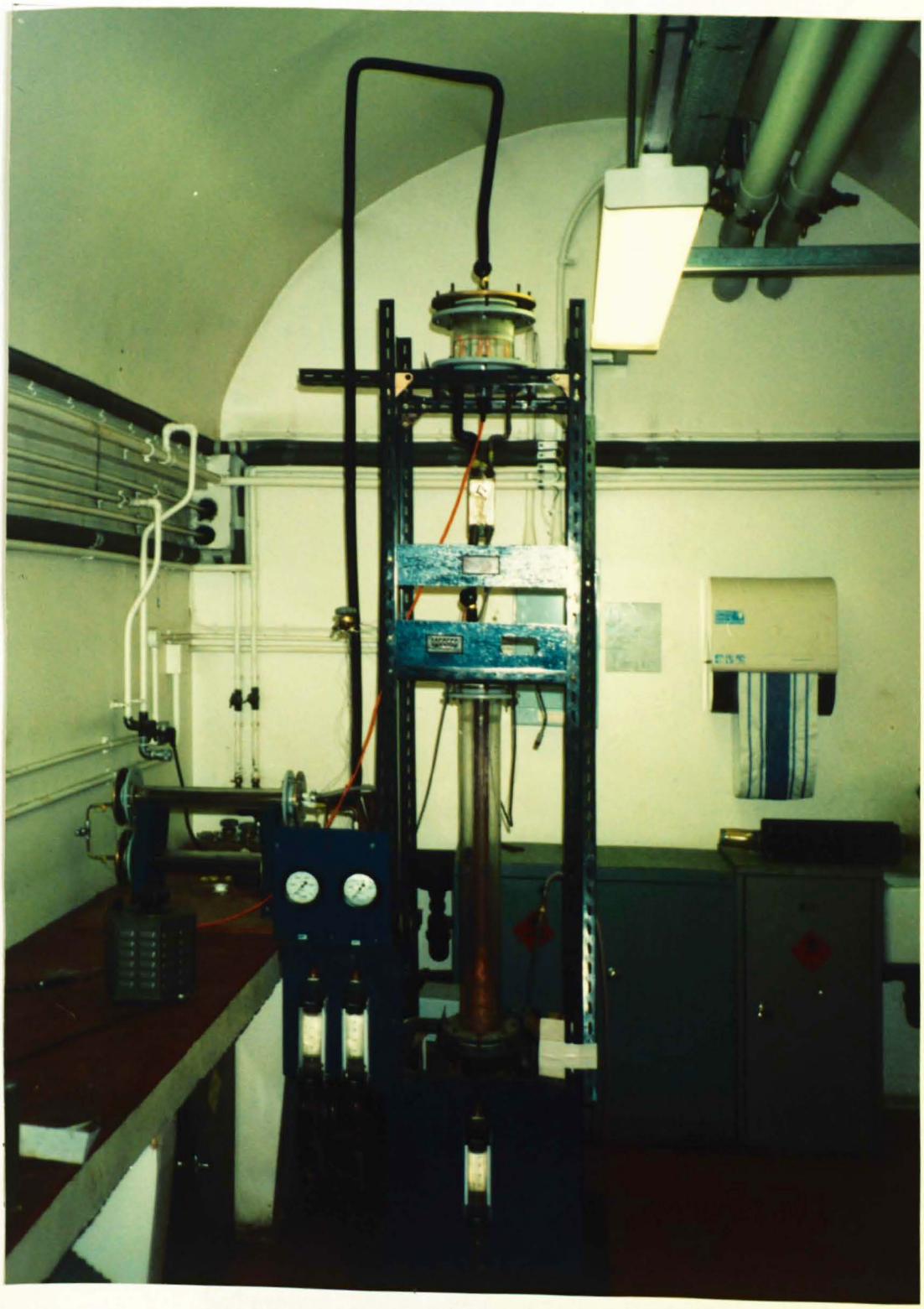

Fig (7.1)

Photograph of the $LiBr/H_2O$ test system

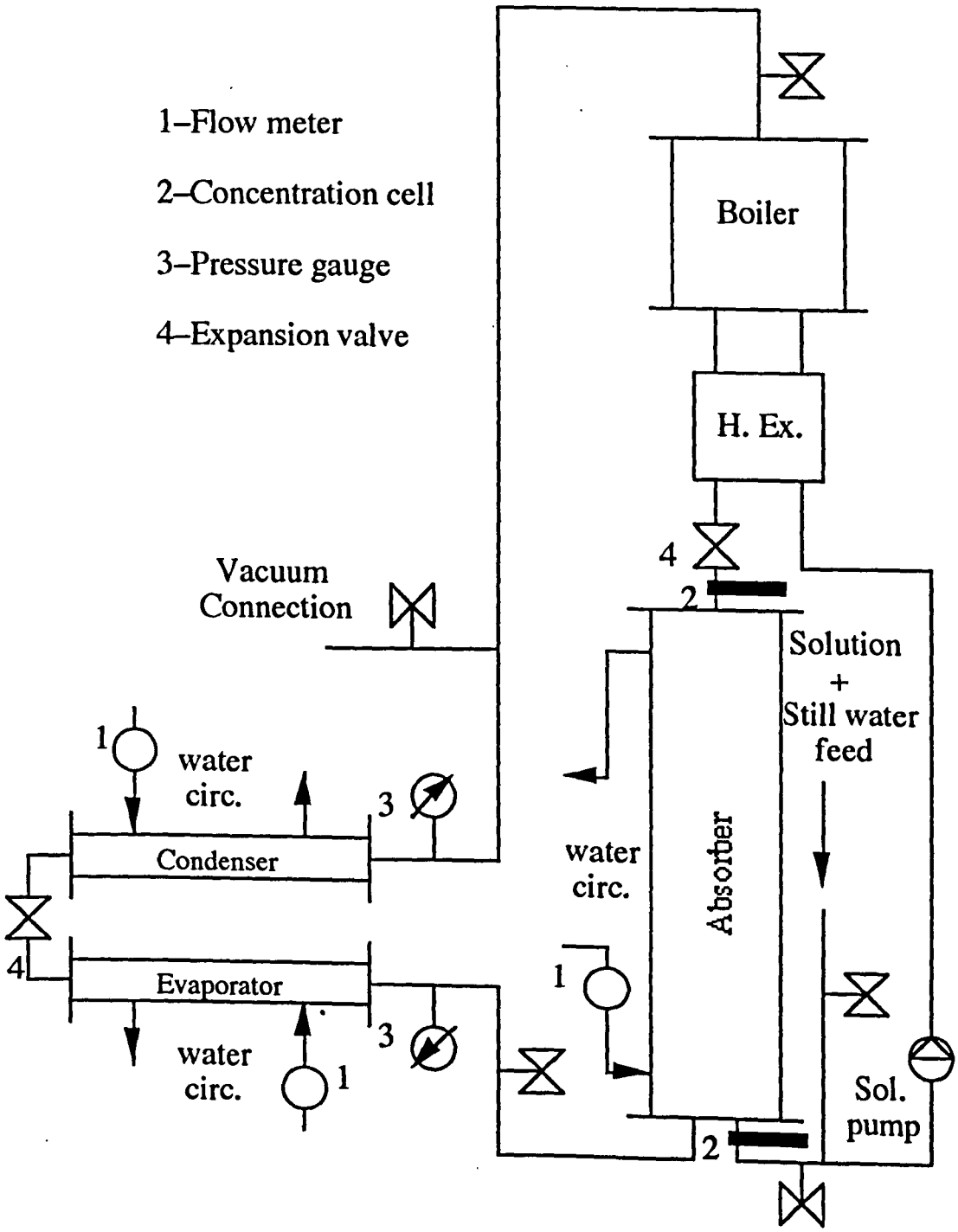

Fig (7.2)

Schematic representation of the $LiBr/H_2O$ test system

7.2–Components Design and Description :

The system is primarily made of proprietary glass vessels and copper tubings. The glass being the containing vessel of the main components. Glass was selected because it gives clear sight of the solution, its level, and the physical processes it undergoes which help identify and solve any problems that may arise. The copper tubing formed the connecting pipework and the water circuits inside the condenser, evaporator, and absorber.

The main components will now be discussed in detail.

7.2.1– Condenser :

Sizing :

The condenser was sized using the following typical conditions :

* The effectiveness (E_C) was selected to be 0.5
* The cooling water flow rate ($\dot{m}_{wc}$) and temperature (T_{wc}) are 0.04 kg/s and 20 °C respectively
* The condensation temperature is 40 °C
* 6.4 mm copper tubes with negligible thickness and thermal resistance circulate the cooling water in the condenser and on which condensation takes place
* The cooling water properties were taken at its inlet temperature.

The Reynold's Number calculated from the formula :

$Re = \frac{4\ \dot{m}_{wc}}{N\ \pi\ D\ \mu}$ was found to be 2122

where N is the number of parallel water tubes.

The Dittus–Boetler equation [49] for the Nusselt Number

$Nu = 0.023\ Re^{0.8}\ Pr^{0.4}$ gave a value of 24

The heat transfer coefficient from the cooling water to the tube wall was then calculated as :

$$h_{ci} = \frac{Nu\ K_w}{D} = 2400\ W/m^2\ K$$

The heat transfer from the tube wall to the condensate film was obtained from the formula [49] :

$$h_{co} = 0.728\ \left[\frac{g\ \rho_l\ (\rho_l - \rho_v)\ K_w^3\ h_{fg}}{M\ \mu_l\ (T_{csat} - T_{cs})\ D}\right]^{0.25}$$

which gave a value of 12224 $W/m^2\ K$

where T_{csat} is the saturation temperature of the condenser, T_{cs} is the temperature of the tube surface, and M is the number of vertical tiers of horizontal tubes.

The overall thermal resistance was then calculated as :

$$R_c = \frac{1}{h_{ci}} + \frac{1}{h_{co}} = 5E\text{-}4\ m^2\ K/W$$

and the overall heat transfer coefficient was obtained as :

$$U_c = \frac{1}{R_c} = 2000 \text{ W/m}^2 \text{ K}$$

The surface area of the cooling water tubes needed was then :

$$A = \frac{NTU \, \dot{m}_{wc} \, C_{pw}}{U_c}$$

where the number of transfer units, NTU was calculated from

$$NTU = -\ln(1 - E_c) = -\ln(1 - 0.5) = 0.69$$

and $A = 0.06 \text{ m}^2$

Description :

Mounted horizontally, the condenser is made of a glass tube 500 mm long and has an internal diameter of 50 mm. Each end of the tube is fitted with a teflon O–ring that is pressed against a brass disc by means of six M6 bolts and nuts that join the disc to the flange which encircles the tapered end of the glass tube. By tightening the screws the O–rings seal off the tube and hold the operational sub–atmospheric pressure.

Soldered to one of the brass discs are two copper tubes which carry the cooling water in and out of the condenser. The two 12.7 mm diam. pipes lead, through two small chambers, to two sets of pipes, each set is composed of four 6.4 mm diam. copper pipes, these pipes circulate the cooling water in and out of the condenser keeping the entrance and exit of the cooling water at one end of the condenser and therefore easing the vacuum sealing problem. The copper tubes have enough surface area to perform the required duty.

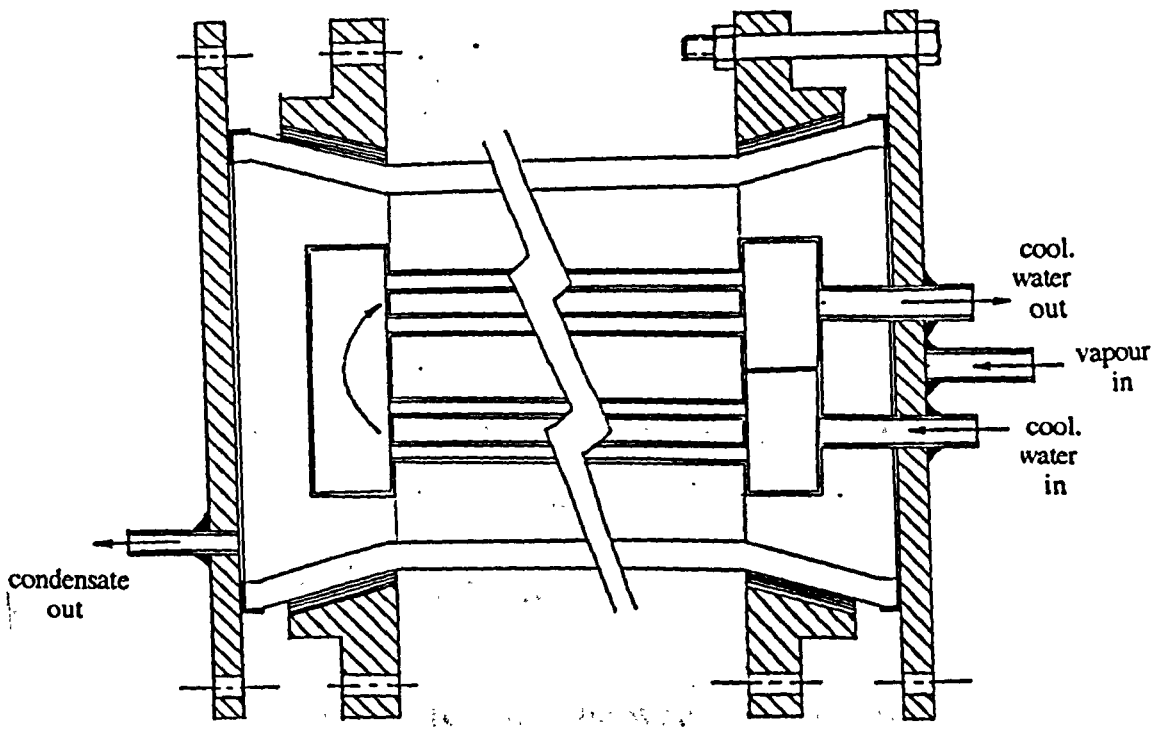

Fig (7.3)

The condenser

The refrigerant vapour coming from the boiler enters the condenser at one end and occupies the space inside the glass tube, and when it contacts the cold water tubing it will condense and drips to the bottom of the glass tube. When the condensate reaches the level of the outlet port at the other end of the condenser it will flow out towards the evaporator through the expansion valve mounted in the connecting 6.4 mm copper tube. See condenser configuration in fig (7.3).

7.2.2– Evaporator :

Sizing :

Taking an evaporation temperature of 3 °C and using the same criteria adopted to size the condenser, the internal heat transfer coefficient was calculated as :

$h_{ei} = 2829\ W/m^2 K$

The heat transfer coefficient from the tube wall to the surrounding condensate was obtained from the correlation [49] :

$$h_{eo} = 5.56\ (\Delta T)^3\ (\frac{p}{pa})^{0.4} = 3874\ W/m^2 K$$

where (ΔT) is the difference between evaporator's saturation temperature and the surface temperature of the tubes, and $(\frac{p}{pa})$ is the ratio of the evaporator pressure to the atmospheric pressure.

The overall thermal resistance was calculated as :

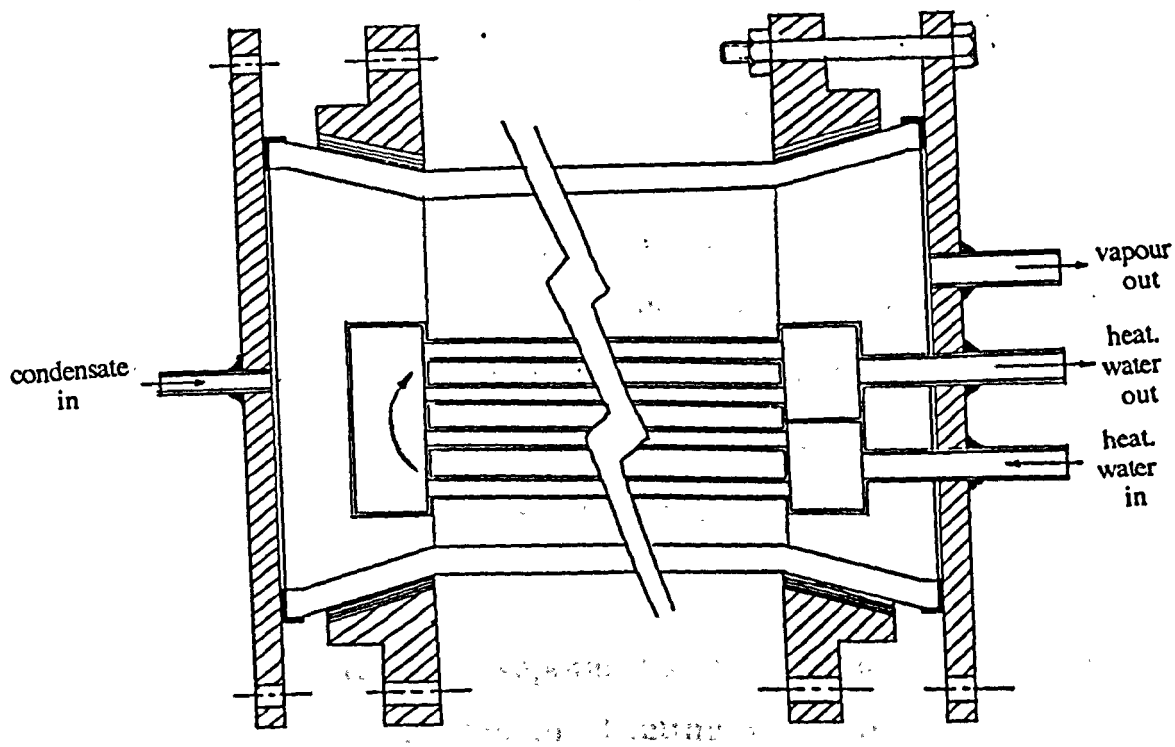

Fig (7.4)

The evaporator

$$R_e = \frac{1}{h_{ei}} + \frac{1}{h_{eo}} = 6E\text{-}4 \text{ m}^2 \text{K/W}$$

and the overall heat transfer coefficient was given by :

$$U_e = \frac{1}{R_e} = 1666 \text{ W/m}^2 \text{K}$$

The area needed was therefore

$$A = \frac{NTU \, \dot{m}_{we} \, C_{pw}}{U_e} = 0.07 \text{ m}^2$$

Description :

The evaporator, seen in fig (7.4), is very similar to the condenser in shape and size. It has the same glass tube body, the same sealing arrangements, and the heating water is circulated in the same manner. The only difference is that the heating water is circulated in six 6.4 mm diam. copper tubes–three in each direction of the flow–and they occupy the lower semi–circle of the glass tube allowing enough space for the rising refrigerant vapour and having enough exchange area to match that calculated above.

The refrigerant enters the evaporator at one end and starts to build up a head. When it reaches the heating water tubes it starts to evaporate. The vapour leaves the evaporator through the 12.7 mm diam. port positioned higher than the inlet port at the other end.

7.2.3–Absorber :

Sizing :

The following conditions were adopted to facilitate the sizing of the absorber :

* the heat effectiveness of the absorber was taken to be 0.12
* the mass flow rate of the cooling water and its temperature were chosen to be 0.25 kg/s and 20 °C respectively

It is noted that the small value chosen for the heat effectiveness of the absorber was based on the knowledge of typical values of such effectivenesses gained from the absorber simulation analysis of chapter 4. The relatively large coolant mass flow rate, on the other hand, was necessary to cope with the heat of absorption.

NTU was obtained from the absorber's simulation programme of chapter 4 as 0.15 and U_a was obtained from the finite difference method [26] as 1.21 kW/m^2 K.

The absorber area was then calculated to be

$$A = \frac{NTU\ \dot{m}_w\ C_{pw}}{U_a} = 0.13\ m^2.$$

Description :

The absorber, designed to be of the falling film type, was made of a glass tube 1000 mm long and 150 mm bore. It was mounted vertically and had the same sealing arrangements as the condenser and evaporator.

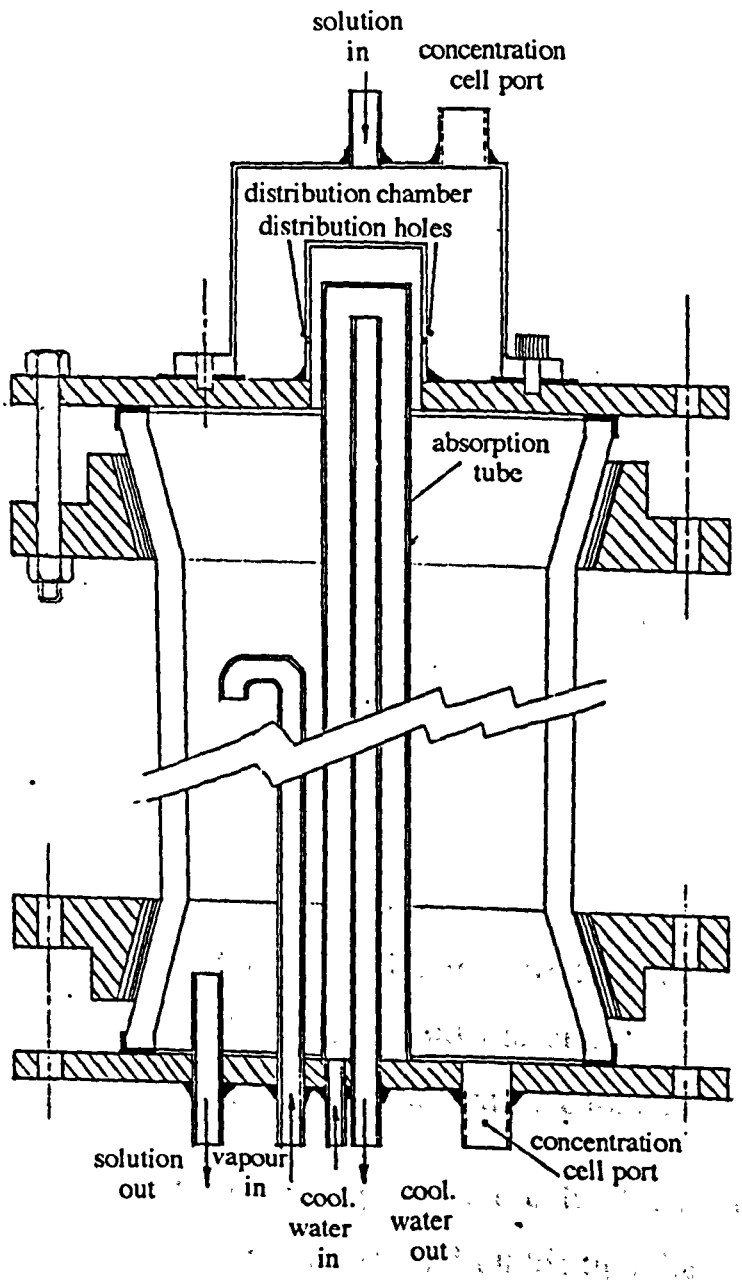

Fig (7.5)

The absorber

The absorption tube was a 41.3 mm diam. copper pipe chosen to give the area calculated above. The tube was sealed at the top end, while its bottom end was soldered to the bottom brass disc. The absorption tube was situated at the centre of the glass tube. The absorbent flows downwards on the exterior of this tube while the cooling water circulates inside it. The vertical mounting of the tube was chosen to improve the wettability of the absorber tube since it will decrease the minimum wetting rate of the solution [64].

The cooling water enters the absorption tube through a hole drilled in the bottom disc. It rises to fill the whole tube before leaving through the 12.7 mm diam. outlet copper pipe which is concentric with the absorption tube. This arrangement ensures that the inside surface of the absorption tube is always in contact with cooling water and the cooling is done in a contra–flow mode.

At the top of the absorber is the distribution chamber, sealed with an O–ring and screwed to the top brass disc. It was made of two concentric brass cylinders. The inner cylinder had eight 1 mm diam. holes distributed at its bottom around the circumference. It encircled the top of the absorption tube with a small clearance in between.

The strong solution coming from the heat exchanger enters the distribution chamber from the top, and builds up a head inside, this head drives the flow out of the distribution holes in a jet form directly into the surface of the absorption tube. The solution then flows down the length of the tube in a thin film. The vapour from the evaporator is admitted to the absorber through a 12.7 mm diam. copper tube which is

extended to about half the height of the absorber, to ensure even distribution of the vapour, and bent at the top to prevent any liquid solution from getting into the vapour line.

The water vapour is absorbed by the descending film producing a weaker solution of LiBr in water. The diluted solution is then pumped out of the absorber through an 12.7 mm diam. outlet tube which was raised about 20 mm above the base of the absorber to maintain a small solution head necessary to keep the tip of the concentration measuring cell immersed. The absorber configuration is shown in fig (7.5).

7.2.4– Solution Pump :

The solution is pumped from the absorber to the boiler through the heat exchanger by means of a prestaltic pump. the pump is driven by a variable speed motor that has a range of 50–600 RPM. The pump head has three stainless steel rollers that press a plastic tube against the pump head casing, and as it rotated it pushed the solution in the direction of rotation. The tube had a thickness/bore ratio of 2.6/4.8 mm which was thought to be enough to withstand the pressure difference across its wall. However this was later proven to be not entirely true and will be discussed in greater detail later in this chapter.

The pump covered a wide range of flow rates and being a positive displacement type the flow is linearly proportional to the speed of rotation. This is shown on the calibration curve of fig (7.6).

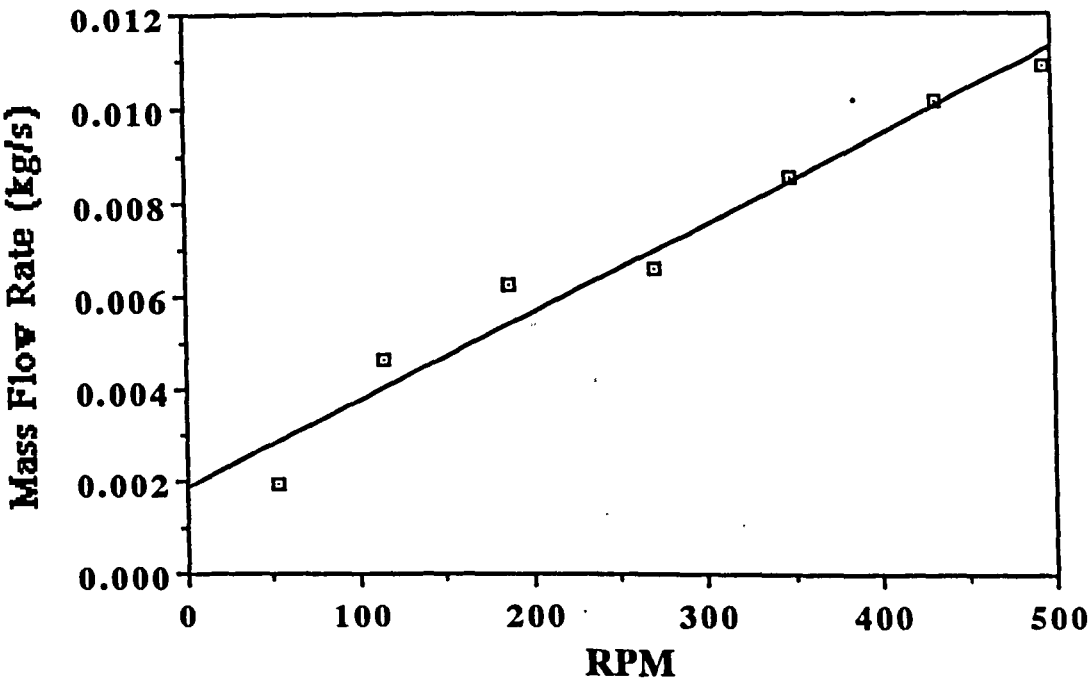

Solution pump calibration curve for $LiBr/H_2O$ at concentration of 52%

Fig (7.6)

7.2.5– Heat Exchanger :

Sizing :

Allowing a 50 °C difference between the temperature of the solution leaving the absorber and that of the solution entering the boiler and taking a solution mass flow rate of 0.01 kg/s, the heat capacity of the heat exchanger was calculated as : $Q = \dot{m} C_p \Delta T = 900$ W

Description :

The plate heat exchanger, mounted between the boiler and the absorber, was a proprietary device with a contact area of 0.5 square meters and an exchange capacity of 1 kW. In the heat exchanger, the cooler weak solution pumped from the absorber is preheated before entering the boiler, and the hotter strong solution coming down from the boiler is precooled before going into the absorber.

7.2.6– Boiler :

The boiler, shown in fig (7.7), was a vertically mounted glass tube sealed at both ends in the same way as the other components. The electrical heating element of the boiler was soldered to the base disc and was connected to a power variac and a voltmeter. The use of the power variac allowed the heat input to be varied between 0 and 3 kW.

The weak solution enters the boiler at the bottom, gets heated and boils off some of its water content. The solution then leaves the boiler through an outlet pipe that was raised above the base disc by 120 mm to

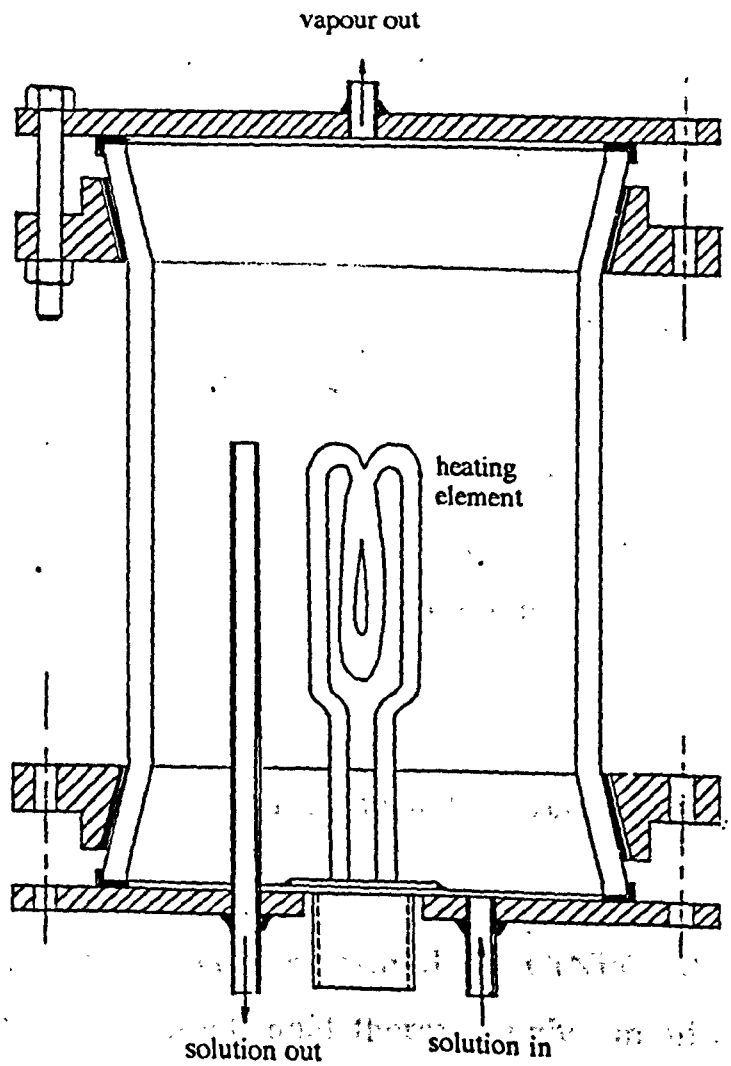

Fig (7.7)

The boiler

ensure that the heating element was completely immersed in the solution. The vapour given off by the solution leaves the boiler through a top pipe and passes to the condenser to repeat the refrigerant's cycle.

The system was fitted with a connection between the absorber and the solution pump to feed the $LiBr/H_2O$ solution and the distiled water. Another connection, fitted in the vapour line between the boiler and the condenser, was used to connect the vacuum pump. Both connections were fitted with shut–off valves.

7.2.7–Water Circuits :

The system was fitted with three water circuits to cool the condenser and absorber and to provide the cooling load for the evaporator.

The three circuits were connected to the hot and cold water supply to allow the control of the temperature and in parallel to each other to enable separate control of their mass flow rates.

7.3–Measurements :

The measurements of various quantities were taken in the following manner :

The temperatures were measured by CrNi/CrAl thermocouples connected to two multichannel thermocouple amplifiers with digital display.

The Pressure was measured at the two levels of the cycle by two EDWARDS–GC16 dial gauges with pressure range of 0–1050 mbar

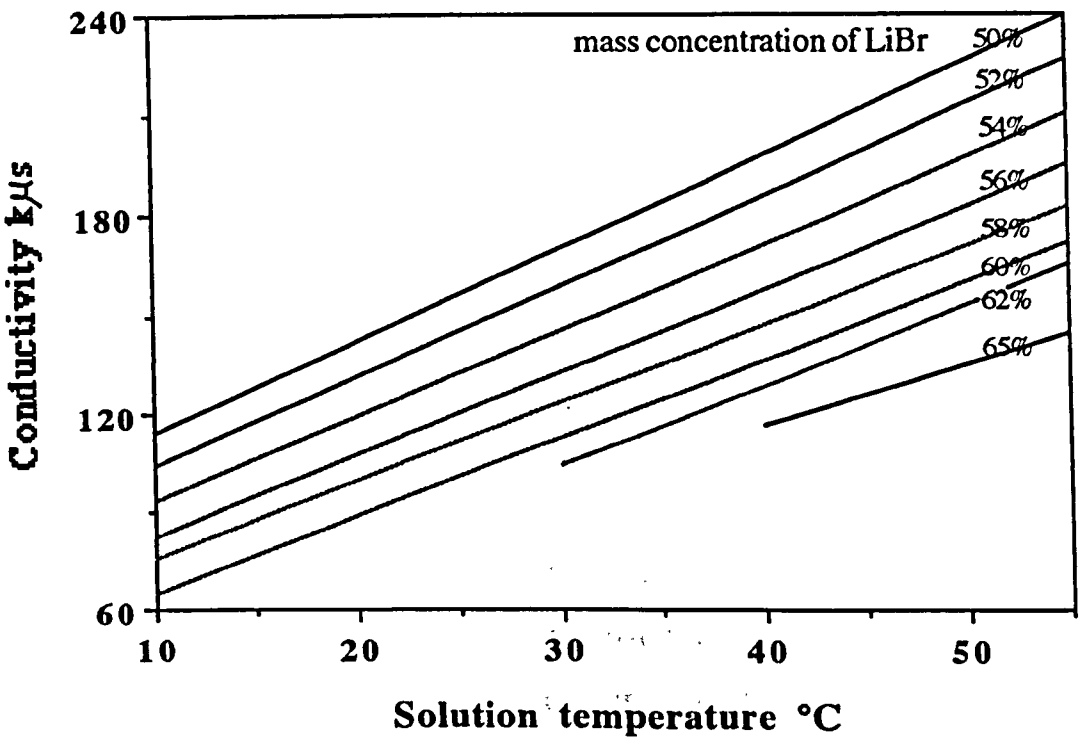

Calibration chart of the Lithium Bromide/Water solution.

Fig (7.8)

absolute. The low pressure gauge was fitted to the vapour line connecting the evaporator to the absorber, while the high pressure gauge was connected to the vapour line entering the condenser.

The cooling water flow rates were measured by three float flow meters connected to each of the three water circuits while the solution's flow rate was obtained from the calibration line of fig (7.6) after measuring the speed of rotation of the pump by a flash tacometer.

Concentration measurements were taken by two Russell–CDC conductivity cells one of which was mounted at the distribution chamber to measure the strong concentration while the other was placed at the bottom of the absorber to measure the weak concentration. The cells were connected to a Russell–CD800 conductivity metre. The concentration cells, though not normally used for high concentrations, were used here because of their convenience, in relation to other methods e.g. weighing and titration, and for their reasonable price, as compared to densometers. The conductivity readings were converted into mass concentration using the calibration chart (fig (7.8)) produced by Ibrahim [26] who used the cells for the same range of concentrations.

7.4–Rig Operation :

Air was evacuated from the system using an oil vacuum pump to a vacuum level of about 0.1 mbar (0.075 mm Hg) which, as discussed in chapter 6, is sufficient for this application. After many trials The system was thought to be reasonably sealed and the vacuum tests of the system showed acceptable rates of pressure increase due to degassing

and minor leaks. Typically, it would take about five hours for the pressure to increase one mbar. This seemed reasonable considering that the low level working pressure of the system was calculated at about 12 mbar (corresponding to a saturation temperature of 10 °C for water vapour).

A $LiBr/H_2O$ solution at a concentration of 52% was fed into the boiler and the absorber before the boiler's heating element was switched on and the test started.

During the course of the test several problems became evident. One of which was, as mentioned earlier, the plastic tube of the solution pump. This was chosen on the basis of durability, chemical compatibility with the solution, and the ability to perform under vacuum as recommended by the manufacturer. However, during the test the section of the tube that was in the pump head and subject to the pressure from the rollers tended to deform permanently, lose its elasticity and decrease its cross sectional area and hence decreasing the flow rate of the solution. This problem was overcome by regularly changing the position of the tube with respect to the pump head putting a new section of it in the pump head and relieving the old one. Fortunately, there was enough length in the tube to last the whole period of the test without having to change the tube completely. However, this was a considerable inconvenience.

Another problem was the blockage of the distribution holes of the absorber by LiBr salt crystals and corrosion residuals. This interrupted the test and the distribution chamber had, at one point, to be dismantled

to be unblocked and cleaned before the test could continue. However, the blockage continued to affect some of the holes during the running of the tests which affected the wetting of the absorber's tube by the absorbent. This contributed to the poor values of the absorber's mass and heat effectivenesses as will be discussed later.

The loss of vacuum also presented a problem. The low pressure built up to about 40 mbar and no evaporation could take place below a temperature of about 30 °C. This was accounted for by adjusting the temperature of the load water to the appropriate level. However, this measure affected the temperature of the cooling water to the condenser and the absorber because they were connected to the same water circuit as the evaporator which meant that they had to be cooled at the same, relatively high, temperature.

Another problem was the condensation of the vapour in the pressure gauges. This was due to a positioning error whereby the gauges were connected at low points with respect to the condenser and evaporator which allowed the condensation to accumulate. However, since this did not have an apparent effect on the pressure readings, and since the gauges were used only as an indication rather than accurate measurement devices, no effort was made to eradicate this problem.

A number of tests were undertaken. However, the number was restricted because of the very limited time available to complete the work. The results from some were most unreasonable in that the inlet concentration of the absorber was lower than that at the outlet, i.e.,

negative concentration variation. The results presented here are representative of the reasonable sets obtained.

7.5–Results and Discussion :

The input and output data of the representative tests are presented in tables (7.1) to (7.5). The input data is presented in the (a) tables, this data consists of the measured input, e.g the cooling water mass flow rates and temperatures, and the calculated system's properties, namely the components' heat effectivenesses calculated from the various temperatures of the cooling water, refrigerant, and absorbent, and the mass effectiveness of the absorber and the boiler calculated from the concentrations of the absorbent and the equilibrium concentrations at the corresponding temperatures. These values were used in the overall simulation programme of chapter 3 to obtain the analytical output results shown on the second column of the (b) tables while the experimental outputs are shown on the first column. The complete test results and the printouts of the programme results are presented in the appendix.

The first thing to note is the fairly good estimate of the experimental evaporation and condensation temperatures by the programme. In all five tests the analytical evaporation temperature stayed within less than three degrees of the experimental temperature keeping the difference between 0.7% and 5% in four tests and 10% in the worst case test (based on the experimental results as reference). The analytical condensation temperature in three of the five tests was within less than 1.5 degrees from the experimental temperature keeping the difference

at about 3%. The difference percentage in temperature in the remaining two tests were 16% and 8.6%. There was a disagreement between the two sets of results in the absorber's inlet temperature ranging between 10% and 35% this is thought to be due to the lack of insulation of the heat exchanger which caused the loss of temperature at the absorber's inlet. At the absorber's outlet however the agreement between the two results was better ranging between 1% and 9% in four tests with the fifth test having a difference of about 18%. The difference between the analytical and experimental results in the boiler's inlet and outlet temperatures were the largest ranging between 2.5% to 77% and 6% to 66% respectively with the experimental results consistently smaller than those of the analysis. This could be explained by the large heat losses associated with the high temperatures of the boiler and the heat exchanger and indeed the accuracy of the measuring equipments. The concentration showed good consistency between the two results in three of the five tests where the difference stayed below 5%. In the other two tests the analytical concentrations were quite high.

The effectivenesses of the various components calculated from the experimental data of temperatures and concentrations showed various degrees of fluctuations. The effectivenesses of the evaporator, condenser, boiler, and absorber were generally lower than the practical values. this is contributed to by the presence of air which, as discussed earlier, has huge impact on heat and mass transfer. The evaporator's effectiveness varied between 0.27 and 0.64, and the condenser's effectiveness was quite low with a range between 0.023 and 0.074. Despite much thought no explanation for these extremely low values of

the condenser's effectiveness could be found. The heat exchanger's effectiveness was quite consistent with a range of 0.76 to 0.8. The mass effectiveness of the absorber varied between about 0.05 and 0.15 while the boiler's mass effectiveness varied between 0.28 and 0.88. As pointed out earlier the poor values of the absorber's mass effectiveness could be attributed, in addition to the effect of air, to the incomplete wetting of the absorber's tube due to the blockage of some of the distribution holes. According to visual estimation, the dry area ranged between 20% to 40% of the total area of the absorption tube. The same factors also affected the heat effectiveness of the absorber which ranged between 0.034 and 0.1.

Neglecting the small amount of power required by the solution pump the overall enthalpy balance of the system can be written as :

$$\dot{Q}_{evap} + \dot{Q}_{boil} = \dot{Q}_{cond} + \dot{Q}_{absorb} + \dot{Q}_{loss}$$

Applying this balance, it is found that the system suffered heat losses of 0.2, -0.03, 0.17, 0.5, and 0.6 kW in the respective five tests (the negative value is most likely to be the result of a measurement error) which points to an inadequate insulation of the system. This resulted in a discrepancy between the values of heat ratios predicted by the model and the actual ones. In only one of the five tests, which possibly has an erratic evaporator capacity, the programme underestimated the heat ratio. The rest of the experimental heat ratios stayed quite below those predicted by the model. The discrepancy ranged between 156% to 23% This is to be expected since the model does not account for thermal losses from the system. The size of the losses of each test was generally

proportional to its average temperature (defined as the arithmetic mean of the cycle's temperatures). However, this was found to be a general trend and not a strict one, for example test 4 has an average temperature of 45.98 °C and 0.5 kW heat loss, whereas test 5 has an average temperature of 45.82 °C and a heat loss of 0.6 kW. This is explained by the fact that the losses are functions of the temperature difference between the system and the ambient and are not dependant solely on the system's temperature. Unfortunately, the ambient temperature was not recorded in this experimental work.

It is evident from the above discussion that there is some discrepancy between the analytical and experimental results. This is believed to be largely due to the heat losses from the system, through lack of insulation, and the possible measurement errors. This is to be expected given the difficulty of constructing and operating a $LiBr/H_2O$ system with all the possible and actual problems that were discussed earlier. Despite this, the programme succeeded in predicting to a good degree of accuracy some of the key quantities of the system e.g the evaporation and condensation temperatures as well as the strong and weak concentrations of the solution.

The fact that the system lacked proper insulation needs to be explained. Now, while the pipework of the system was insulated, its main components were left uninsulated because insulating them would have denied the visual access which was the reason for making them out of glass. It was felt that this compromise was necessary in order to further the understanding of the absorption system and the physical processes it undergoes. However, in order to asses the contribution of

the heat losses to the discrepancy between the analytical and the experimental results an estimation of the heat loss from each component of the system was obtained based on a free convective heat transfer between the component and the surroundings for test 4 (having the highest average temperature). These estimations were then incorporated into the components' enthalpy balances in the programme and a set of results were obtained and compared to the original analytical set as well as the experimental one. The results that clearly show better agreement with the experimental data are presented in table (7.6). However, including the heat losses permanently in the code will require the knowledge of the heat transfer areas and coefficients, i.e., the size, geometry, and orientation of the different components as well as some information about the surroundings. This amounts to either (a) simulating a specific system in a specific location, as is the case in [8], which will contradict the generality of the code, or (b) creating a complex code with complicated calculations and a large number of inputs, to be specified by the user, which will complicate the process of converging into a solution. Of course, because of the experimental requirements, the heat losses from this rig have been large. In practice, where more extensive insulation would be incorporated, then these heat losses would be very much reduced and the programme, where heat losses are ignored, should give a more accurate simulation.

Thus it is believed that the programme provides a valuable means of estimating the performance of the $LiBr/H_2O$ system and could be extended to cater for other absorption combinations. However, it is recommended that further improved experimental work be carried out

with further data obtained and compared. Alternatively, data from a commercially available $LiBr/H_2O$ refrigeration system should be used to validate the accuracy of the model.

Quantity	Value
Pump flow rate (kg/s)	6.5 E-3
Evaporator heating water flow rate (kg/s)	.0833
Condenser cooling water flow rate (kg/s)	.1
Absorber cooling water flow rate (kg/s)	.133
Evaporator heating water temperature (C)	32.
Condenser cooling water temperature (C)	32.
Absorber cooling water temperature (C)	32.
Evaporator effectiveness	.375
Condenser effectiveness	.074
Heat exchanger effectiveness	.8
Absorber mass effectiveness	.15
Absorber heat effectiveness	.081
Boiler mass effectiveness	.375
Heat input (kw)	.816

Table (7.1a)

Input conditions of test 1

Quantity	experimental	analytical
Evaporator temp. (C)	30.4	27.6
Condenser temp. (C)	49.7	50.96
Absorber inlet temp.(C)	38.2	49.88
Absorber outlet temp.(C)	32.1	37.83
Boiler inlet temp. (C)	66.4	83.53
Boiler outlet temp. (C)	91.5	98.08
Strong concentration	.58	.566
Weak concentration	.55	.544
Evaporator capacity (kw)	.21	.576
Condenser capacity (kw)	.545	.586
Absorber capacity (kw)	.28	.805
Heat ratio	.257	.705

Table (7.1b)

Comparison between the experimental and analytical output of test 1

Quantity	Value
Pmp flow rate (kg/s)	6.5 E-3
Evaporator heating water flow rate (kg/s)	.0833
Condenser cooling water flow rate (kg/s)	.1
Absorber cooling water flow rate (kg/s)	.2
Evaporator heating water temperature (C)	32.4
Condenser cooling water temperature (C)	32.4
Absorber cooling water temperature (C)	32.4
Evaporator effectiveness	.44
Condenser effectiveness	.066
Heat exchanger effectiveness	.76
Absorber mass effectiveness	.096
Absorber heat effectiveness	.06
Boiler mass effectiveness	.741
Heat input (kw)	.816

Table (7.2a)

Input conditions of test 2

Quantity	experimental	analytical
Evaporator temp. (C)	30.6	28.98
Condenser temp. (C)	52.	51.73
Absorber inlet temp.(C)	44.	48.477
Absorber outlet temp.(C)	32.8	32.52
Boiler inlet temp. (C)	71.5	80.82
Boiler outlet temp. (C)	93.7	98.99
Strong concentration	.57	.594
Weak concentration	.55	.574
Evaporator capacity (kw)	.28	.524
Condenser capacity (kw)	.545	.533
Absorber capacity (kw)	.587	.806
Heat ratio	.34	.642

Table (7.2b)

Comparison between the experimental and analytical outputs of test 2

Quantity	Value
Pmp flow rate (kg/s)	6.5 E-3
Evaporator heating water flow rate (kg/s)	.0833
Condenser cooling water flow rate (kg/s)	.1
Absorber cooling water flow rate (kg/s)	.233
Evaporator heating water temperature (C)	32.
Condenser cooling water temperature (C)	32.
Absorber cooling water temperature (C)	32.
Evaporator effectiveness	.64
Condenser effectiveness	.056
Heat exchanger effectiveness	.77
Absorber mass effectiveness	.07
Absorber heat effectiveness	.034
Boiler mass effectiveness	.882
Heat input (kw)	.816

Table (7.3a)

Input conditions of test 3

Quantity	experimental	analytical
Evaporator temp. (C)	30.9	29.9
Condenser temp. (C)	53.3	52.2
Absorber inlet temp.(C)	43.1	56.4
Absorber outlet temp.(C)	32.2	35.4
Boiler inlet temp. (C)	72.4	104.2
Boiler outlet temp. (C)	96.4	126.7
Strong concentration	.58	.698
Weak concentration	.565	.676
Evaporator capacity (kw)	.244	.466
Condenser capacity (kw)	.503	.474
Absorber capacity (kw)	.39	.808
Heat ratio	.3	.57

Table (7.3b)

Comparison between the experimental and analytical outputs of test 3

Quantity	Value
Pmp flow rate (kg/s)	6.5 E-3
Evaporator heating water flow rate (kg/s)	.1
Condenser cooling water flow rate (kg/s)	.1
Absorber cooling water flow rate (kg/s)	.133
Evaporator heating water temperature (C)	33.4
Condenser cooling water temperature (C)	33.4
Absorber cooling water temperature (C)	33.4
Evaporator effectiveness	.27
Condenser effectiveness	.034
Heat exchanger effectiveness	.79
Absorber mass effectiveness	.049
Absorber heat effectiveness	.055
Boiler mass effectiveness	.278
Heat input (kw)	.75

Table (7.4a)

Input conditions of test 4

Quantity	experimental	analytical
Evaporator temp. (C)	30.8	30.21
Condenser temp. (C)	51.	59.34
Absorber inlet temp.(C)	42.5	57.65
Absorber outlet temp.(C)	34.	31.03
Boiler inlet temp. (C)	75.1	133.27
Boiler outlet temp. (C)	99.2	159.31
Strong concentration	.58	.707
Weak concentration	.57	.69
Evaporator capacity (kw)	.294	.36
Condenser capacity (kw)	.252	.369
Absorber capacity (kw)	.28	.741
Heat ratio	.39	.48

Table (7.4b)

Comparison between the experimental and analytical outputs of test 4

Quantity	Value
Pmp flow rate (kg/s)	6.5 E-3
Evaporator heating water flow rate (kg/s)	.267
Condenser cooling water flow rate (kg/s)	.167
Absorber cooling water flow rate (kg/s)	.1
Evaporator heating water temperature (C)	31.
Condenser cooling water temperature (C)	31.
Absorber cooling water temperature (C)	31.
Evaporator effectiveness	.625
Condenser effectiveness	.023
Heat exchanger effectiveness	.77
Absorber mass effectiveness	.077
Absorber heat effectiveness	.1
Boiler mass effectiveness	.384
Heat input (kw)	.703

Table (7.5a)

Input conditions of test 5

Quantity	experimental	analytical
Evaporator temp. (C)	30.2	30.4
Condenser temp. (C)	53.	57.56
Absorber inlet temp.(C)	38.3	47.6
Absorber outlet temp.(C)	31.2	31.05
Boiler inlet temp. (C)	82.5	84.65
Boiler outlet temp. (C)	96.5	102.998
Strong concentration	.56	.564
Weak concentration	.545	.549
Evaporator capacity (kw)	.56	.416
Condenser capacity (kw)	.35	.426
Absorber capacity (kw)	.294	.694
Heat ratio	.79	.59

Table (7.5b)

Comparison between the experimental and analytical outputs of test 5

Quantity	experimental	analytical (no losses)	analytical (with losses)
Evaporator temp. (C)	30.8	30.21	31
Condenser temp. (C)	51.	59.34	43.83
Absorber inlet temp.(C)	42.5	57.65	45.42
Absorber outlet temp.(C)	34.	31.03	34.56
Boiler inlet temp. (C)	75.1	133.27	73.93
Boiler outlet temp. (C)	99.2	159.31	86.25
Strong concentration	.58	.707	.56
Weak concentration	.57	.69	.55
Evaporator capacity (kw)	.294	.36	.271
Condenser capacity (kw)	.252	.369	.248
Absorber capacity (kw)	.28	.741	.417
Heat ratio	.39	.48	.36

Table (7.6)

The improved analytical predictions due to including the heat losses

8–Discussion :

8.1–Discussion of Present Work :

A computer model that simulates a $LiBr/H_2O$ water chiller has been developed in chapter 3. The model gives the temperatures, concentrations, and flow rates around the cycle and will compute the components duty and the overall heat ratio. To perform, it requires only the knowledge of the outside conditions of the cycle and the system's data. For typical working conditions, the model will need about 4 to 6 iterations and will take few seconds to converge into a solution on a time sharing main frame computer. However, depending on how far the seed values are from the solution, the code may need greater number of iterations and time to converge. The effects of various parameters on the system's performance, characterized by the heat ratio, are presented and discussed. As pointed out in chapter 3, constraints of the nature described in [4] were not implemented here because of the limited use of the programme as a simulation of a $LiBr/H_2O$ water chiller and not as a general code covering a wide range of cycles, working fluids, and working conditions as in [4] which necessitated the use of such constraints to allow for the expected deviation of the seed values from the wide range of solutions. For the model presented here there has been very few runs that resulted in a non–physical solution which, for example, had one or more negative temperatures and temperature differences, negative concentrations, and negative flow rates. The use of the heat and mass effectivenesses of the absorber and boiler is more convenient and requires the knowledge of

less inputs than using the transfer areas and coefficients as implemented in [1], [3], and [7]. The simulation has various degrees of success in predicting the performance of the actual system as shown by the comparative analysis with the experimental results obtained from the experimental work that was carried out to validate the model. The model generally overestimates the temperatures of the actual system and its heat ratio with varied deviation. This supports the conclusion that the heat losses from the system which is not accounted for by the model is primarily responsible for the discrepancy. This is in line with the justification given by Grossman and Michelson [4]. The inclusion of the heat losses in the simulation of test no. 4 and the better agreement between the analytical and experimental data that resulted supports the conclusion even further. However, this discrepancy would not be much of a problem in practical systems because they will be better insulated.

In chapter 4 a method of estimating the performance of the absorber was presented. The method, which is suitable for use on PCs due to its simplicity and its limited need of memory, calculates the temperature and concentration of the absorber and its overall effectiveness from given heat and mass transfer coefficients which can be obtained from relevant experimental or analytical data. From the computed temperature and concentration profiles the method can then calculate the heat and mass effectivenesses of the absorber which are used by the overall computer model, of chapter 3, to simulate the performance of the absorber. The method was compared to the hybrid method of Ibrahim [26] and was corrected to give good agreement between the two methods. The method is simpler than the finite difference method

approach even when this approach is reduced to solving the approximated equations for a single space variable by using the "method of lines" as was introduced in [25]. It is also much simpler than the exact solution presented in [22] which was obtained using a set of restrictive conditions. The method, by using predetermined heat and mass transfer coefficients, goes one step further than the simplified method introduced by Perez–Blanco [28] who applied energy and mass balances to the absorber and used values for the mass transfer coefficient calculated by Ruchenstein and Berbente [29] but simplified the heat transfer problem by assuming pure conduction across the absorbent film. The second method of Urakawa et al [27] in which they approximated the concentration and temperature profiles by non–linear algebraic equations is simple enough but appears to be less accurate as they reported some differences between this approach and their own finite difference solution in the temperature field at the entry region.

Although the heat and mass transfer coefficients used by the method in this work represent the case of a smooth falling film type absorber, the method is not limited to such case and can be equally employed for other conditions provided that the correct transfer coefficients are used. The increase in the cooling water flow rate or the absorber's area were found to improve the overall performance of the absorber. A surprising finding was that the temperature of the cooling water can exceed that of the absorbent at the same point of the absorber's length and a "crossing over" of the temperature profiles occurs. This behaviour is unique to absorbers and is attributed to the heat of

absorption and the variation of the absorbent's temperature. It is only possible at high cooling water temperatures and/or low capacity ratios.

The improvement in the heat and mass transfer in the falling film absorbers brought about by the action of waves was analyzed in chapter 5. The analysis uses the data of the velocity profile and the wave characteristics computed by Penev et al [24] as quoted by Beschkov and Boyadjiev [23]. Numerical solution for the energy and diffusion equations was obtained in terms of concentration and temperature at varying Lewis Number and heat of absorption for the wavy and the smooth flow conditions. The results showed that improvements in heat and mass transfer are attained by wavy flow without eddies and mixing since the data computed by Penev et al [24] denies such possibility for flows with two dimensional waves. The improvements are attributed to the vertical component of the velocity, which does not exist in smooth flows, and the convective heat and mass transfers associated with it.

In chapter 6 the presence of a non–condensable gas and its effect on the performance of absorbers were analytically studied. The results from a computer simulation of the impact of air in a $LiBr/H_2O$ absorber were presented in terms of the overall effectiveness of the absorber obtained for varying partial pressure of air (or varying concentration of air in the vapour) and for different values of mass transfer coefficient. The analysis showed that the smallest amount of air results in a significant reduction in effectiveness. This is supported by the work of Burdukov et al [41], Lee and Rose [42], Kotake [43], Galamba et al [44], and Bologa [45]. The study also showed that introducing forced convection into the gas/vapour mixture improves the

performance considerably which is in line with the conclusion of Lee and Rose [42].

8.2–Recommendations for Future Work :

8.2.1–Overall Simulation :

The overall simulation developed in chapter 3 is capable of generating numerous useful data that describes the performance of the $LiBr/H_2O$ refrigeration system. In this work the performance was characterized by the heat ratio defined for a cooling system. However, it is possible, and useful, to produce results that defines the performance in terms of other quantities such as the evaporation temperature. It is also of benefit to use the model to simulate a heat pump system. In this case the performance is characterized by a redefined heat ratio or the condenser/absorber temperature. It is recommended below that the experimental rig be made more reliable and robust. However, it is perhaps easier to validate the simulation by using data from commercially available $LiBr/H_2O$ absorption systems.

8.2.2–Experimental Rig :

The experimental rig, despite some deficiencies, operated in a satisfactory manner. There is, however, a room for improving the design for future work e.g better distribution chamber for the absorber with bigger holes to counteract the blockage by salt and residuals, better insulation, and better vacuum arrangements. The prestaltic pump is probably the best type of solution pump that can be used for such system; it is easy to calibrate and there is no direct contact between the

solution and any of its parts thus eliminating the possibility of corrosion and leakage. However, a tube with more and durable elasticity is required to overcome the problem of permanent plastic deformation. It is unfortunate in this respect that the manufacturer's data can not be relied upon.

8.2.3–Absorber's Performance :

Because it shows considerable potential it will be of great benefit to check further the accuracy of the simplified absorber prediction method introduced in chapter 4 and extend it to other conditions e.g. various flow patterns and working fluids and to see whether the correction obtained in the present work applies generally or if not, a universal correction that accounts for all conditions should be sought. An example for such work is to obtain the heat and mass transfer coefficients from the wavy flow simulated in this work and use them in the absorber prediction method to determine what overall enhancements are obtained as a result of waves.

8.2.4–Effect of Waves :

In performing the calculation of the combined heat and mass transfer in the wavy film flow the mesh size had to be very fine to guarantee a stable solution. As a result the amount of calculation work was large which, consequently, required long execution time and large memory . The memory problem was circumvented by dividing the solution field into several segments as described in chapter 5. However, the lengthy time requirement still needs to be addressed because even if the technique is replaced by the simplified method the finite difference

method is still required to generate the heat and mass transfer coefficients. It would be, therefore, of great interest to investigate whether an hybrid solution, i.e., analytical at the entry region and numerical thereafter, similar to that introduced by Ibrahim [26] can be found for this problem. This would save computational time and memory.

8.2.5–Air Entrainment :

It is noted that the body of literature on the subject of the effects of air presence on the absorption process is very limited. Most of the literature found concentrates on the effects on pure condensation, evaporation, or melting. It is thus recommended that experimental work be conducted in the area of the effects of non–condensable gases on absorption with the results to be used to verify the analytical method presented in this work. This is particularly important because it has been shown that the effect of entrained air has a very significant effect on the performance.

9-Conclusion :

A computer simulation of the complete $LiBr/H_2O$ absorption refrigeration system has been successfully developed. It used heat and mass effectivenesses to characterize the performance of the system's components. The code enabled the assessment of the effects of various conditions on the overall heat ratio (Hr) of the system. Experimental work was carried out in order to validate the code. The programme was found to predict the condensation and evaporation temperatures as well as the concentration variation reasonably well. It predicted other conditions of the system with various degrees of accuracy. The discrepancy was attributed largely to the heat losses from the system. This was further supported by taking these losses into consideration and obtaining better predictions by the code.

A simplified method of predicting the absorber's performance has been described. It was compared to the finite difference method. Differences were found but were eliminated by introducing a correction factor. The method showed clearly that increasing the Cooling ratio (Cr) or the absorber's area will improve the overall performance of the absorber. The analysis also showed the surprising phenomenon that the cooling water temperature can exceed the absorbent temperature at certain points. This is believed to be due to the unusual behaviour of the absorbent which changes phase and varies its temperature at the same time.

The effects of waves and the entrainment of air on the absorber's performance has been analyzed. The attainment of high heat and mass transfer rates by wavy flows at low Reynold's Number (Re) was found to be due to the existence of the vertical velocity component and the heat and

mass convection associated with it. The investigation into the effects of entrained air showed that the presence of air causes a large reduction in its performance of the absorber. However, this reduction can be offset by creating forced convection in the vapour/gas mixture region, thus improving the mass transfer coefficient.

Reference List :

1) Vliet, G. C., Lawson, M. B., and Lithgow
Water–Lithium Bromide Double–Effect Absorption Cooling Cycle Analysis.
ASHRAE Trans. Vol. 88, No. 1, pp. 811–823, 1982.

2) Takeshita, I., Yamamoto, Y., Harada, T., and Watamatsu, N.
Residential Gas–Fired Absorption Heat Pump Based on R22–DEGDME Pair. Part 2 Design, Computer Simulation and Testing of a Prototype.
Int. Journal of Refrigeration, Vol. 7, No. 5, pp. 313–321, 1984.

3) Grossman, G., and Perez–Blanco, H.
Conceptual Design and Performance Analysis of Absorption Heat Pumps for Waste Heat Utilization.
Int. Journal of Refrigeration, Vol. 5, No. 6, pp. 361–370, 1982.

4) Grossman, G., and Michelson, E.
A Modular Computer Simulation of Absorption Systems.
ASHRAE Trans., Vol. 91, No. 2B, pp. 1808–1819, 1985.

5) Grossman, G., and Gommed, K.
A Computer Model for Simulation of Absorption Systems in Flexible and Modular Form.
ASHRAE Trans., Vol. 93, No. 2, pp. 2389–2402, 1987.

6) Gommed, K., and Grossman, G.

Performance Analysis of Staged absorption Heat Pumps: Water–Lithium Bromide Systems.
ASHRAE Trans., Vol. 96, No. 1, pp. 1590–1598, 1990.

7) Iedema, P. D.
Real Process Simulation of a LiBr/Zn Br_2/CH_3OH Absorption Heat Pump.
ASHRAE Trans., Vol. 93, No. 2, pp. 562–574, 1987.

8) Alvares, S. G., and Trepp, Ch.
Simulation of a Solar Driven Aqua–Ammonia Absorption Refrigeration System: Part 1, Mathematical Description and System Optimization.
Int. Journal of Refrigeration, Vol. 10, pp. 40–48, 1987.

9) Butz, D., and Stephan, K.
Dynamic Behaviour of an Absorption Heat Pump.
Int. Journal of Refrigeration, Vol. 12, pp. 204–212, 1989.

10) Hirshburg, R. I., and Florschuetz, L. W.
Laminar Wavy–Film Flow: Part I, Hydrodynamic Analysis.
Journal of Heat Transfer, Vol. 104, pp. 452–458, 1982.

11) Aragaki, T., Nakayama, S., Suzuki, M., and Toyama, S.
Characteristics of Falling Film on a Vertical Tube.
Int. Chemical Eng., Vol. 27, No. 2, pp. 326–333, 1987.

12) Benjamin, T. B.
Wave Formation in Laminar Flow Down and Inclined Plane.
Journal of Fluid Mechanics, Vol. 2, pp. 554–574, 1957.

13) Rotem, Z., and Neilson, J. E.
Exact Solution for Diffusion to Flow Down an Incline.
Canadian J. Chemical Eng., Vol. 47, pp. 341–346, 1969.

14) Hounkanlin, M. A., and Dumargue, P.
Statistical Characteristics of Intermittent Liquid Film Flow.
Int. J. Heat Mass Trans. Vol. 7, No. 3, pp. 223–230, 1986.

15) Iedema, P. D.
The Absorption Heat Pump with Lithium Bromide/Zinc Bromide/Methanol.
PhD Thesis, Dept. of Mech. Eng., Delft University of Technology, the Netherlands, 1984.

16) Tailby, S. T., and Portalski, S.
The Determination of the Wavelength on a Vertical Film of Liquid Flowing Down a Hydrodynamically Smooth Plate.
Trans. Instn. Chemical Engrs., Vol. 40, pp. 114–122, 1962.

17) Stainthorp, E. P., and Allen, T. M.
The Development of Ripples on the Surface of a Liquid Film Flowing Inside a Vertical Tube.
Trans. Instn. Chemical Engrs., Vol. 43, pp. 85–91, 1965.

18) Salazar, R. P., and Marshall, E.
Three–Dimensional Surface Characteristics of a Falling Liquid Film.
Int. Journal of Multiphase Flow, Vol. 4, pp. 487–496, 1978.

19) Brauner, N., and Moalem Maron, D.

Characteristics of Inclined Thin Films, Waviness and the Associated Mass Transfer.
Int. J. Heat Mass Trans., Vol. 25, No. 1, pp. 99–110, 1982.

20) Brauner, N., and Moalem Maron, D.
Modeling of Wavy Flow in Inclined Thin Films.
Chemical Eng. Science, Vol. 38, No. 5, pp. 775–788, 1983.

21) Javdani, K.
Mass Transfer in Wavy Liquid Films.
Chemical Eng. Science, Vol. 29, pp. 61–69, 1974.

22) Grigor'eva, N. I., and Nakoryakov, V. E.
Exact Solution of Combined Heat and Mass Transfer During Film Absorption.
Journal of Eng. Physics Vol. 33, No. 5, pp. 893–898, 1977.

23) Beschkov, V., and Boyadjiev, C.
Numerical Investigation of Gas Absorption in a Wavy Film Flow.
chemical Eng. Comm., Vol. 20, pp. 173–182, 1982.

24) Penev, V., Krylov, S. V., Boyadjiev, CH., and Vorotilin, V. P.
Wavy flow of Thin Liquid Film.
Int. J. Heat Mass Trans., Vol. 15, pp. 1389–1406, 1968.

25) Grossman, G., and Heath, M. T.
Simultaneous Heat and Mass Transfer in Absorption of Gases in Turbulent Liquid Films.
Int. J. Heat Mass Trans., Vol. 27, pp. 2365–2376, 1984.

26) Ibrahim, G. A.
An Investigation into Liquid Film Absorbers for Refrigeration Systems.
PhD Thesis, Dept. of Mech. Eng. King's College, London University, 1991.

27) Urakawa, K., Morioka, I., and Kiyota, M.
Absorption of Water Vapour into Lithium Bromide–Water Solution Film Falling Along a Vertical Plate.
Bulletin of JSME, Vol. 29, No. 258, pp. 4218–4222, 1986.

28) Perez–Blanco, H.
A Model of an Ammonia–Water Falling Film Absorber.
ASHRAE Trans., Vol. 94, No. 1, pp. 467–482, 1988.

29) Ruckenstein, E. and Berbente, C.
Mass Transfer to Falling Liquid Films at Low Reynolds Numbers.
Int. J. Heat Mass Trans., Vol. 11, pp. 743–753, 1968.

30) Cosenza, F., and Vliet, G. C.
Absorption in Falling Water/LiBr Films on Horizontal Tubes.
ASHRAE Trans., Vol. 96, No. 1, pp. 693–701, 1990.

31) Zheng, G., and Worek, W. M.
A Holographic Interferometric Method to Study Combined Heat and Mass Transfer in Film Sorption.
Int. comm. Heat Mass Trans., Vol. 19, No. 4, pp. 531–540, 1992.

32) Budov, V. M., Kir'yanov, B.A, and Shemagin, I. A.

Heat Transfer in the Laminar–Wave Section of Condensation of a Stationary Vapour.
Journal of Eng. physics, Vol. 52, No. 6, pp. 647–648, 1987.

33) Oliver, D. R., and Atherinos, T. E.
Mass Transfer to Liquid Films on an Inclined Plane.
Chemical Eng. Science, Vol. 23, pp. 525–536, 1968.

34) Pokusaev, B. O., Levonyan, G. A., and Pribaturin, N. A.
Effect of Waves at the Interfacial Boundary on the Desorption of a Gas from the Bulk of a Liquid.
Journal of Eng. Physics Vol. 53, No. 5, pp. 1292–1296, 1987.

35) Ruckenstein, E., and Berbente, C.
Mass Transfer in Wave Flow.
Chemical Eng. Science, Vol. 20, pp. 795–801, 1965.

36) Beschdov, V., Boyadjiev, C., and Peev, G.
On the Mass Transfer Into a Falling Laminar Film with Dissolution.
Chemical Eng. Science, Vol. 33, pp. 65–69, 1978.

37) Portalski, S. and Clegg., A. J.
Interfacial Area Increase in Rippled Film Flow on Wetted Wall Columns.
Chemical Engng. Science, Vol. 26, pp. 773–784, 1971.

38) Howard, D. W., and Lightfoot, E. N.
Mass Transfer to Falling Films.
AICHE Journal, Vol. 14, No. 3, pp. 458–467, 1968.

39) Moalem Maron, D., and Brauner, N.
Flow Patterns in Wavy Thin Films: Numerical Simulation.
Int. comm. Heat Mass Trans., Vol. 16, pp. 655–666, 1989.

40) Usmanov, A. G., Bol'shov, V. P., Mishchenko, A. P., Fatkullin, G. Sh., and Sergeenko, E. S.
Optical Investigation of Heat and Mass Transfer in Vapour Condensation from Vapour–Gas Mixtures.
Journal of Eng. Physics Vol. 53, No. 6, pp. 1369–1373, 1987.

41) Burdukov, A. P., Bufetov, N. S., Deriy, N. P., Dorokhov, A. R., and Kazakov, V. I.
Experimental Study of the Absorption of Water Vapour by Thin Films of Aqueous Lithium Bromide.
Heat Trans.–Soviet Research, Vol. 12, No. 3, pp. 118–123, 1980.

42) Lee, W. C., and Rose, J. W.
Forced Convection Film Condensation on a Horizontal Tube with and without Non–Condensing Gases.
Int. J. Heat Mass Trans., Vol. 27, No. 4, pp. 519–528, 1984.

43) Kotake, S.
Effects of a Small Amount of Noncondensable Gas on Film Condensation of Multicomponent Mixtures.
Int. J. Heat Mass Trans., Vol. 28, No. 2, pp. 407–414, 1985.

44) Galamba, D., Dhir, V. K., and Kaveh Taghavi

Analytical and Experimental Investigation of Simultaneous Melting–Condensation on a Vertical Wall in the Presence of Noncondensable gas.
Int. J. Heat Mass Trans., Vol. 29, No. 12, pp.1869–1880, 1986.

45) Bologa, M. K., Savin, I. K., and Didkovsky, A. B.
Electric–Field–Induction Enhancement of Vapour Condensation Heat Transfer in the Presence of a Non–Condensable Gas.
Int. J. Heat Mass Trans.,Vol. 30, No. 8, pp. 1577–1587, 1987.

46) Abdullahi, M.
Estimation of Air Traces in Steam–air Mixtures Subjected to Dropwise condensation.
Int. comm. Heat Mass Trans. Vol. 14, No. 3, pp. 347–351, 1987.

47) Leibundgut, H. J., Schamaun, J., Schuepbach, R., and Stierlin, H.
Absorption Type Heat Pump with Inert Gas for Domestic Heating.
Int. Congress of Refrigeration, Paris, Vol. 2, pp. 531–537, 1983.

48) Young, J., and Makiya, G. A. A. S.
Thermal Behaviour of a Diffusion–Absorption Refrigerator.
Int. Congress of Refrigeration, Paris, Vol. 2, pp. 729–735, 1983.

49) Incropera, F. P., De Witt, D. P.
Fundamentals of Heat Transfer.
John Wiley & Sons, 1981.

50) ASHRAE, Handbook of Fundamentals, 1985.

51) Patterson, M. R., and Perez–Blanco, H.

Numerical Fits of the Properties of Lithium–Bromide Water Solutions
ASHRAE Trans., Vol. 94, No. 2, pp. 2059–2075, 1988.

52) Lee, K. L. C.
Computer Modelling of Lithium Bromide/Water Vapour Absorption Refrigeration System Using Presumed Values of Heat & Mass Transfer Effectivenesses.
M.Sc. Thesis, King's College, London University, 1989.

53) Borse, G. J.
Fortran 77 and Numerical Methods for Engineers.
PWS–KENT Publishing Company, 1985.

54) Treybal, R. E.
Mass Transfer Operation.
Third Edition, McGraw–Hill Book Company, 1985.

55) Press, W. H., Flannery, B. P., Teukolsky, S. A., and Vetterling,W.T.
Numerical Recipes.
Cambridge University Press, 1986.

56) Nakoryakov, V. E., and Grigor'eva, N. I.
Calculation of Heat and Mass Transfer in Non–Isothermal absorption on the Initial Portion of a Down Flowing Film.
Teoreticheskie Osnory Khimicheskoi Tekhnolgii, Vol. 14, No. 4, pp. 305–309, 1980.

57) Nakoryakov, V. E., and Grigor'eva, N. I.

Combined Heat and Mass Transfer During Absorption in Drops and Films.
Journal of Eng. Physics Vol. 32, No. 3, pp. 243–247, 1977.

58) Johnson, L. W., and Riess, R. D.
Numerical Analysis
Second Edition, Addison Wesley, 1982.

59) Ibrahim, G. A., and Vinnicombe, G. A.
A Hybrid Method to Analyse the Performance of Falling Film Absorbers.
Int. J. Heat Mass Trans., Vol. 36, No. 5, pp. 1383–1390, 1993.

60) Yan, Wei–Mon
Effects of Film Evaporation on Laminar Mixed Convection Heat and Mass Transfer in a Vertical Channel.
Int. J. Heat Mass Trans., Vol. 35, No. 12, pp. 3419–3429, 1992.

61) Meredith, F. H.
Refrigeration technicians pocket book.
Butterworths London, 1981.

62) Guthrie, A.
Vacuum Technology.
J. Willey & Sons, 1963.

63) Gosney, W. B.
Principles of Refrigeration.
Cambridge University Press, 1982.

64) Moalem Maron, D., Ingel, G., and Brauner, N.
Wettability and Break–Up of Thin Films on Inclined Surfaces with Continuous and Intermittent Feed.
Desalination, Vol. 42, pp. 87–96, 1982.

Appendix :

Appendix I–Mathematical Methods :

Appendix I.1–Newton–Raphson Iteration Method :

To illustrate the method of Newton–Raphson, a pair of simultaneous nonlinear equations are considered.

$$F1(x,y) = 0 \tag{1a}$$

$$F2(x,y) = 0 \tag{1b}$$

Expanding using truncated Taylor series gives

$$F1(x_1,y_1) = F1(x_0,y_0) + h\frac{\partial}{\partial x}F1(x_0,y_0) + k\frac{\partial}{\partial y}F1(x_0,y_0) = 0 \tag{2a}$$

$$F2(x_1,y_1) = F2(x_0,y_0) + h\frac{\partial}{\partial x}F2(x_0,y_0) + k\frac{\partial}{\partial y}F2(x_0,y_0) = 0 \tag{2b}$$

where $x_1 = x_0 + h$ and is a better solution of x than x_0, and $y_1 = y_0 + k$ and is a better solution of y than y_0 . From eqns (2a) and (2b)

$$-F1(x_0,y_0) = h\frac{\partial}{\partial x}F1(x_0,y_0) + k\frac{\partial}{\partial y}F1(x_0,y_0)$$

$$-F2(x_0,y_0) = h\frac{\partial}{\partial x}F2(x_0,y_0) + k\frac{\partial}{\partial y}F2(x_0,y_0)$$

in matrix form

$$\begin{bmatrix} \frac{\partial F1}{\partial x} & \frac{\partial F1}{\partial y} \\ \frac{\partial F2}{\partial x} & \frac{\partial F2}{\partial y} \end{bmatrix} \begin{bmatrix} h \\ k \end{bmatrix} = \begin{bmatrix} -F1 \\ -F2 \end{bmatrix} \tag{3}$$

The algorithm starts by choosing seed values for x and y, evaluating the functions F1 and F2 and their derivatives $\frac{\partial F1}{\partial x}$, $\frac{\partial F1}{\partial y}$, $\frac{\partial F2}{\partial x}$, and $\frac{\partial F2}{\partial y}$ then solving the matrix (3) for h and k. x and y are then replaced by x+h and y+k respectively and used to repeat the procedure until |F1| and |F2| approaches zero or a preset tolerance.

Appendix I.2–Gauss Elimination Method:

Gauss elimination technique with partial pivoting is illustrated here in graphical representation :

Original Matrix :
$$\begin{bmatrix} a11 & a12 & a13 \\ a21 & a22 & a23 \\ a31 & a32 & a33 \end{bmatrix} \begin{bmatrix} x1 \\ x2 \\ x3 \end{bmatrix} = \begin{bmatrix} c1 \\ c2 \\ c3 \end{bmatrix}$$

Partial Pivoting :
$$\begin{bmatrix} a11 & a12 & a13 \\ 0 & a'22 & a'23 \\ 0 & 0 & a''33 \end{bmatrix} \begin{bmatrix} x1 \\ x2 \\ x3 \end{bmatrix} = \begin{bmatrix} c1 \\ c'2 \\ c''3 \end{bmatrix}$$

Back Substitution : $x3 = \frac{c''3}{a''33}$

$$x2 = \frac{(c'2 - a'23\ x3)}{a'22}$$

$$x1 = \frac{(c1 - a12\ x2 - a13\ x3)}{a11}$$

Appendix I.3–Fourth Order Runge–Kutta Method :

This is a standard method of integrating ordinary differential equations, i.e., for an arbitrary differential equation of the form :

$$\frac{dy}{dx} = f(x,y)$$

the Runge–Kutta solution at the next x step will be :

$$y_{i+1} = y_i + \frac{\Delta x}{6}(K_1 + 2K_2 + 2K_3 + K_4)$$

where

$$K_1 = f(x_i, y_i)$$

$$K_2 = f(x_i + \frac{\Delta x}{2}, y_i + \frac{\Delta x}{2} K_1)$$

$$K_3 = f(x_i + \frac{\Delta x}{2}, y_i + \frac{\Delta x}{2} K_2)$$

$$K_4 = f(x_i + \Delta x, y_i + \Delta x\, K_3)$$

Appendix I.4–Predictor–Corrector Method :

The method used in this text is the Adams–Bashfroth–Moulton scheme. For the ordinary differential equation :

$$\frac{dy}{dx} = f$$

the method amounts to predicting the solution at the next x point using the current solution together with the functions at the past 3 points i.e.,

$$y_1 = y_0 + \frac{\Delta x}{24}(55\, f_0 - 59\, f_{-1} + 37\, f_{-2} - 9\, f_{-3})$$

the function f_1 is calculated from the predicted value y_1 and is then used in the corrector step to calculate a better value of y_1 i.e.,

$$y_1 = y_0 + \frac{\Delta x}{24}(9\, f_1 + 19\, f_0 + 37\, f_{-1} - 9\, f_{-2})$$

It is clear that the method needs 4 initial values to start the solution process. This is a disadvantage compared with the Runge–Kutta method.

Appendix II–Experimental Results :

Quantity	Test 1	Test 2	Test 3	Test 4	Test 5
T1 (°C)	49.7	52.0	53.3	51.0	53.0
T2 (°C)	23.9	23.7	23.9	24.4	26.1
T3 (°C)	23.9	23.5	23.5	23.6	25.1
T4 (°C)	30.4	30.6	30.9	30.8	30.2
T5 (°C)	32.1	32.8	32.2	34.0	31.2
T6 (°C)	31.2	31.6	31.6	32.7	30.0
T7 (°C)	66.4	71.5	72.4	75.1	82.5
T8 (°C)	91.5	93.7	96.4	99.2	96.5
T9 (°C)	43.3	46.4	46.8	46.5	45.3
T10 (°C)	38.2	44.0	43.1	42.5	38.3
T11 (°C)	33.3	33.7	33.2	34.0	31.5
T12 (°C)	31.4	31.6	31.3	32.7	30.5
T13 (°C)	32.5	33.1	32.4	33.9	31.7
T14 (°C)	32.0	32.4	32.0	33.4	31.0
Strong concentration	.58	.57	.58	.58	.56
Weak concentration	.55	.55	.565	.57	.545
Pump flow rate (kg/s)	.0065	.0065	.0065	.0065	.0065
water flow rate to evaporator (kg/s)	.0833	.0833	.0833	.1	.267
water flow rate to condenser (kg/s)	.1	.1	.1	.1	.167
water flow rate to absorber (kg/s)	.133	.2	.233	.133	.1
Heat input (kw)	.816	.816	.816	.750	.703

Table (II.1) Experimental results

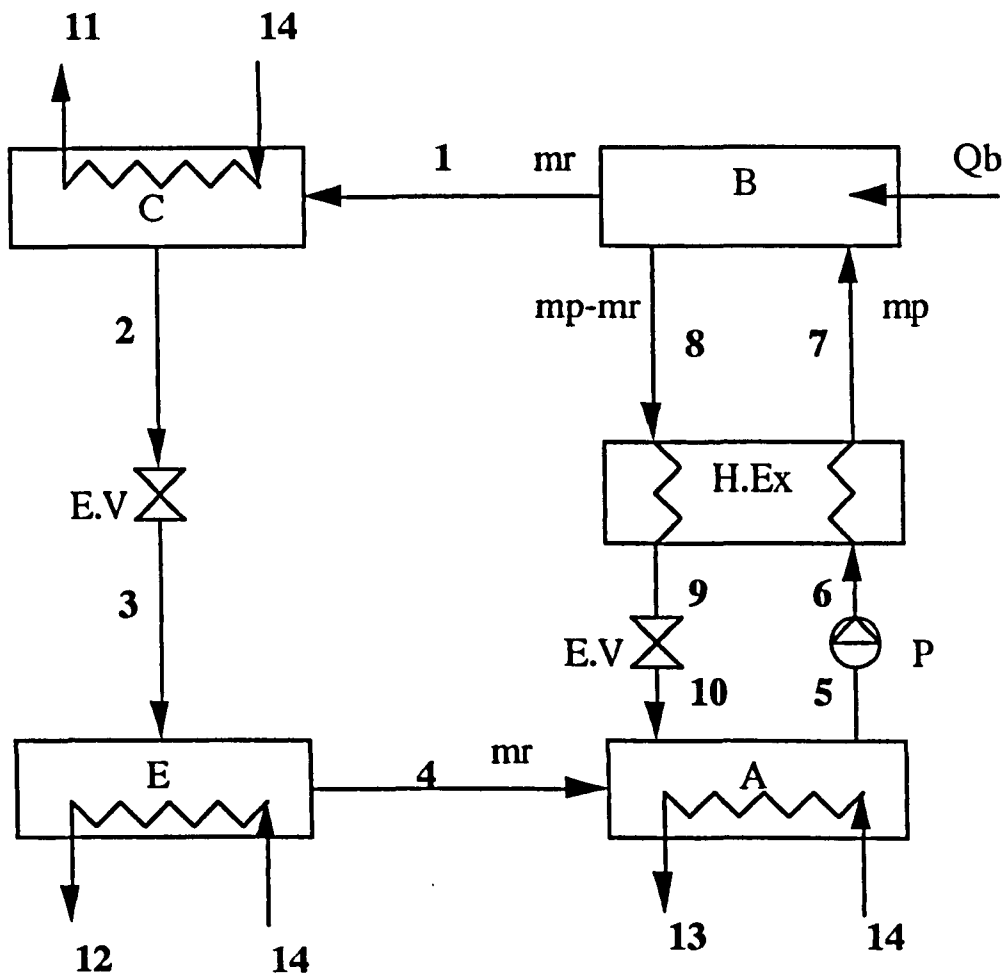

Fig (II.1)

Schematic representation of the $LiBr/H_2O$ system with the thermocouples positions

```
Refrigerant Mass Flow          =   2.4602606E-04 Kg/S
Evaporator Temp                =    27.59122     C
Condenser Temp                 =    50.96013     C
Absorber Inlet Temp            =    49.88076     C
Absorber Outlet Temp           =    37.82986     C
Boiler Inlet Temp              =    83.53008     C
Boiler Outlet Temp             =    98.08439     C
Strong Mass Ratio              =   0.5658454     Kg/Kg
Weak Mass Ratio                =   0.5444280     Kg/Kg

Heat Ratio =  0.7054730

System Capacity   =  0.5756660    KW
Condenser Capacity=  0.5864748    KW
Absorber Capacity =  0.8051935    KW
Boiler Capacity   =  0.8160000    KW

Converged To Solution In          4 Iterations

      The Set Of Conditions For The Above Results Is :

Pump Flow Rate                          =   6.5000001E-03Kg/S
Evaporator Heating Water Flow Rate      =   8.3300002E-02Kg/S
Condenser  Cooling Water Flow Rate      =   0.1000000    Kg/S
Absorber   Cooling Water Flow Rate      =   0.1330000    Kg/S
Evaporator Heating Water Temp.          =    32.00000    C
Condenser  Cooling Water Temp.          =    32.00000    C
Absorber   Cooling Water Temp.          =    32.00000    C
Evaporator Effectiveness                =   0.3750000
Condenser  Effectiveness                =   7.4000001E-02
H.Exchange Effectiveness                =   0.8000000
Absorber Mass Effectiveness             =   0.1500000
Absorber Heat Effectiveness             =   8.1000000E-02
Boiler Mass Effectiveness               =   0.3750000
```

Fig (II.2)

Computer printout of test 1

```
Refrigerant Mass Flow          =   2.2389671E-04 Kg/S
Evaporator Temp                =    28.98139     C
Condenser Temp                 =    51.73180     C
Absorber Inlet Temp            =    48.47703     C
Absorber Outlet Temp           =    32.52410     C
Boiler Inlet Temp              =    80.81874     C
Boiler Outlet Temp             =    98.99464     C
Strong Mass Ratio              =   0.5944183     Kg/Kg
Weak Mass Ratio                =   0.5739432     Kg/Kg

Heat Ratio =  0.6418501

System Capacity   =  0.5237496   KW
Condenser Capacity=  0.5333257   KW
Absorber Capacity =  0.8064243   KW
Boiler Capacity   =  0.8160000   KW

Converged To Solution In          5 Iterations

      The Set Of Conditions For The Above Results Is :

Pump Flow Rate                          =   6.5000001E-03Kg/S
Evaporator Heating Water Flow Rate      =   8.3300002E-02Kg/S
Condenser  Cooling Water Flow Rate      =   0.1000000    Kg/S
Absorber   Cooling Water Flow Rate      =   0.2000000    Kg/S
Evaporator Heating Water Temp.          =    32.40000    C
Condenser  Cooling Water Temp.          =    32.40000    C
Absorber   Cooling Water Temp.          =    32.40000    C
Evaporator Effectiveness                =   0.4400000
Condenser  Effectiveness                =   6.6000000E-02
H.Exchange Effectiveness                =   0.7600000
Absorber Mass Effectiveness             =   9.6000001E-02
Absorber Heat Effectiveness             =   5.9999999E-02
Boiler Mass Effectiveness               =   0.7410000
```

Fig (II.3)

Computer printout of test 2

```
Refrigerant Mass Flow          =   1.9906381E-04 Kg/S
Evaporator Temp                =    29.91074     C
Condenser Temp                 =    52.24682     C
Absorber Inlet Temp            =    56.38974     C
Absorber Outlet Temp           =    35.38928     C
Boiler Inlet Temp              =    104.2431     C
Boiler Outlet Temp             =    126.6956     C
Strong Mass Ratio              =    0.6976509    Kg/Kg
Weak Mass Ratio                =    0.6762852    Kg/Kg

Heat Ratio =  0.5705619

System Capacity    =  0.4655786   KW
Condenser Capacity=  0.4739376   KW
Absorber Capacity  =  0.8076409   KW
Boiler Capacity    =  0.8160000   KW

Converged To Solution In          5 Iterations

        The Set Of Conditions For The Above Results Is :

Pump Flow Rate                          =   6.5000001E-03Kg/S
Evaporator Heating Water Flow Rate      =   8.3300002E-02Kg/S
Condenser  Cooling Water Flow Rate      =   0.1000000    Kg/S
Absorber   Cooling Water Flow Rate      =   0.2330000    Kg/S
Evaporator Heating Water Temp.          =    32.00000    C
Condenser  Cooling Water Temp.          =    32.00000    C
Absorber   Cooling Water Temp.          =    32.00000    C
Evaporator Effectiveness                =   0.6400000
Condenser  Effectiveness                =   5.6000002E-02
H.Exchange Effectiveness                =   0.7700000
Absorber Mass Effectiveness             =   7.0000000E-02
Absorber Heat Effectiveness             =   3.4000002E-02
Boiler Mass Effectiveness               =   0.8320000
```

Fig (II.4)

Computer printout of test 3

```
Refrigerant Mass Flow          =   1.5593458E-04 Kg/S
Evaporator Temp                =    30.20872     C
Condenser Temp                 =    59.34349     C
Absorber Inlet Temp            =    57.64915     C
Absorber Outlet Temp           =    31.03080     C
Boiler Inlet Temp              =    133.2675     C
Boiler Outlet Temp             =    159.3120     C
Strong Mass Ratio              =   0.7070094     Kg/Kg
Weak Mass Ratio                =   0.6900483     Kg/Kg

Heat Ratio =  0.4802239

System Capacity    =  0.3601679    KW
Condenser Capacity=  0.3687088    KW
Absorber Capacity  =  0.7414590    KW
Boiler Capacity    =  0.7500000    KW

Converged To Solution In          5 Iterations

      The Set Of Conditions For The Above Results Is :

Pump Flow Rate                          =   6.5000001E-03Kg/S
Evaporator Heating Water Flow Rate      =   0.1000000    Kg/S
Condenser  Cooling Water Flow Rate      =   0.1000000    Kg/S
Absorber   Cooling Water Flow Rate      =   0.1330000    Kg/S
Evaporator Heating Water Temp.          =    33.40000    C
Condenser  Cooling Water Temp.          =    33.40000    C
Absorber   Cooling Water Temp.          =    33.40000    C
Evaporator Effectiveness                =   0.2700000
Condenser  Effectiveness                =   3.4000002E-02
H.Exchange Effectiveness                =   0.7925000
Absorber Mass Effectiveness             =   4.9300000E-02
Absorber Heat Effectiveness             =   5.5000000E-02
Boiler Mass Effectiveness               =   0.2780000
```

Fig (II.5)

Computer printout of test 4

```
Refrigerant Mass Flow          =   1.7973452E-04 Kg/S
Evaporator Temp                =    30.40217     C
Condenser Temp                 =    57.56343     C
Absorber Inlet Temp            =    47.59861     C
Absorber Outlet Temp           =    31.05064     C
Boiler Inlet Temp              =    84.65353     C
Boiler Outlet Temp             =    102.9984     C
Strong Mass Ratio              =   0.5643718     Kg/Kg
Weak Mass Ratio                =   0.5487661     Kg/Kg

Heat Ratio =  0.5925199

System Capacity    =  0.4165415    KW
Condenser Capacity=  0.4257199    KW
Absorber Capacity  =  0.6938225    KW
Boiler Capacity    =  0.7030000    KW

Converged To Solution In          5 Iterations

      The Set Of Conditions For The Above Results Is :

Pump Flow Rate                          =   6.5000001E-03Kg/S
Evaporator Heating Water Flow Rate      =   0.2667000    Kg/S
Condenser  Cooling Water Flow Rate      =   0.1667000    Kg/S
Absorber   Cooling Water Flow Rate      =   0.1000000    Kg/S
Evaporator Heating Water Temp.          =    31.00000    C
Condenser  Cooling Water Temp.          =    31.00000    C
Absorber   Cooling Water Temp.          =    31.00000    C
Evaporator Effectiveness                =   0.6250000
Condenser  Effectiveness                =   2.3000000E-02
H.Exchange Effectiveness                =   0.7700000
Absorber Mass Effectiveness             =   7.7000000E-02
Absorber Heat Effectiveness             =   0.1000000
Boiler Mass Effectiveness               =   0.3840000
```

Fig (II.6)

Computer printout of test 5